University of Southampton

A Plane Wave Basis Method for the Vibration Analysis of Membranes and Plates

by

Laurent Jacques Willocq

Thesis submitted for the degree of Master of Philosophy at the faculty of Engineering and Applied Science

October 1997

UNIVERSITY OF SOUTHAMPTON

ABSTRACT

FACULTY OF ENGINEERING AND APPLIED SCIENCE
AERONAUTICS AND ASTRONAUTICS

Master of Philosophy

A PLANE WAVE BASIS METHOD FOR THE VIBRATION ANALYSIS OF MEMBRANES AND PLATES

by Laurent Jacques Willocq

A new boundary method for modelling structural vibrations, called the *Plane Wave Basis Method*, is developed to estimate the natural frequencies and mode shapes of membranes and plates with various boundary conditions.

Since its formulation may be derived from the *Indirect Boundary Element Method*, this method is studied and applied to the vibration of arbitrary shaped membranes and clamped plates. Furthermore, a new boundary element technique that deals with equations of the type $\mathcal{L}u = b(x, y)$ is presented. Based on the spatial Fourier transform, it may be used with any type of fundamental solution and does not need any domain integration. This approach has been applied to determine the forced response of membranes to surface waves.

The alternative formulation using the plane wave basis method is based on use of the *Trefftz functions* or T-function. Thus, the Trefftz methodology is introduced and one of its application, called the *Exterior Boundary Element Method* or *Modified Trefftz Method*, is applied to the vibration of clamped membranes.

In both cases, the plane wave basis formulation expresses the transverse displacement as a superposition of propagating waves and evanescent waves. This method is highly effective in simplifying the programming and reducing the computational expense. The vibration of clamped membranes and of square, triangular, trapezoidal, rhombic and elliptical plates with different boundary conditions such as clamped, simply supported, sliding clamped, point supported, free and combinations of the aforementioned, are analysed. In most of the cases, the results agree well with the exact values or the values which have been found so far by various other approximate methods. However, problems are encountered when dealing with free polygonal plates; it is thought that the reason for this is attributable to the corner points. Although several different models of corners were studied, none of them was found to be satisfactory.

Contents

List of Figures

List of Tables

Acknowledgements

The author wishes to thank Prof. R. Langley and Dr. N. Bardell for their patience and guidance throughout the year. Their precious help during the most critical parts of this research is gratefully acknowledged.

A special thank is given to Prof. Y. Urata, of the Department of Mechanical Engineering at the Shizuoka Institute of Science and Technology, for his help in explaining certain aspects of his work.

The author wishes to thank the Ecole Nationale Supérieure d'Ingénieurs de Constructions Aéronautiques for its financial support for this research.

The author thanks his parents without whose encouragement and loving support, this work may never have been completed.

Notation and Abbreviations

$\|\ \|$	the norm of a vector in $\mathbb{R}^2$
∇	gradient
IBEM	Indirect Boundary Element Method(s)
DBEM	Direct Boundary Element Methods(s)
EIBEM	Exterior Indirect Boundary Element Method(s)
PWBM	the Plane Wave Basis Method
ABFM	the Approximate Bessel-function Method
FEM	the Finite Element Method
arg	the argument of a complex number
$\mathbb{C}$	the set of all complex numbers
$c([M])$	condition number of the matrix $[M]$
$\det[M]$	the determinant of the matrix $[M]$
$\delta(\mathbf{x})$	the Dirac delta distribution
$dS_{\mathbf{x}}$	the infinitesimal surface element
$dC_{\mathbf{x}}$	the infinitesimal curve element
$\frac{\partial}{\partial \mathbf{n}}$, $\partial_{\mathbf{n}}$, $\frac{\partial}{\partial \mathbf{n}_x}$	the normal derivative (at $\mathbf{x}$ or with respect to the $\mathbf{x}$-variable)
D	flexural rigidity of a plate; $D = \frac{Eh^3}{12(1-\nu^2)}$
E	Young's modulus

$\mathcal{F}$	the Fourier transform, $\mathcal{F}(f)(\nu) = \hat{f}(\nu) = \frac{1}{2\pi}\int_{\mathbb{R}^2} e^{i(x_1\nu_1+x_2\nu_2)}\,dx_1dx_2$
$\mathcal{F}^{-1}$	the inverse Fourier transform
$\Gamma(\mathbf{x})$	the gamma function
h	thickness of plate
$H_\alpha^{(1)}$,$H_\alpha^{(2)}$	Hankel functions of the first and the second kinds of order α
I_α	modified Bessel function of order α
J_α	Bessel function of order α
k	eigenvalue of the boundary value problem; $k = \omega\frac{\sigma h}{\rho}$ for a membrane, and $k^4 = \frac{\omega^2\rho h}{D}$ for a plate
λ	nondimensional eigenvalue or eigenfrequency $\lambda = ka$, with a the reference length
M_{ij}	elements of matrix $[M]$
$[M]^t$	the transpose of matrix $[M]$
$\mathbf{n}$, $\mathbf{n_x}$	the unit normal vector pointing outward on the boundary $\partial\Omega$ of a bounded domain Ω (at $\mathbf{x} \in \partial\Omega$)
$\mathbb{N}$	the set of all nonnegative integers
ν	Poisson's ratio
ω	circular (angular) frequency of free vibration
Ω	an open domain in $\mathbb{R}^2$: Ω is usually simply connected and bounded with smooth boundary $\partial\Omega$; $\bar{\Omega} = \Omega \cup \partial\Omega$
r, θ	polar co-ordinates
ρ	mass per unit of area
$\mathbb{R}$	the set of real numbers
$\mathbb{R}^N$	the N-dimensional real Euclidean space
s	arc length parameter along $\partial\Omega$

$\mathbf{s}$	counterclockwise unit tangential vector to the boundary $\partial\Omega$
σ	shear stress
$\mathbf{x}$	the point or the vector of co-ordinates (x_1, x_2)
x_1, x_2	Cartesian co-ordinates
X_1, X_2	co-ordinate axes of Cartesian co-ordinate system
$\mathbb{Z}$	the set of integers

1. Introduction

1.1 General remarks

Since the early days of manned flight, the importance of structural analysis has been recognised from the design stage through to full scale testing. In particular, the dynamic response of the airframe to external loading actions must be appreciated in order to ensure its structural integrity - the literature is full of accounts of system failures brought about by resonance and excessive vibration of components [2, 1, 3]. Till the 1950s, such studies were done by using gross models, with only a few degrees of freedom. However, the advent of high-speed digital computers made it possible to analyse moderately complex systems and to generate approximate solutions. The introduction of the Finite Element Method (FEM) enabled aeronautical engineers to use digital computers to conduct numerically detailed vibration analysis of complex mechanical and structural systems displaying many thousands of degrees of freedom. This technique discretizes the domain of the problem under consideration into a number of elements or cells. The governing equations are then approximated over the region by functions which fully or partially satisfy the boundary conditions.

Alternative procedure is to use approximating functions that satisfy the governing equations in the domain but not the boundary conditions. These techniques are called boundary methods. Although they have developed slowly up to the present time, they are now being re-examined, mainly because they offer an elegant and economic alternative to the domain methods such as the FEM. One major advantage of the boundary methods over the FEM is a significant reduction of dimensionality, i.e. in the BEM, a two-dimensional region is quantified by its one-dimensional boundary or perimeter. Consequently, the discretization is much simpler. The computer programs require much less memory space, and are generally easier to develop. However, both approaches - domain and boundary ones - should be considered to be complementary more than exclusive, and there are already several examples of mixed methods based on the simultaneous use of a boundary method and the FEM.

There are two main approaches for the formulation of boundary methods: one is based on the use of boundary integral equations (BIE) and the other one on the use of complete systems of solutions. In numerical applications, the first method has received most of the attention.

It has been known for a long time that it is possible to formulate boundary integral equations with singular kernels (due to the use of Green's functions or fundamental solutions) to solve a boundary value problem. However, the BIE as a numerical technique has its origin in the 1960s. It was called the boundary element method (BEM) in order to emphasise the boundary discretization character of the method in contrast with the FEM. The BIE used at that time

were primarily formulated from Green's formula, which is commonly referred to as the *direct approach* or Direct Boundary Element Method (DBEM). However, an alternative approach to the BIE, the *indirect approach* or IBEM, using ideas from Potential Theory to represent the solution as a superposition of layer potentials, leads to greatly simplified systems, and, as a consequence, is much easier to compute.

The second type of boundary method, based on the use of complete systems of solutions is frequently associated with the name of Trefftz, who first described such a boundary method in 1926. Though this type of boundary method avoids the use of singular integrals, unlike the BIE, it has received less attention. This situation may be due to the common, but false, belief that complete systems of solutions have to be constructed specifically for a given region. However, frequently systems of solutions are completely independent of the detailed shape of the region considered, and this method has recently been used in many fields by choosing different sets of complete functions.

1.2 Literature survey

The origin of integral equation approach to boundary value problems in elasticity is closely related to the work done in the latter half of the 19th century on potential theory [43]. It also borrows greatly from the work on integral equations reported by Fredholm [23], published in 1903. With aid of digital computers, it became possible to solve non-trivial, engineering-type problem using their numerical implementation. Pioneering work in this direction was done by Jawson [41] and Symm [41] in Potential Theory and elastostatic. However, all these works were based on the direct approach. Indeed, the Indirect Boundary Element Method (IBEM) has always been less popular, despite its closer link with Potential Theory.

Furthermore, applications of the BEM to the vibrations of structures are scarce. Since, in the frequency-domain, the dynamical equation of the membrane reduces to the Helmholtz equation, the works done on the eigenvalues and eigenmodes of the Helmholtz equation [13, 73, 57], published in the mid 1970s, can be considered to be first results of such a application.

Among them, the work by Cassot and Extremet [13] is probably the first application of the BEM to treat this problem. They used the indirect approach to express not only the distribution of the sound field inside a circular cavity, but also to determine the eigenfrequencies of the Neumann problem associated with this circular shape. To do so, they use the complex determinant in order to obtain the eigenfrequencies, and they concluded that the eigenvalues should be determined as the local minima of the determinant.

On the other hand, Tai and Shaw [73] used the direct approach to find the eigenfrequencies and the eigenmodes of a triangular domain associated with the

Neumann problem. Instead of using the complex determinant, they preferred to search for common roots of the determinant for the real and imaginary parts of the complex matrix.

The first directly applicable result to a clamped membrane is found in the work by De Mey [57]. The author of this reference used the indirect approach to calculate the eigenfrequencies of circular and rectangular domain for the Dirichlet problem, e.g. with a clamped boundary. However, he noticed that looking for common root of the determinant of the real and imaginary part can lead to discrepancies between the results, and hence less accurate results.

Hutchinson [37] employed the direct BEM with only the real part of the Green's function. Although such a procedure greatly simplified the calculation, it produced spurious roots which complicate the determination of the eigenvalues because of the need to look at the modal shapes.

The first application of the boundary integral equations to the vibration of plates is usually credited to Vivoli and Filippi [82] in which they used the indirect method of solution employing layer potentials up to the third order. By determining the minima of the complex determinant, they obtained the eigenfrequencies of an arbitrary shaped plate with a clamped and partially clamped-partially free boundary. Comparing the results with experimental ones, they concluded that even if the relative error is quite high (up to 6% in the case of the mixed boundary conditions), such results are still valid for engineering purpose. That work was preceded by a series of papers by Vivoli [79, 81, 80] and by Vivoli and Filipi [22, 21].

The direct approach was implemented by Hutchinson and Wong [38] who applied this method to clamped and simply supported plates. As in the membrane problem, they used only the real part of the fundamental solution which led to spurious roots. However, they concluded, by comparing their results with known finite elements solutions, that the BEM leaded to greater accuracy at higher frequency, but because of the greater computational complexity, it was not a superior method.

Niwa, Kobayashi and Kitahara [62] formulated the plate boundary element equations using both layer potentials (indirect method) and the Green's formula (direct method) using the classical fundamental solution. In doing so, they used the complex determinant and studied two types of element, the straight line segment and the curved line segment.

A more detailed study of all these eigenvalue problems, and more general elastodynamic eigenvalue problems, can be found in the book by Kitahara [47].

Finally, the special indirect BEM of Heuer and Irschik [35] developed for frequency analysis of polygonal membranes and plates should also be mentioned. In this work, the authors used a finite-domain Green's function so that only part of the

boundary has to be discretized. The dynamic analysis of parallelogram plates is then obtained by considering the analogous membrane problems.

However, in all the previous work, the singular character of the integrals used, due to the fundamental solution, incurred a sizeable computational overhead. Hence, some derived methods which eliminated these singularities were investigated. In the case of the indirect approach (which is the one studied in this work), the Exterior Indirect Boundary Element Method (EIBEM) is one of them. In this technique, the source points are located not on the boundary of the domain but outside it, on an imaginary exterior boundary, thus suppressing the singularities. This simple idea was discovered independently by several researchers who, sometimes not quoting each other, gave it different names. Thus, it was called regular Indirect Boundary Element Method (RIBEM) [85], method of fundamental solutions [55, 8], source function method [19], exterior collocation boundary element method [7], charge simulated method exterior collocation method and modified Trefftz method [66].

In fact, the EIBEM is closely related to the other approach cited previously, namely the Trefftz method. The difference between these two methods is chiefly dependent upon the choice of the trial functions. But, since the fundamental solutions used in the EIBEM are part of Kupradze's functions (the Kupradze functions, introduced by Kupradze [48] in the middle 1960s, are fundamental solutions with concentrated forces applied to a surface exterior to the investigated region and modelling the unknown solution inside it), one can the use the standard Trefftz method.

No work can be found which applies this method to the study of eigenfrequencies of membranes and plates. However, some results obtained by researchers in other fields, such as stress analysis [66, 84], fluid flow problems [66], propagation of waves in structures [24], elastostatic [87], thermal analysis [85, 30], study of magnetic fields [36] and waveguides [42] can be used to validate this work, especially regarding the study of the most two important parameters in the EIBEM: the shape of the exterior surface holding the source points, and its distance from the surface of the original problem.

Until now, the most common way to define the exterior shape was the homothetic contour of the original boundary, and many authors [42, 24, 87, 36, 30] situate the sources on straight lines perpendicular to the surface. Wearing and Sheikh [85] defined an optimised contour for the corner zone. However, some authors such as Bogomolny [8] proposed a circular exterior boundary and others [55] gave the algorithm for optimising the contour by the mean of the least squares and the theory of approximation by γ-polynomials. According to Heise [31], the profile of the imaginary boundary placed on the source points can be taken regardless of the real boundary profile, but the accuracy of the results and the conditioning of the matrices are very dependent on the type of profile chosen. The distance between the imaginary and the real boundary can also greatly influence the efficiency of the

method. Most of the researchers [42, 55, 24, 87, 85, 36, 30] agree on the presence of a range of acceptability for this parameter. This range is problem-dependent but if the distance is too small, the problem becomes singular and if the distance is too big, the matrices become linearly dependent, hence singular and ill-conditioned. Several ways to overcome the distance dependency were investigated. Thus, Mathon and Jonhston [55] used a scaled fundamental solution and noticed a better convergence of their results. Fu *et al.* [24] used a coarse discretization of the boundary to reduce the number of exterior points and to have a better conditioned matrix, and Honma *et al.* [36] preferred to use smaller elements to overcome the ill-conditioning.

However, Zielinski [89] observed an increase in the solution accuracy but simultaneous deterioration of the matrix conditioning with the increase of the distance.

As it has just been seen, the distinction between the Trefftz method and the BEM may be less obvious than it first appeared, since the latter can lead to a trefftzian formulation. However, the set of functions used in the Trefftz method fulfill the governing equations inside the domain and *on its boundary.* This particularity eliminates the standard BEM approach which applies functions fulfilling the differential equations everywhere *but* the boundary.

In the case of the classical Trefftz method, few results concerning its application to the eigenvalues problems have been published. Herrera [32] gave it a sound mathematical background and he derived the complete systems of solutions, which were latter called T-functions, for bounded and unbounded regions, for the reduced Helmholtz equation [33] in two- and three-dimensional problems in the late 1970s. Similar systems were also derived by the same author for the Laplace equation [32] and the biharmonic equation [32]. There are two approaches for using these systems, namely the *direct* and the *indirect* approaches. In the direct formulation, which is relatively new [15, 16], the weighted residual expression of the governing equation is derived by taking the T-functions as the weighting functions, and then the boundary integral equation is obtained by applying twice the Gauss-Green formula to it. Such a method was applied to the study of water wave diffraction around a structure [15] (modelled by the Helmholtz equation) and to Kirchhoff plate bending [16].

The indirect formulation of the Trefftz method, which is considered to be the original one presented by Trefftz, approximates the solution of the problem by the superposition of the T-functions and then the unknown parameters are determined so that the approximate solution satisfies the boundary condition by means of collocation, the least squares or the Galerkin method [46]. Hence, in the case of vibration of structures, the eigenfrequencies are obtained by a determinant search similar to the one encountered in the BEM. Although this method is fairly old and the question of completeness for the plate is still not settled, the first application of this method to the problem of plate vibrations was undertaken by Conway [17],

and Conway and Farnham [18] in the early 1960s. In these articles, Conway *et al.* satisfied an equation verified by the moment quantity which is similar to the Helmholtz equation, and then, using the well-known solutions of the plate vibration in polar co-ordinates (which was latter proven to be T-functions by Herrera [33]) and the collocation method, they obtained the classical eigenvalue problem to be solved by the eigenfrequencies, i.e. the eigenfrequencies being the roots of a determinant.

A series of articles [60, 61, 58, 59] by Nagaya on the vibrations of plates must also be noted. The author of these references used the same solution as Conway [18] to express the displacement for an arbitrary shaped plate. However, unlike in the Trefftz method, the unknown coefficient were determined by applying to the resulting boundary conditions the method of Fourier expansion.

One of the first applications of the Trefftz method to the vibration of membranes was realised by Urata and Nakagawa [78] in 1993. Indeed, without acknowledging the similarity with the Trefftz methodology, they expressed the displacement of the membrane by a system of propagating plane waves. By applying the weighted residual method and the collocation method, they derived the eigenfrequencies of rectangular and circular membranes for the Neumann and Dirichlet problems. It must be remarked that such a system of plane waves had already bee proposed as alternative T-functions for the Helmholtz equation by Herrera [34] in 1981.

A subsequent article by Urata [77] (in Japanese) expressed of the transverse displacement of a plate as the sum of propagating and evanescent waves. However, instead of using this expression, he derived four expressions using sinusoidal functions and hyperbolic functions to represent the different symmetries of the modes. Then applying the collocation method and the method of weighted residuals (or more precisely, the method of virtual work), he was able to determine the natural frequencies of clamped circular, elliptic, square and rhombic plates and of square and rhombic plates with free edges.

In a recent article [75], Urata used another expression of the transverse displacement, which had already been used by Nagaya, e.g. the polar co-ordinate solution of the plate equation, to examine the lateral vibrations of different plates. In doing so, he applied the collocation method and remarked that, although this method is one of the simplest, the accuracy obtained was perfectly acceptable. However, Urata encountered several problems with the modelling of corners, and offered some improvements in another article [76].

1.3 Motivation

As just seen, the application of boundary methods to the study of vibrations are scarce, despite the fact that such methods have been widely applied in other areas. Furthermore, the simplest formulation - the indirect approach - has known little

success. Hence, this thesis describes a computational and theoretical investigation of the application of indirect boundary methods to the vibration of two types of structure: membranes and plates, and a new and simpler method is proposed. This method can be derived from the two formulations of the boundary method, the BIE approach or the Trefftz method.

1.4 Scope

In this work, the emphasis is laid on the indirect formulation of the boundary methods, and the classical formulation of the IBEM is assessed for both membranes and plates. In doing so, a simple technique which enables the forced response of these structures to be determined is implemented.

Then, in order to improve the computer efficiency of this method, the application of the EIBEM to the vibration of membranes is studied. Since such an application is new, some difficulties to optimise the parameters are encountered. It also appears that such a method may lack the versatility of the IBEM. Hence, a derived formulation is investigated.

This derived formulation is obtained by considering the asymptotical form of the EIBEM, which aims to express the displacement field inside the structure by a superposition of plane waves. Such a formulation can also be derived from the Trefftz method, as it was shown by Herrera [33] for the case of the Helmholtz equation. This formulation is then applied to several different plates and some results are presented for different planforms typically encountered in aeronautics. Although this formulation has already been applied to membrane vibration [78], its application to plate vibrations constitutes an original contribution.

1.5 Organisation of the dissertation

This dissertation is divided into five chapters, a list of references and seven appendices.

Chapter 2 presents the Indirect Boundary Element Method and its application to the vibration of damped and undamped clamped membranes and of clamped plates. A new technique to determine the forced response of a membrane is also presented, and two types of excitation are considered, a point force and a plane wave force.

Chapter 3 presents the Exterior Indirect Boundary Element Method and the principle of the Trefftz methodology. In order to highlight the main characteristics of the EIBEM, the simple case of the membranes is considered. Comments are included on the different ways to optimise the parameters introduced by this

method. The Trefftz method is then briefly described and the usual T-functions, for the problems of membrane and the plate vibrations, are presented. Since these T-functions have already been applied to the study of vibration of these two structures [17, 18, 77, 75, 76], the reader is referred to these works for further information.

Chapter 4 introduces the new set of functions used in this work. Based on the work by Herrera [32], they represent propagating and evanescent plane waves, thus the name given to this derived Trefftz method, the Plane Wave Basis Method. By applying the discretization used in the Trefftz methodology and the collocation method, it is shown that such functions can be applied to the analyses of vibrations of membranes and plates with various shapes and boundary conditions. Although most of the eigenfrequencies and the modes obtained by using this method are found to be accurate, problems with ill-conditioning and with free corner points are encountered. Hence, other discretization methods, such as the weighted residual method and the Galerkin method, along with different models of free corner points are investigated. Since none of them lead to satisfactory results, a derived formulation of the PWBM is studied. It is shown that such a formulation constitutes an approximation of the Bessel functions used in the usual T-functions. However, such a method did not give accurate values but for free rectangular plates.

Chapter 5 presents the final conclusions of the current research.

Appendix A presents the special functions used in this research and some useful relations between them.

Appendix B presents some results concerning the matrix algebra.

Appendix C presents the modal expansion of a vibrating damped square membrane. Such expressions are used to assess the accuracy of the forced response technique developed in Chapter 2.

Appendix D presents the derivation of the new set of functions for the case of the plate from the solution of the differential equation in polar co-ordinates.

Appendix E introduces the different expression of the boundary quantities for a plane wave. Such expressions are used while implementing the new method.

Appendix F presents an application of the weighted residual method and the Galerkin method to the new method. It is shown that care must be taken when using these methods because of the spurious roots they introduce.

Appendix G presents the boundary condition which should be implemented for a discontinuous point along a free edge.

Finally, a list of technical references is presented.

2. The boundary element method

The boundary element method (BEM) is based on the discretization of the integral equations representating the system. There are two types of boundary element methods: the *indirect* method and the *direct* method. The first technique is the oldest and comes from the potential theory. It employs fictitious quantities (source densities) to express the integral equations [47, 14]. The second one only employs quantities that have a clear physical meaning (displacement, stress, etc.) [11, 9, 52].

2.1 Principle

2.1.1 The Indirect Boundary Element Method (IBEM)

Integral formulation

Let Ω be an open domain of $\mathbb{R}^2$ with smooth boundary $\partial\Omega$ (more precisely, a Lyapunov surface as defined in [41]). Let $\mathcal{L}$ be a differential operator on Ω and $\{B_i\}_{i=1,\dots,m}$ be m differential operators giving the homogeneous boundary conditions of the problem. A *boundary value problem* is represented by the following system:

$$\begin{cases} \mathcal{L}u + b = 0 & \text{on } \Omega \\ B_i(u) = 0 \quad (i = 1, \dots, m) & \text{on } \partial\Omega \end{cases} \tag{2.1}$$

where the body force b is given.

A *fundamental solution*, $G(\mathbf{x}, \mathbf{y})$, of (2.1) is by definition a solution (in the sense of distributions) of the equation:

$$\mathcal{L}G(\mathbf{x}, \mathbf{y}) + \delta(\mathbf{x} - \mathbf{y}) = 0, \quad \mathbf{x}, \mathbf{y} \in \mathbb{R}^2 \tag{2.2}$$

where $\delta(\mathbf{x}, \mathbf{y})$ is a Dirac delta function which goes to infinity at the point $\mathbf{x} = \mathbf{y}$ and is equal to zero elsewhere. It has the following property:

$$\int_\Omega u(\mathbf{y})\delta(\mathbf{x} - \mathbf{y})\, dS_\mathbf{y} = u(\mathbf{x}), \quad \forall \mathbf{x} \in \mathbb{R}^2 \tag{2.3}$$

Physically, $G(\mathbf{x}, \mathbf{y})$ is the response at $\mathbf{x}$ to a concentrated unit source located at $\mathbf{y}$ and generated in an infinite medium.

The indirect formulation of (2.1) is obtained by using *layer potentials*. In the classical potential theory for Laplace's equation, harmonic functions can be represented by layer potentials and it has been shown that analogous results to the classical potential theory can be deduced for steady-state elastodynamics [47, 14]. Here, using the formulation of Vivoli [81], a layer potential of order q, $\tilde{U}^q$, is a solution of:

$$\mathcal{L}\tilde{U}^q = \partial_\mathbf{n}^q(\mu_q\, \delta_{\partial\Omega}) \tag{2.4}$$

where μ_q is the *source density* of the layer, $\partial_{\mathbf{n}}^q$ is the qth derivative in the direction of the unit outward normal to the boundary $\partial\Omega$, $\mathbf{n}$, and $\delta_{\partial\Omega}$ is the Dirac measure with support $\partial\Omega$:

$$\delta_{\partial\Omega}(\mathbf{x}) = \begin{cases} 1, & \text{for } \mathbf{x} \text{ on } \partial\Omega, \\ 0, & \text{otherwise.} \end{cases} \tag{2.5}$$

$\tilde{U}^q$ can be written as in [82]:

$$\tilde{U}^q(\mathbf{x}) = (-1)^q \int_{\partial\Omega} \mu_q(\mathbf{y}) \partial_{\mathbf{n}}^q G(\mathbf{x}, \mathbf{y})\, dC_{\mathbf{y}} \tag{2.6}$$

where $G(\mathbf{x}, \mathbf{y})$ is a fundamental solution previously defined.

Hence, the indirect formulation of (2.1) is:

$$u(\mathbf{x}) = \int_{\Omega} b(\mathbf{y}) G(\mathbf{x}, \mathbf{y})\, dS_{\mathbf{y}} + \sum_{q \in I} (-1)^q \int_{\partial\Omega} \mu_q(\mathbf{y}) \partial_{\mathbf{n}}^q G(\mathbf{x}, \mathbf{y})\, dC_{\mathbf{y}} \tag{2.7}$$

with $I \subset \mathbb{N}$.

In the following, the body force b is assumed to be zero. By applying the m boundary conditions B_i to (2.7), the following system of integral equations with respect to μ_q is derived:

$$\sum_{q \in I} (-1)^q \lim_{\mathbf{x} \to \mathbf{X}} B_i \left(\int_{\Gamma} \mu_q(\mathbf{y}) \partial_{\mathbf{n}}^q G(\mathbf{x}, \mathbf{y})\, dC_{\mathbf{y}} \right) = 0, \quad (i = 1, \ldots, m), \quad \forall \mathbf{X} \in \partial\Omega \tag{2.8}$$

Since the fundamental solution presents a discontinuity at $\mathbf{x} = \mathbf{y}$, some care must be taken when dealing with the integrals. It may be required to use the Cauchy Principal Value and a free term representating the "jump" on the boundary. A rigorous treatment of these singularities can be found in the book by Chen and Zhou [14] and in the series of articles by Vivoli *et al.* [81, 21, 82].

Having m boundary conditions to satisfy, m potential layers will be taken. Furthermore, as a lower order potential is preferable from the computational point of view [47], it is customary to have $I = \{0, \ldots, m-1\}$.

Numerical Analysis

For the purposes of numerical computation, the boundary $\partial\Omega$ is divided into n suitable intervals Γ_j so that $\partial\Omega = \Gamma_1 \cup \Gamma_2 \cup \ldots \cup \Gamma_n$. The points that subdivide the boundary will be referred as *interval points* and will be denoted $\mathbf{x}^{j \pm \frac{1}{2}}$. It is important when choosing the interval points that any corners of $\partial\Omega$ are included, which ensures that each interval Γ_j is smooth. The source densities μ_q are then approximated by step-functions:

$$\begin{aligned} \mu_q(\mathbf{x}) = \mu_q^j, \quad \forall \mathbf{x} \in \Gamma_j, \quad & (j = 1, \ldots, n), \\ & (q = 1, \ldots, m), \end{aligned} \tag{2.9}$$

where μ_q^j are constant. Hence, the system (2.8) is approximated by

$$\sum_{j=1}^{n}\sum_{q=0}^{m-1}(-1)^q \lim_{\mathbf{x}\to\mathbf{X}} B_i\left(\mu_q^j \int_{\Gamma_j} \partial_{\mathbf{n}}^q G(\mathbf{x},\mathbf{y})\, dC_{\mathbf{y}}\right) = 0, \quad (i=1,\ldots,m), \quad \forall \mathbf{X}^j \in \Gamma_j \tag{2.10}$$

To solve this equation, the method of *collocation* or *point-matching* is used, and (2.10) is applied at one particular point in each interval Γ_j of $\partial\Omega$. These points are called *nodal points* and will be denoted $\mathbf{x}^j$, as shown on Figure 1.

As it was remarked by Jawson *et al.*[41], this method of discretizing an integral equation is a particular case of the method of moments, and more generally of the weighted residual method.

Hence, (2.10) is approximated by a system of homogeneous linear equations:

$$\sum_{j=1}^{n}\sum_{q=0}^{m-1} A_{lj}^{qi}\mu_q^j = 0, \quad \begin{matrix}(i=1,\ldots,m),\\ (l=1,\ldots,n)\end{matrix} \tag{2.11}$$

with

$$A_{lj}^{qi} = \lim_{\mathbf{x}\to\mathbf{x}^l}(-1)^q B_i\left(\int_{\Gamma_j} \mu_q(\mathbf{y})\partial_{\mathbf{n}}^q G(\mathbf{x},\mathbf{y})\, dC_{\mathbf{y}}\right), \quad \mathbf{x}^l \in \Gamma_l \tag{2.12}$$

All integrals are then evaluated numerically with respect to the remark stated previously.

2.1.2 The Direct Boundary Element Method (DBEM)

An exhaustive presentation of this method is beyond the scope of this work. For further information, reference should be made to any of the following references [52, 11, 12, 10, 47]

In elastodynamics, the DBEM can be derived from the dynamical reciprocal theorem (Somigliana's Formula) [47], the weighted residuals method [11] or from the Green's function method [52]. It makes use of the fundamental solution to obtain an integral representation of the system inside the domain Ω with respect to u and to its boundary data. The integral equation is then taken to the boundary and a system of constraint equations between the boundary quantities is derived. The last step of this method is a numerical discretization of the domain and the evaluation of the integrals.

2.2 Application of the IBEM to a membrane

A membrane is a continuum possessed of axial stiffness in tension, but offering no flexural resistance. Membranes are extensively used in machine design for pumps, compressors, pressure regulators, etc.

Membrane vibration have been subjects of many investigations as special cases of plate vibrations. Indeed, in the case of the IBEM, the formulation of the problem for a membrane is closely related to the one of a plate.

2.2.1 Case of a vibrating undamped membrane

In the derivation of the differential equation of the equilibrium of a membrane occupying the area Ω, it is assumed that the lateral displacements v are small and thus the tensile force per unit length acting on the middle surface ($\sigma_x h = \sigma_y h = \sigma h$) is constant. Furthermore, the displacement on the boundary is assumed to be zero (homogeneous Dirichlet condition). From [72], the following differential equation of motion is obtained for the free transverse vibration of a membrane:

$$\rho \frac{\partial^2 v}{\partial^2 t} - \sigma h \nabla^2 v = b, \ \mathbf{x} \in \Omega \tag{2.13}$$

where ρ is the mass of the membrane per unit area and b is the distributed transverse load per unit area. The boundary of the membrane being fixed, v satisfies:

$$B(v)(\mathbf{x}, t) = 0, \ \mathbf{x} \in \partial\Omega, \ t \geq 0. \tag{2.14}$$

where B is the differential operator introduced in Section 2.1.1. In this case, B is defined by

$$B(w) = w \tag{2.15}$$

Through out this work, the time dependency will be removed by assuming harmonic motions with an angular frequency ω, i.e.

$$v(\mathbf{x}, t) = e^{-i\omega t} w(\mathbf{x}) \tag{2.16}$$

$$b(\mathbf{x}, t) = e^{-i\omega t} q(\mathbf{x}) \tag{2.17}$$

where i denotes $\sqrt{-1}$ when it is not used as an index in the subscripts. Furthermore, in order to simplify the formulation of the problem, the following reduced force p will be used

$$p(\mathbf{x}) = \frac{q(\mathbf{x})}{\sigma h} \tag{2.18}$$

Hence, the following Dirichlet problem is derived:

$$\begin{cases} k^2 w(\mathbf{x}) + \nabla^2 w(\mathbf{x}) = -p(\mathbf{x}), & \mathbf{x} \in \Omega, \\ w(\mathbf{x}) = 0, & \mathbf{x} \in \partial\Omega \end{cases} \tag{2.19}$$

where the wave number k is related to the angular frequency ω by

$$k = \frac{\omega}{c} \tag{2.20}$$

where c, the velocity of transverse waves in the membrane, is defined by

$$c = \sqrt{\frac{\sigma h}{\rho}} \tag{2.21}$$

Indirect integral representation for the free vibrations of a membrane

By replacing p in (2.19) by the Dirac delta function introduced in Section 2.1.1, the equation satisfied by the fundamental solution of the Helmholtz equation is obtained. In this case, there are an infinity of fundamental solutions:

$$G(\mathbf{x},\mathbf{y}) = \lambda H_0^{(1)}(k\|\mathbf{x}-\mathbf{y}\|) + \zeta\overline{H_0^{(1)}(k\|\mathbf{x}-\mathbf{y}\|)}, \quad \lambda,\, \zeta \in \mathbb{C} \tag{2.22}$$

where λ and ζ are arbitrary constants independent of $\mathbf{x}$ and $\mathbf{y}$, and $H_0^{(1)}$ is the Hankel function of order 0 of the first kind (see Appendix A for definition). In order to distinguish between the solutions, the radiation condition introduced by Sommerfeld [70] is used thus:

$$\left(\frac{\partial}{\partial r} - ik\right) G(kr) = \mathcal{O}(|r|^{3/2}), \quad \text{when } r \to \infty \tag{2.23}$$

That means that only outgoing waves are present in the infinite membrane or, from the point of view of energy, that no energy is reflected by points at infinity.

The asymptotical expressions of the Hankel functions introduced in (2.22) are [4]:

$$H_0^{(1)}(z) \approx \left(\frac{2}{\pi z}\right)^{1/2} e^{+i(z-\pi/4)}, \text{ for } |z| \to \infty, \tag{2.24}$$

and

$$\overline{H_0^{(1)}(z)} \approx \left(\frac{2}{\pi \bar{z}}\right)^{1/2} e^{-i(\bar{z}-\pi/4)}, \text{ for } |z| \to \infty \tag{2.25}$$

Hence, $H_0^{(1)}(z)$ and $\overline{H_0^{(1)}(z)}$ represent *outgoing* waves and *in-going* waves respectively. Therefore, according to the Sommerfeld condition (2.23), the fundamental solution can uniquely be determined and written as [14]:

$$G(\mathbf{x},\mathbf{y};k) = \frac{1}{4} i H_0^{(1)}(k\|\mathbf{x}-\mathbf{y}\|) \tag{2.26}$$

Since there is only one boundary condition to fulfill, the transverse displacement, w, is represented by a simple-layer potential [14]:

$$w(\mathbf{x}) = \int_{\partial\Omega} \mu(\mathbf{y}) G(\mathbf{x},\mathbf{y};k)\, dC_{\mathbf{y}} \tag{2.27}$$

Numerical solution

As explained in Section 2.1.1, the boundary $\partial\Omega$ is divided into n elements Γ_j. Here, the elements are straight line segments and the n nodes $\mathbf{x}^j$ are the centre points of these segments. Hence, (2.11) can be written as:

$$\sum_{j=1}^{n} A_{ij}(k)\mu_j = 0, \quad (i = 1, \ldots, n) \tag{2.28}$$

with

$$A_{ij}(k) = \lim_{\mathbf{x}\to\mathbf{x}^i} \int_{\Gamma_j} G(\mathbf{x}, \mathbf{y}; k)\, dC_{\mathbf{y}}, \quad \mathbf{x}^i \in \Gamma_i \tag{2.29}$$

When i and j are different, $G(\mathbf{x}^i, \mathbf{y}; k)$ does not contain a singularity on Γ_j. Hence, the integral in A_{ij} can be approximated by the mid-ordinate rule for integration:

$$\int_{\Gamma_j} G(\mathbf{x}, \mathbf{y}; k)\, dC_{\mathbf{y}} \approx L_j G(\mathbf{x}, \mathbf{x}^j; k) \tag{2.30}$$

where L_j is the length of the segment Γ_j. Thus,

$$A_{ij}(k) \approx L_j G(\mathbf{x}^i, \mathbf{x}^j; k), \quad i \neq j \tag{2.31}$$

But, if i and j are equal, $G(\mathbf{x}^i, \mathbf{y}; k)$ becomes singular for $\mathbf{y} = \mathbf{x}^j$. However, according to [14], the following results can be obtained:

$$\lim_{\mathbf{x}\to\mathbf{x}_i} \int_{\Gamma_j} G(\mathbf{x}, \mathbf{y}; k)\, dC_{\mathbf{y}} = \frac{i}{2k} \int_0^{k|\Gamma_j|/2} H_0^{(1)}(\tau)\, d\tau \tag{2.32}$$

For $z \in \mathbb{C}$,

$$\int_0^z H_0^{(2)}(\tau)\, d\tau = zH_0^{(1)}(z) + \frac{\pi z}{2}\left[\mathcal{H}_0(z)H_1^{(1)}(z) - \mathcal{H}_1(z)H_0^{(1)}(z)\right] \tag{2.33}$$

where $\mathcal{H}_0$ and $\mathcal{H}_1$ are respectively the Struve functions of order 0 and 1 (see Appendix A for definition).
Hence, $A_{ii}(k)$ can be written as:

$$\begin{aligned} A_{ii}(k) &= \frac{1}{4}i|\Gamma_i|\{H_0^{(1)}(\tfrac{1}{2}k|\Gamma_i|) + \frac{\pi}{2}[\mathcal{H}_0(\tfrac{1}{2}k|\Gamma_i|)H_1^{(1)}(\tfrac{1}{2}k|\Gamma_i|) && (2.34)\\ &- \mathcal{H}_1(\tfrac{1}{2}k|\Gamma_i|)H_0^{(1)}(\tfrac{1}{2}k|\Gamma_i|)]\} && (2.35)\end{aligned}$$

The set of equations (2.28) can be expressed in matrix form as:

$$[A(k)]\vec{\mu} = \vec{0} \tag{2.36}$$

where

$$[A(k)] = [A_{ij}(k)]_{n\times n} \tag{2.37}$$

$$\vec{\mu} = \begin{pmatrix} \mu_1 \\ \vdots \\ \mu_n \end{pmatrix} \tag{2.38}$$

From the eigenvalues k of the boundary value problem (2.19), the eigenfrequencies $\lambda = ka$, where a is a reference length dimension of the vibrating membrane, are obtained.

The necessary and sufficient condition for which (2.36) has a non-trivial solution is the well-known

$$\det[A(k)] = 0 \tag{2.39}$$

Approximate eigenfrequencies can be obtained by computing the roots of this determinant.

Numerical tests

The previous method was implemented in FORTRAN-77 on a SPARC station 2. Two techniques for solving (2.39) were investigated. In the first one, the real and the imaginary part of the determinant were solved separately. This method was first used by De Mey [57]. However, it was noticed that the roots of the real part and the imaginary part never coincided perfectly, because of the approximations introduced by the numerical procedure. Indeed, some discrepancies were found between the two roots when using this method. This problem was remarked by Kitahara [47] and he proved that the search of the local minima of the absolute value of the determinant instead of its root was preferable from a computational point of view. Therefore, the second method, which consisted in finding the minimum of:

$$\mathrm{f}(k) = |\det[A(k)]| \tag{2.40}$$

was preferred. The determinant was calculated by Croutz factorisation implemented in a NAG subroutine [64]. The minimum was determined by plotting the curve of $\mathrm{f}(k)$ using the software package MATLAB [54].

Through all this work, the dimensionless eigenfrequency parameter $\lambda = ka$, where a is a reference length, will be used when possible. However, it must be noted that all the calculations were conducted for the parameter k.

Three types of membranes were investigated: a skew membrane, a pentagonal membrane and an arbitrary quadrilateral membrane.
For the skew membrane shown in Figure 9, the eigenfrequencies $\lambda = ak$, where a the edge length of the skew membrane, were tested for various skew angle ψ and compared with the ones obtained by Durvasula [20] using the Rayleigh-Ritz method. The average relative error was 0.4% as shown in Table 1.
The eigenfrequencies k for the pentagonal membrane shown on Figure 10 were compared with the ones found by Kim [45] using the software ANSYS[1] and 1114 finite elements. Again, as shown in Table 2, the results are in perfect agreement with those reported in [45].
The last case to be examined was an arbitrary quadrilateral membrane shown in

[1] A commercial Finite Element package developed by Swanson Analysis System, Inc.

Figure 11. The results were again compared to the ones in [45] (see Table 3), and the average relative error was found to be slightly superior to the previous ones and equal to 0.72%.

2.2.2 Case of a vibrating damped membrane

Here only linear damping will be considered. The linear damping force is $\tau\,\partial v/\partial t$, proportional to the velocity. It is also known as the *viscous damping force* and τ as the coefficient of damping.

Hence, (2.13) becomes:

$$\rho\frac{\partial^2 v}{\partial t^2} + \tau\frac{\partial v}{\partial t} - \sigma h\nabla^2 v = b,\ \tau \geq 0, \tag{2.41}$$

In the steady-state regime, the following Helmholtz equation is obtained:

$$\nabla^2 w + (k^2 + ik\gamma)w = -p, \tag{2.42}$$

where p, k and w are given by (2.18), (2.20) and (2.16) respectively, and the coefficient γ is given by

$$\gamma = \frac{\tau}{\rho c} \tag{2.43}$$

where c is the velocity of the wave motion in the undamped membrane, The Dirichlet condition for this problem is again $w(\mathbf{x}) = 0,\ \mathbf{x} \in \partial\Omega$.
This Helmholtz equation (2.42) is similar to the previous one (2.13), and hence the same type of layer potential and fundamental solution can be used.

Furthermore, the radiation condition (2.23) ensures that the *evanescent* transverse wave introduced by the damping decays at infinity.

The discretization of Section 2.1.1 was adopted and a complex equation similar to (2.39) was obtained.

The effect of damping on the forced response of a square membrane will be shown in Section 2.2.3.

2.2.3 Forced response of a membrane

For boundary problems with body force, the full form of (2.7) must be considered. Because of the domain integral

$$\int_\Omega b(\mathbf{y})G(\mathbf{x},\mathbf{y})\,dS_\mathbf{y}, \tag{2.44}$$

its discretization is no longer restricted to the boundary $\partial\Omega$. The simplest way to deal with this integral is to subdivide the region Ω into a series of internal cells

Ω_e, and a numerical integration performed on each of them. In this case, for each collocation point $\mathbf{x}^i$, the domain integral (2.44) can be written as:

$$b_i = \sum_{e=1}^{K} \int_{\Omega_e} b(\mathbf{y}) G(\mathbf{x}^i, \mathbf{y})\, dS_{\mathbf{y}}, \tag{2.45}$$

where K is the total number of cells describing the domain Ω. However the subdivision of the domain into cells is cumbersome and time-consuming. Moreover, the integration over the whole domain has to performed as many times as the total number of nodes. This not only affects the efficiency of the method and but also causes the BEM to lose its main advantage which is the boundary-only formulation problem.

Hence, several methods to transform the domain integral occurring in (2.7) into its equivalent boundary form have been proposed [5, 65, 63]. They can be classified into two categories: the *particular solution* method and the *Galerkin vector* method. The former was proposed by Azevado and Brebbia [5] and used in conjunction with the DBEM. It consisted in splitting the solution u of (2.1) into a particular solution and the solution of the associated homogeneous equation:

$$u = \bar{u} + \hat{u} \tag{2.46}$$

where $\bar{u}$ is the solution of the homogeneous equation and $\hat{u}$ is a particular solution such that:

$$\mathcal{L}\hat{u} = b, \quad \text{in } \Omega \tag{2.47}$$

Then, by integrating by parts, the domain integral is reduced to an integral computed only along the boundary $\partial\Omega$, which is similar to the direct boundary formulation.

In the case where the particular solution was not known (and this occurs in the majority of cases), thus it was proposed to interpolate the body force b with some interpolation functions for which particular solutions were available and then proceed as before. This method was called the Dual Reciprocity method [65].

The latter method is related to the Galerkin technique and permits conversion of domain integrals to boundary integrals for a restricted selection of body force terms, i.e. those obeying the Laplace equation

$$\nabla^2 b = 0 \tag{2.48}$$

The transformation to the boundary is accomplished through integration by parts and the use of higher fundamental solutions derived from a recurrent relation involving the Laplace equation [63]. The Multiple Reciprocity Method, developed by Nowak and Brebbia [63], generalises this concept.

Because the previous methods can be cumbersome to implement, a new technique has been investigated. This method is based on the particular solution method. However, instead of looking for a particular solution over the domain Ω, this approach makes use of the particular solution for the *whole space* $\mathbb{R}^2$. As a result, it is relatively easy to find this type of particular solution through the use of a spatial Fourier transform. The method is described in detail in the remainder of this section.

General Theory

In the case of the membrane vibration, the transverse displacement w is expressed as:

$$w = \bar{w} + \hat{w} \tag{2.49}$$

where $\bar{w}$ is the solution of the homogeneous Helmholtz equation (2.19) and is equal to (2.27):

$$\bar{w}(\mathbf{x}) = \int_{\partial\Omega} G(\mathbf{x}, \mathbf{y}; k)\, dC_{\mathbf{y}}, \tag{2.50}$$

and $\hat{w}$ is the particular solution for an *infinite membrane*:

$$\nabla^2 \hat{w}(\mathbf{x}) + k^2 \hat{w}(\mathbf{x}) = -p(\mathbf{x}), \quad \mathbf{x} \in \mathbb{R}^2 \tag{2.51}$$

Let $\mathcal{F}$ be the spatial Fourier transform defined over $\mathbb{R}^2$ such as:

$$\mathcal{F}(\hat{w}) = \hat{W}(\boldsymbol{\nu}) = \frac{1}{2\pi} \int_{-\infty}^{\infty} \int_{-\infty}^{\infty} \hat{w}(\mathbf{x}) e^{i(x_1\nu_1 + x_2\nu_2)}\, dx_1 dx_2 \tag{2.52}$$

and,

$$\mathcal{F}(p) = P(\boldsymbol{\nu}) = \frac{1}{2\pi} \int_{-\infty}^{\infty} \int_{-\infty}^{\infty} p(\mathbf{x}) e^{i(x_1\nu_1 + x_2\nu_2)}\, dx_1 dx_2 \tag{2.53}$$

Hence, (2.51) is written as:

$$(\nu_1^2 + \nu_2^2)\hat{W}(\boldsymbol{\nu}) - k^2 \hat{W}(\boldsymbol{\nu}) = P(\boldsymbol{\nu}) \tag{2.54}$$

Alternatively, (2.54) can be rearranged to give:

$$\hat{W}(\boldsymbol{\nu}) = \frac{P(\boldsymbol{\nu})}{(\nu_1^2 + \nu_2^2) - k^2} \tag{2.55}$$

The required particular solution of (2.51) is therefore:

$$\hat{w}(\mathbf{x}) = \mathcal{F}^{-1}\left(\frac{P(\boldsymbol{\nu})}{(\nu_1^2 + \nu_2^2) - k^2}\right) \tag{2.56}$$

where $\mathcal{F}^{-1}$ is the inverse spatial Fourier transform. Substituting $\hat{w}$ in (2.19) and applying this result to all the collocation points produces the following system:

$$[A(k)]\vec{\mu} = \vec{F} \tag{2.57}$$

where $[A(k)]$ is the matrix defined in Section 2.1.1 and $\vec{F}$ is defined by:

$$\vec{F} = \begin{pmatrix} -\hat{w}(\mathbf{x}^1) \\ \vdots \\ -\hat{w}(\mathbf{x}^n) \end{pmatrix} \tag{2.58}$$

Hence, $\vec{mu}$ is uniquely determined and the transverse displacement of the membrane is easily computed.

For the sake of simplicity, this technique will be applied to a point force and to a surface force but it can easily be generalised to describe several other types of force.

Point force

A point force is defined by

$$p_{\mathbf{z}}(\mathbf{x}) = A\,\delta(\mathbf{x} - \mathbf{z}) \tag{2.59}$$

where A is the amplitude of the reduced force.
Since the particular solution for a point force is the fundamental solution of the Helmholtz equation, the following equation can also be derived from the results presented in Section 2.2 and written as:

$$w(\mathbf{x}) = \int_{\partial\Omega} \mu(\mathbf{y}) G(\mathbf{x}, \mathbf{y}) dC_y - AG(\mathbf{z}, \mathbf{x}) \tag{2.60}$$

This result can easily be obtained by replacing $b(\mathbf{x})$ by $p_{\mathbf{z}}(\mathbf{x})$ in the integral over the domain Ω.
Using this technique, it was possible to determine the point force response of an undamped and a damped square membrane shown in Figure 15. These results were obtained for $n = 56$ boundary elements, a step-size $\Delta\lambda$ equal to 0.005 and $\gamma = 0.01$. The point force was applied at the point $(0.2, 0.2)$ and the response was observed at the point $(0.5, 0.5)$. The amplitude of the reduced point force was equal to 1.

In the case of an undamped membrane, the forced response should be infinite, which is not the case here. This suggests that the numerical method has introduced a *numerical damping*, a phenomenon that will be studied later.

Surface force

A time-harmonic surface force is a plane propagating wave acting on the entire membrane. Its reduce expression is:

$$p(\mathbf{x}) = A\,e^{-i\mathbf{u}\cdot\mathbf{x}} \tag{2.61}$$

where A represents the amplitude of the exciting wave, which has the wavelength $2\pi/\sqrt{(u_1^2 + u_2^2)}$. The tangent of the direction of propagation is given by the ratio

u_1/u_2 of the wavenumber.

Hence, the spatial Fourier transform of this force is the well-known formula

$$P(\boldsymbol{\nu}) = \delta(\mathbf{u} - \boldsymbol{\nu}) \tag{2.62}$$

Substituting the above relation in (2.56) gives an equation satisfied by the particular solution $\hat{w}$, namely

$$\hat{w}(\mathbf{x}) = A\mathcal{F}^{-1}\left(\frac{\delta(\mathbf{u} - \boldsymbol{\nu})}{(\nu_1^2 + \nu_2^2 - k^2)}\right) \tag{2.63}$$

Hence, the following expression is obtained:

$$\hat{w}(\mathbf{x}) = A\frac{e^{i(u_1 x_1 + u_2 x_2)}}{u_1^2 + u_2^2 - k^2} \tag{2.64}$$

Figure 16 shows the forced response of a square membrane to a plane wave force. The wavenumbers a_1 and a_2 are both taken equal to 20 and the amplitude A is equal to 1. The number of boundary elements and the step-size of the mesh were chosen to include at least 4 points on each half sine-wave. Using this technique, the first five modes of the pentagonal membrane, shown on Figure 17, were determined.

2.2.4 Numerical damping

The presence of numerical damping was quite obvious from some of the previous results. Further tests were conducted in order to investigate it.

Using a modal expression of the transverse displacement, the relation between the magnitude of the modal participation factor Λ_1 of a square membrane of unit edge length and the damping coefficient γ was studied at the first eigenfrequency. The case of a uniform pressure load was considered and the reduced force p was taken to be unity.

It can be shown (see Appendix C) that, in that case,

$$\Lambda_1 = \frac{16p}{\pi^3\sqrt{2}\gamma} \tag{2.65}$$

Hence,

$$\frac{1}{\Lambda_1} = 2.74\gamma \tag{2.66}$$

From Figure 18, it can be seen that the linearity is preserved by the numerical application, and it is found that the slope of the numerical curve is equal to 2.71, thus the relative error is equal to 1.09%. Hence, it can be concluded that the

numerical damping has almost no effect when some physical damping is added.

In fact, it can be inferred from before that the paradoxical damping observed when plotting the force response of an undamped membrane is mainly due to the difficulty of exactly pinpointing the eigenfrequency. Indeed, if $k = k_1 + \varepsilon$, the theoretical expression of the force response of an undamped membrane will become (Appendix C) :

$$\Lambda = \frac{16p}{\pi^2\sqrt{2k_1\varepsilon}}. \tag{2.67}$$

Hence, even small values of ε will greatly decrease the value of the amplitude of the transverse displacement.

2.3 Application of the IBEM to a plate

In this section, the free vibration of an undamped plate will be studied. It was not the purpose of this work to carry out an exhaustive study of the application of the IBEM to a plate; an excellent monograph by [47] has already been published on this subject. However, this section will highlight the particularities of the application of the IBEM to a free vibrating plate.

After showing the governing equations for the plate vibration, the fundamental solution along with the plate potentials will be given. The boundary integral formulation will then be applied to the case of clamped plates.

2.3.1 Governing equation of thin plates

In what follows, the small deflection plate theory will be applied. This theory is based on the Kirchoff and Love assumptions as stated by Szilard [72]:

1. The material of the plate is elastic, homogeneous, and isotropic.
2. The plate is initially flat.
3. The thickness of the plate is small compared to its other dimensions. The smallest dimension of the plate is at least ten times larger than its thickness.
4. The deflections are small compared to the plate thickness, i.e. the maximum deflection is less than one fiftieth of the small span length.
5. The slopes of the deflected middle surface are small compared to unity.
6. The deformations are such that straight lines, initially normal to the middle surface, remain straight lines normal to the middle surface.
7. The deflection of the plate is produced by displacement of points of the middle surface normal to its initial plane.

8. The stresses normal to the middle surface are of negligible order of magnitude.

Under these assumptions, the following governing equation of vibration is derived:

$$\nabla^4 v + \frac{\rho h}{D}\frac{\partial^2 v}{\partial t^2} = \frac{b}{D}, \tag{2.68}$$

where v is the lateral displacement, b is the load per unit area, ρ is the density per unit area, h is the thickness and D is the flexural rigidity of the plate and is equal to

$$D = \frac{Eh^3}{12(1-\nu^2)}, \tag{2.69}$$

where E denotes the Young's modulus and ν is the the Poisson's ratio.

In the steady-state domain, assuming the notations introduced in Section 2.2.1, (2.68) becomes:

$$\nabla^4 w(\mathbf{x}) - k^4 w(\mathbf{x}) = p(\mathbf{x}), \quad \forall \mathbf{x} \in \Omega \tag{2.70}$$

where k satisfies:

$$k^4 = \frac{\omega^2 \rho h}{D} \tag{2.71}$$

and,

$$p(\mathbf{x}) = \frac{q(\mathbf{x})}{D} \tag{2.72}$$

In order to define the different boundary conditions, let $\mathbf{n}$, $\mathbf{s}$, and s be the unit outward normal vector to $\partial\Omega$, the counterclockwise unit tangential vector and the arc length parameter along $\partial\Omega$ respectively. Unless stated otherwise, the boundary conditions are derived for straight segments, i.e. the radius of curvature of the boundary curve is infinite.

The boundary conditions may be prescribed as deflection, slope, bending moment and equivalent shear force, thus [56]

$$w \tag{2.73}$$

$$\partial_{\mathbf{n}} w \tag{2.74}$$

$$M_n w = \Delta w - (1-\nu)\partial_{\mathbf{s}} w \tag{2.75}$$

$$V_n w = \partial_{\mathbf{n}} \Delta w + (1-\nu)\partial_{\mathbf{s}} \left(\frac{\partial^2 w}{\partial \mathbf{n} \partial \mathbf{s}} \right) \tag{2.76}$$

where the moment and the equivalent shear M_n and V_n are so defined as multiplying the ones usually defined by $-1/D$. Using the notations introduced in Section 2.1.1, the homogeneous boundary conditions are expressed as the combination of these quantities as follows:

$$B_i(w)(\mathbf{x}) = 0, \quad (i = 1, 2) \ \ \forall \mathbf{x} \in \partial\Omega \tag{2.77}$$

Here, $B_i\,(i=1,2)$ have the following meanings: combinations of (2.73) and (2.74), (2.73) and (2.75), (2.75) and (2.76) and (2.74) and (2.76) mean the clamped, simply supported, free and sliding-clamp boundary conditions, respectively. The last boundary condition is rarely seen but will be used later, and brief description of it can be obtained in [14].

2.3.2 Integral equation for a clamped plate

The fundamental solution of (2.70) is [82, 47, 62]:

$$G(\mathbf{x},\mathbf{y};k)=-\frac{i}{8k^2}\left[H_0^1(ik\|\mathbf{x}-\mathbf{y}\|)-H_0^1(k\|\mathbf{x}-\mathbf{y}\|)\right]. \tag{2.78}$$

with the notations previously introduced.

It can be easily shown that this fundamental solution satisfies the Sommerfeld condition (2.23) which ensures its uniqueness.

Noting that the boundary conditions enforce two conditions on $\partial\Omega$, the lateral displacement w can be represented as the sum of two layer potentials, of order zero and one [62]:

$$w(\mathbf{x})=\int_{\partial\Omega}G(\mathbf{x},\mathbf{y};k)\mu_0(\mathbf{y})\,dC_{\mathbf{y}}-\int_{\partial\Omega}\partial_{\mathbf{n_y}}G(\mathbf{x},\mathbf{y};k)\mu_1(\mathbf{y})\,dC_{\mathbf{y}},\ \forall\mathbf{x}\in\Omega \tag{2.79}$$

As stated previously, the potentials may become discontinuous on the boundary $\partial\Omega$. However, in the case of a clamped plate, no jump conditions are introduced [81] and the integrals are convergent. Hence, the following system is derived from (2.8):

$$\left\{\begin{array}{l}\lim\limits_{\mathbf{x}\to\mathbf{X}}\int_{\partial\Omega}G(\mathbf{x},\mathbf{y};k)\mu_0(\mathbf{y})\,dC_{\mathbf{y}}-\int_{\partial\Omega}\partial_{\mathbf{n_y}}G(\mathbf{x},\mathbf{y};k)\mu_1(\mathbf{y})\,dC_{\mathbf{y}}=0\\ \qquad\qquad\qquad\qquad\qquad\qquad\qquad\qquad\qquad\qquad\qquad\qquad\forall\mathbf{X}\in\partial\Omega\\ \lim\limits_{\mathbf{x}\to\mathbf{X}}\partial_{\mathbf{n_x}}\left[\int_{\partial\Omega}G(\mathbf{x},\mathbf{y};k)\mu_0(\mathbf{y})\,dC_{\mathbf{y}}-\int_{\partial\Omega}\partial_{\mathbf{n_y}}G(\mathbf{x},\mathbf{y};k)\mu_1(\mathbf{y})\,dC_{\mathbf{y}}\right]=0\end{array}\right. \tag{2.80}$$

2.3.3 Numerical Procedures

Using the collocation method introduced in Section 2.1.1, the following linear system is obtained for a clamped plate:

$$\left.\begin{array}{l}\sum\limits_{j=1}^{n}A_{ij}^{01}(k)\mu_0^j+\sum\limits_{j=1}^{n}A_{ij}^{11}(k)\mu_1^j=0\\ \sum\limits_{j=1}^{n}A_{ij}^{02}(k)\mu_0^j+\sum\limits_{j=1}^{n}A_{ij}^{12}(k)\mu_1^j=0\end{array}\right\}\ (i=1,\ldots,n) \tag{2.81}$$

with

$$A_{ij}^{01} = \lim_{\mathbf{x}\to\mathbf{x}^i} \int_{\Gamma_j} G(\mathbf{x},\mathbf{y};k)\, dC_{\mathbf{y}}, \tag{2.82}$$

$$A_{ij}^{11} = \lim_{\mathbf{x}\to\mathbf{x}^i} \int_{\Gamma_j} G(\mathbf{x},\mathbf{y};k)(-\frac{\partial\zeta}{\partial\mathbf{n}_{\mathbf{y}}})\, dC_{\mathbf{y}}, \tag{2.83}$$

$$A_{ij}^{02} = \lim_{\mathbf{x}\to\mathbf{x}^i} \int_{\Gamma_j} G'(\mathbf{x},\mathbf{y};k)(\frac{\partial\zeta}{\partial\mathbf{n}_{\mathbf{x}}})\, dC_{\mathbf{x}}, \tag{2.84}$$

$$A_{ij}^{12} = \lim_{\mathbf{x}\to\mathbf{x}^i} \int_{\Gamma_j} \left[G''(\mathbf{x},\mathbf{y};k) - \frac{1}{\zeta}G'(\mathbf{x},\mathbf{y};k)(\frac{\partial\zeta}{\partial\mathbf{n}_{\mathbf{x}}})(-\frac{\partial\zeta}{\partial\mathbf{n}_{\mathbf{y}}}) + \frac{1}{\zeta}G'(\mathbf{x},\mathbf{y};k)(\mathbf{n}_{\mathbf{y}}\cdot\mathbf{n}_{\mathbf{x}})\right] dC_{\mathbf{x}} \tag{2.85}$$

where $\zeta = \|\mathbf{x}-\mathbf{y}\|$ In these expressions, the prime indicates the differentiation with respect to the argument; $\partial r/\partial\mathbf{n}_{\mathbf{x}}$ and $\partial r/\partial\mathbf{n}_{\mathbf{y}}$ mean the differentiation with respect to the outward normal direction on the points $\mathbf{x}$ and $\mathbf{y}$ respectively of $\|\mathbf{x}-\mathbf{y}\|$.
The expressions of the derivatives of G can be found in the book by Kitahara [47].

In the case in which i and j elements do not coincide with each other, the approximation of Section 2.2.1 is used. For the case $i = j$, the Bessel functions included in the fundamental solution G are approximated at a point $\mathbf{y}$ by the series expansion up to the appropriate power of $\|\mathbf{x}-\mathbf{y}\|$, these series are then integrated term on the segment Γ_j under consideration and differentiated at an interior point of $\mathbf{x} \in \Gamma_j$ up to the required order, and, finally, the limit $\mathbf{x} \to \mathbf{x}^i$ is taken. The resulting formulae can be found in [47, 81].

2.3.4 Numerical results

The present method was applied to a clamped square plate and a clamped skew plate with a skew angle $\psi = 45°$. Table 5 and Table 4 show the different eigenfrequencies $\lambda = ka$, with a being equal to the edge length as shown in Figure 9, along with the results obtained by Bardell [6] who used the Hierarchical Finite Element Method. Figure 19 shows the general trend of the logarithm of the absolute value of the determinant for the square clamped plate.
A brief inspection of the absolute relative errors in Table 5 and Table 4 shows that, although the relative errors are well within 1%, the accuracy of the results begins to deteriorate for higher eigenfrequencies.

2.4 Conclusion

In this chapter, the Indirect Boundary Element Method has been presented. This method was then applied to the vibration analysis of different types of membranes and of clamped plates. Furthermore, a new and simple method for determining the forced response of such structures was introduced. Through this method, the modes and the forced response of a damped and undamped membrane of arbitrary

shape was determined. This method can easily be extended to the case of a plate as it will be shown in Chapter 4.

However, the purpose of this chapter was not only to introduce some techniques which will be used later in this work, but also to specify some of the drawbacks of the Indirect Boundary Element Method.

The construction and the use of a fundamental solution can become very tedious. Indeed, even for the simple case of the clamped plate, the treatment of the singularity required some lengthy calculations. Moreover, it has been remarked in the work of Kitahara [47] that the IBEM is not efficient for mixed boundary conditions.

3. The EIBEM and other related Trefftz methods

In this chapter a derived version of the IBEM, called the Exterior Indirect Boundary Element Method or EIBEM, will be presented. This method was pioneered by Kupradze [48], and was shown to be part of the family of Trefftz methods [32]. Hence, the Trefftz method will also be introduced.

However, far from being a detailed presentation of the EIBEM and of the Trefftz methodology, the objective of this chapter is to highlight some particularities of these methods by some simple examples. Hence, the EIBEM will be applied to the vibrations of simple membranes.

3.1 The Exterior Indirect Boundary Element Method (EIBEM)

3.1.1 Principle

As has been seen in Chapter 2, one of the major drawback of the IBEM, and the boundary element methods in general, is the use of singular fundamental solutions. Indeed, since the fundamental solutions are dependent upon the inverse of the distance between field and source points, the integrals become singular when the location of the field and source points coincide. In the EIBEM, such problems are eliminated by moving the source points to a position outside the field boundary. In this work, this method is studied by applying it to the vibration of clamped membranes. In Section 2.2, the transverse displacement w of a membrane was expressed by the following integral equation:

$$w(\mathbf{x}) = \int_{\partial\Omega} \mu(\mathbf{y}) G(\mathbf{x}, \mathbf{y}; k)\, dC_{\mathbf{y}}, \tag{3.1}$$

where G is the fundamental solution, $\mathbf{x}$ is the load point, $\mathbf{y}$ are the source points and $\mu(\mathbf{y})$ is the source density of point $\mathbf{y}$.
In the EIBEM, the source points $\mathbf{y}$ are moved to an imaginary source boundary Θ enclosing the physical boundary $\partial\Omega$ of the problem as shown on Figure 2.
Hence, (3.1) is rewritten as

$$w(\mathbf{x}) = \int_{\Theta} \mu(\mathbf{y}) G(\mathbf{x}, \mathbf{y}; k)\, dC_{\mathbf{y}}, \quad \forall \mathbf{x} \in \overline{\Omega} = \Omega \cup \partial\Omega, \tag{3.2}$$

Obviously, the integral in (3.2) is no longer singular.
By applying the boundary condition for a clamped membrane, the source density μ can be determined by:

$$\int_{\Theta} \mu(\mathbf{y}) G(\mathbf{X}, \mathbf{y}; k)\, dC_{\mathbf{y}} = 0, \quad \forall \mathbf{X} \in \partial\Omega \tag{3.3}$$

3.1.2 Numerical analysis

The equation (3.3) is treated numerically in a way similar to the one presented in Section 2.1.1. Hence, the boundary which holds the source points, here Θ, is discretized in n elements Θ_j and an equation similar to 2.10 is obtained. To solve this equation, the collocation scheme is applied at n nodal points $\mathbf{x}^j$ chosen on $\partial\Omega$. Hence, an equation similar to (2.28) is deduced

$$\sum_{j=1}^{n} A'_{ij}(k)\mu_j = 0, \quad (i = 1, \ldots, n) \tag{3.4}$$

with

$$A'_{ij}(k) = \int_{\Theta_j} G(\mathbf{x}^i, \mathbf{y}; k)\, dC_{\mathbf{y}} \tag{3.5}$$

Furthermore, the Θ_j will be taken as straight segments and $A'_{ij}(k)$ will be approximated by the mid-ordinate rule of integration, hence

$$A'_{ij}(k) \approx L_j G(\mathbf{x}^i, \mathbf{y}^j; k) \tag{3.6}$$

with $\mathbf{y}_j$ the mid-point of segment Θ_j and L_j is the length of the element Γ_j. Thus, (3.4) can be expressed in matrix form as:

$$[A'(k)]\vec{\mu} = \vec{0} \tag{3.7}$$

where

$$[A'(k)] = \left[A'_{ij}(k)\right]_{n\times n}$$

$$\vec{\mu} = \begin{pmatrix} \mu_1 \\ \vdots \\ \mu_n \end{pmatrix} \tag{3.8}$$

Therefore, it can be seen that the EIBEM greatly simplifies the numerical calculation by avoiding singularities in the fundamental solution. However, two new parameters are introduced: the shape of the exterior boundary Θ and its distance from the physical boundary. As it was remarked by [89] and as it will be seen in the next section, these free parameters influence the convergence of the solutions and determine the effectiveness of the method.

3.1.3 Application to a membrane

When using the EIBEM, it has been common [24, 89, 36, 67] to assess the effects of the shape of the exterior boundary and its distance from the real one upon the accuracy of the solution. These effects can be classified into two categories depending on the values computed. The first category concerns the effects of these parameters upon the determination of the eigenfrequencies. The second category includes their effects upon the forced response of the membrane, thus the determination of the mode shapes.

The Condition number and its influence upon the force response

In the present case, the forced response is determine by the technique presented in Section 2.2.3. Hence, a linear system similar to one previously seen can be deduced:

$$[A'(k)]\vec{\mu} = \vec{F} \tag{3.9}$$

where $[A'(k)]$ is the matrix defined in previously and $\vec{F}$ is the defined by:

$$\vec{F} = \begin{pmatrix} -\hat{w}(\mathbf{x}^1) \\ \vdots \\ -\hat{w}(\mathbf{x}^n) \end{pmatrix} \tag{3.10}$$

where $\hat{w}$ is a particular solution of the problem.

To measure the sensitivity of such system which respect to changes in the matrix $[A'(k)]$ and the right-hand side $\vec{F}$, it is usual to use a criterion based on the *condition number with respect to inversion* [86]. It must be noted that the use of such a criterion is frequently encountered in works on the EIBEM [24, 89, 36, 67].
Usually, the condition number of the matrix $[B]_{n\times n}$ is defined by [86]:

$$c([B]) = \|[B]\|_2 \, \|[B]^{-1}\|_2 \tag{3.11}$$

with $\|\cdot\|_2$ is the 2-norm defined in Appendix B. If $c([B])$ is large, then $[B]$ is said to be *ill-conditioned*, i.e. the linear system is very sensitive to small changes. Although $c(\cdot)$ depends on the underlying norm, if $[B]$ is ill-conditioned in an α-norm, then $[B]$ will also be ill-conditioned in a β-norm because all the norms are equivalent on $\mathbb{R}^n$. Hence, the norm $\|\cdot\|_1$ will be chosen, because of its availability in the NAG subroutines [64]. A more detailed description of the condition number can be found in books by Wilkinson [86], Golub [26] or Stewart [71].

Study on the accuracy of the eigenfrequencies

It would be interesting to use also the condition number to evaluate the effect of the parameters upon the accuracy of the eigenfrequencies.

It has been said in Section 2.2.1, that the eigenfrequencies of the problem are the local minima of the following function of k

$$|\det[A'(k)]| \tag{3.12}$$

Unfortunately, as remarked by Golub [26], there is little correlation between $\det([B])$ and the condition number $c([B])$, thus, the condition number does not give any indication of the sensitivity of the determinant. Furthermore, even if the matrix $[A(k)]$ is ill-conditioned, i.e. nearly singular, and its determinant is

very small, e.g. the order of 10^{-120}, it might still be possible to identify accurately the local minima. This is indeed the case, as will be shown in the next section.

Therefore, it is thought that one of the criteria which can be used when studying the accuracy of the eigenfrequencies is the "smoothness" of the curve $|\det[A'(k)]|$. Indeed, if the value of the determinant reaches the machine precision, the curve will present some oscillations which will render the determination of the eigenfrequencies impossible.

Another criterion applicable here is the absolute relative error of the eigenfrequencies. However, this assumes that the accurate values for the problem are known, which is rarely the case. Hence, this criterion will seldom be used.

Applications

As it will be seen later, by varying the two parameters, i.e. the shape of the exterior boundary and its distance from the physical one, it is possible to increase the condition number of the matrix. Hence, in order to show the effect of the condition number of the matrix $[A'(k)]$, the forced response at an arbitrary point of a clamped square membrane to a plane wave travelling in the direction $(-10.0, -10.0)$ was determined for two different values of $\mathrm{c}([A'(k)])$. Figure 20 (a) and on Figure 20 (b) show the real part of the forced response of such a membrane. In the case of Figure 20 (a), the condition number is the order of 10^1. Figure 20 (b) was obtained for a condition number $c([A'(k)]) \approx 10^9$. A simple look at Figure 20 (b) shows that this latter response is incorrect on account of the high condition number. However, by plotting the determinant of the same ill-conditioned matrix, it was found that the first two eigenfrequencies were not only easy to distinguish but also accurate as it may be seen on Figure 21, thus confirming what has been said in the previous section.

The two parameters which are thought to affect the condition number were then studied. First, the relation between the condition number and the distance between the two boundaries, δ, was examined, with regard to a square membrane and an homothetic exterior boundary Θ as shown on Figure 3. Figure 22 shows the results of the analysis for δ in the range $[0.001, 1.000]$ and for two different values of the eigenfrequency λ. From this figure, it is possible to conclude that having the sources too far away from the boundary $\partial\Omega$ will destroy the linear independence in the matrix $[A'(k)]$ and increase its condition number. It may also be remarked that for a given δ, the condition number is lower for a higher value of k.

The influence of the distance δ upon the accuracy of the eigenfrequencies was then investigated. Using again an homothetic exterior boundary, the first and the sixth eigenfrequencies λ of a circular membrane were determined for different values of δ and compared with the theoretical values found in Zhou [14]. The absolute relative error is shown on Figure 23. It can be seen from this figure that when the imaginary boundary is too close to real boundary, the singular nature

of the fundamental solution necessitates special treatment of integration in the neighbourhood of the source points so as to ensure the accuracy of the results. Since the EIBEM was used to avoid such case, it is necessary to locate the exterior boundary further away from the real boundary.

Hence, from the previous examples, it may be concluded that if the exterior boundary is too far away from the real boundary, the forced response of the membrane will be misleading, and if it is too close to the real boundary, the eigenfrequencies will be inaccurate. Therefore, a region must be sought between the two extremes which yields a stable solution. For example, in the case of the square plate, such a region is obtained for $\delta \in [0.09, 0.18]$.

The influence of the shape of the boundary upon the condition number was then examined. It was chosen to evaluate the condition number of the matrix for a square membrane and for an exterior boundary of circular shape as shown on Figure 4 (a) and (b). Two methods to locate the collocation points $\mathbf{x}^j$ on the real boundary were investigated: Method (a) (see Figure 4 (a)), an homothetic collocation of the load points on $\partial\Omega$; Method (b) (see Figure 4 (b)), an equidistant collocation of the load points on $\partial\Omega$.

The condition number was then plotted for different values of the radius R of a circular exterior boundary and for $\lambda = 4.0$. The results are shown on Figure 24. When comparing Figure 24 and Figure 22, it is obvious that the shape of the exterior boundary influences the condition number. Furthermore, from Figure 24 it may be inferred that the way of fitting the collocation points (equidistant or homothetic collocation) also influences the condition number. Such phenomenon has already been noticed by Zieliński [90] for Laplace's equation $\nabla^2 w = 0$. In Table 6, the absolute relative errors of the first seven frequencies of this square plate is determined for the two different shapes of exterior boundary Θ along with the results obtained by using an homothetic exterior boundary Θ. The results are compared with the theoretical values and the absolute relative error is indicated in parenthesis next to each value. As can be seen, using the circular exterior boundary together with the homothetic collocation gives the best results. Note that this type of collocation was seen to have the highest condition number, thus confirming that the matrix may be ill-conditioned but still yields accurate results.

3.2 The Trefftz methodology

In section 3.1.2, by applying a discretization of the boundary along with the mid-ordinate rule of integration, the following equation was obtained

$$w(\mathbf{x}) = \sum_{j=1}^{n} G(\mathbf{x}, \mathbf{y}^j; k)\mu_j, \quad \forall \mathbf{x} \in \overline{\Omega}, \quad \mathbf{y}^j \in \Theta \tag{3.13}$$

This equation was then applied to the collocation points $\mathbf{x}^i$ on the boundary $\partial\Omega$ to determine the values of the source density.
The representation of w in the EIBEM (3.13), is very similar to the one obtained by another method known as the Trefftz method.

In this section, the indirect formulation of this method will be presented. The aim of this presentation is to highlight the close links between the existing indirect boundary methods such as the IBEM, and more precisely the EIBEM, and the new method which has been developed in this work and which will presented in the next chapter.

3.2.1 Principle

In the indirect formulation Trefftz method, the solution of the problem is approximated by the superposition of the functions satisfying the governing equation in the domain Ω (including its boundary $\partial\Omega$), and the unknown parameters are determined so that the approximate solution satisfies the boundary conditions by means of the collocation or other weighted residual methods. Hence, in the case of the membrane, the transverse displacement at an arbitrary point $\mathbf{x}$ will be written as:

$$w(\mathbf{x}) = a_1 w_1^* + a_2 w_2^* + \ldots + a_n w_n^* \tag{3.14}$$

where the w_j^* satisfies exactly the Helmholtz equation in the domain Ω and the a_j are the unknown parameters.
Hence, if the functions w_j^* are taken equal to the fundamental solutions appearing in the discretized formulation of the EIBEM of (3.13)

$$w_j^* = G(\mathbf{x}, \mathbf{y}^j; k), \quad \mathbf{y}^j \in \Theta \tag{3.15}$$

and if the unknown parameters a_j are considered to be the unknown source densities μ_j, it is obvious that the discretized EIBEM represents an indirect Trefftz formulation. Indeed, the n fundamental solutions $G(\mathbf{x}, \mathbf{y}^j; k)$ satisfy exactly the Helmholtz equation in Ω since the source points are placed on the imaginary boundary Θ surrounding Ω. Because of the similarities between these two formulation, the EIBEM was given the name of modified Trefftz method by Patterson *et al.* [66].

When using a system of solutions to treat differential equations, a major requirement is that the system be complete. The most direct criterion of completeness for such systems is completeness with respect to the metric of the space in which the differential operator is defined. For application to boundary value problems, this must be related to the metric of suitable spaces of boundary values. A criterion of completeness possessing these properties was proposed by Herrera [32] and was called c-completeness or *T-completeness*. The system of functions which satisfy the T-completeness are called *T-functions*. The same author has also shown that under general conditions a system which is T-complete for a region has this property for

any region which contains the first one. However, it is outside the scope of this work to present the T-completeness criterion and its algebraic formulation, and reference should be made to the book by Herrera [32]. It must be noted that the highly abstract mathematical formulation of this criterion renders it difficult to use.

3.2.2 Application of the Trefftz method to the membrane

As has been seen earlier, the system of fundamental solutions used in the discrete EIBEM can be used as a system of solutions in the Trefftz methodology. The proof of its completeness was given by Kupradze [48]. Herrera [32] presented another version of the proof by using the T-completeness. It is worth noting that a set of T-functions for a particular problem are not necessarily unique. Hence, in the case of the reduced Helmholtz equation ($\nabla^2 w + w = 0$), another set of T-functions was derived by Herrera [33], who applied the separation of variables in a unit circle and obtained the following T-complete system

$$\begin{cases} J_j(r)\cos j\theta, \\ J_{j+1}(r)\sin j\theta \end{cases} \tag{3.16}$$

Such system can easily be extended to the standard Helmholtz equation [15].

3.2.3 Application to a plate

In the case of a vibrating plate and its related boundary value problem, no work can be found on T-complete systems. However, by using the separation of variables in the unit circle, which is considered to be a powerful procedure for obtaining systems of functions which are T-complete in arbitrary regions by Herrera [32], it is possible to obtain the following classical system of functions which satisfy the equations of motion of a plate in polar co-ordinates:

$$\begin{cases} J_j(kr)\cos j\theta \\ J_{j+1}(kr)\sin(j+1)\theta \\ I_j(kr)\cos j\theta \\ I_{j+1}(kr)\sin(j+1)\theta \end{cases} \tag{3.17}$$

These functions will be called *Heuristic T-functions*. The terminology was first used by Zieliński [89] to characterise the functions which fulfill the governing differential equations, but the T-completeness of which is not proved.

3.3 Conclusion

In this chapter, the Trefftz method, along with one of its application, the EIBEM or modified Trefftz method, has been presented. Some applications of the EIBEM to the vibration of membranes were presented, and it was found that this method was simpler to implement and more efficient than the IBEM (a comparison of the CPU

execution time is given in Chapter 4). However, it was remarked that the additional parameters introduced, such as the distance between the two boundaries, the shape of the imaginary boundary, and the location of the load points, could influence the accuracy of the solutions. Therefore, as it was remarked by Zieliński [89], the EIBEM cannot be applied directly without earlier numerical tests, and that such optimisation can result in final higher computational costs than the IBEM. The link between the Trefftz method and the EIBEM was then described, and a brief presentation of the general indirect Trefftz method was given.

Two sets of functions which satisfied the Helmholtz equation and the dynamic equation of the plate were given. In the case of the Helmholtz equation, the system of functions was said to be T-complete, i.e. to represent completely the transverse displacement in a vibrating membrane regardless of its shape. However, in the case of the plate, the system was not found to possess such a property, and the functions were considered to be heuristic T-function.
As mentioned earlier, such systems are not unique, and the in next chapter, two new simpler systems of such functions will be derived.

4. The Plane Wave Basis Method (PWBM)

4.1 Principle

In this section, a method to represent the general solutions of the membrane equation and of the plate equation as a linear combination of plane waves which have the same wave number and travel in different directions will be presented. Since this technique, called the Plane Wave Basis Method or PWBM, can either be viewed as a version of the classical Trefftz method or as an extension of the EIBEM, the two ways to formulate it will be presented for the membrane equation. The case of the plate equation will then be straightforward to derive from the results for the Helmholtz equation.
In all the following, the domain Ω occupied by the membrane or the plate will be considered as a *bounded* and *simply connected region.* Therefore, ring-shaped domains and deeply concave domains will be excluded.

4.1.1 Plane waves basis for a membrane

It was shown in Section 3.2.2 that the transverse displacement w of a membrane at $\mathbf{x}$ can be expressed by the system of T-complete functions:

$$\begin{cases} J_j(kr)\cos j\theta \\ J_{j+1}(kr)\sin j\theta \end{cases} \tag{4.1}$$

where r, θ are the polar co-ordinates of $\mathbf{x}$ and k is wave number introduced in Chapter 2.
Using this property, the following proposition can be stated [32]:

> Let $\{\mathbf{e}_1, \mathbf{e}_2, \ldots\}$ be a system of unit vectors in $\mathbb{R}^2$, which is dense in the unit circle. Then the system
>
> $$\mathcal{B}_m = \{e^{-ik\mathbf{e}_1\cdot\mathbf{x}},\ e^{-ik\mathbf{e}_2\cdot\mathbf{x}}, \ldots\} \tag{4.2}$$
>
> of plane waves which propagate in the directions $\mathbf{e}_1, \mathbf{e}_2, \ldots$, is T-complete for the Helmholtz equation.

A complete proof of this statement can be found in the work by Herrera [32, 33].
By writing

$$\mathbf{e}_\alpha = \begin{pmatrix} \cos\xi_\alpha \\ \sin\xi_\alpha \end{pmatrix}, \alpha = 1, 2, \ldots$$

where the sequence of angles $\{\xi_1, \xi_2, \ldots\}$ is dense in the interval $[-\pi, \pi[$, the following system of functions can be derived

$$\mathcal{B}'_m = \{u_{\xi_1}, u_{\xi_2}, \ldots\} \quad \text{with } u_{\xi_i}(\mathbf{x}) = e^{ikr\cos(\xi_i - \theta)}$$

This system is equivalent to the system $\mathcal{B}_m$. Hence, the general expression of the solution w of the Helmholtz equation can be written [78]:

$$w(\mathbf{x}) = \int_{-\pi}^{\pi} D(\xi) e^{-ikr\cos(\xi-\theta)}\, d\xi, \tag{4.3}$$

Or, in the Cartesian co-ordinates system,

$$w(\mathbf{x}) = \int_{-\pi}^{\pi} D(\xi) e^{-ik(x_1\cos\xi + x_2\sin\xi)}\, d\xi, \tag{4.4}$$

where $D(\xi)$ is the amplitude of the plane wave travelling in the ξ-direction.

The plane waves can also be regarded as an approximation of the circular wave emitted from a very far point source. Indeed, from the EIBEM formulation (see Section 3.1), w can be expressed as:

$$w(\mathbf{x}) = \int_{\Theta} \mu(\mathbf{y}) G(\mathbf{x}, \mathbf{y}; k)\, dC_{\mathbf{y}} \tag{4.5}$$

where μ is the source density and Θ is the exterior boundary. Since, the exterior boundary can have any shape [89], let Θ be a circle of radius R. Furthermore, when R tends to infinity, the asymptotical form of the Hankel function of first order is found to be:

$$H_0^{(1)}(k\zeta) \approx \left(\frac{2}{\pi k\zeta}\right)^{1/2} e^{+i(k\zeta-\pi/4)}, \quad \text{for } \zeta \to \infty \quad \text{where } \zeta = \|\mathbf{x}-\mathbf{y}\| \tag{4.6}$$

Hence, if $\mathbf{x} = (r, \theta)$ and $\mathbf{y} = (R, \xi)$, (4.5) can be rewritten as:

$$w(\mathbf{x}) \approx \int_{-\pi}^{\pi} \left\{ \mu(R,\xi) \left(\frac{2}{\pi kR}\right)^{1/2} e^{+i(kR-\pi/4)} \right\} e^{-ikr\cos(\xi-\theta)}\, d\xi, \tag{4.7}$$

where

$$\zeta = R - r\cos(\xi-\theta) + \mathcal{O}(1/R), \quad \text{when } R \gg r$$

and it is now obvious that (4.7) is equivalent to (4.3).

4.1.2 Plane wave basis for a plate

As remarked by Manolis and Beskos [52], the question of T-completeness is still not settled. However, by using the following heuristic T-functions, seen in Section 3.2.3:

$$\begin{cases} J_j(kr)\cos j\theta \\ J_{j+1}(kr)\sin(j+1)\theta \\ I_j(kr)\cos j\theta \\ I_{j+1}(kr)\sin(j+1)\theta \end{cases} \tag{4.8}$$

a new T-heuristic system of propagating and evanescent plane waves can be obtained (see Appendix D for its derivation):

$$\mathcal{B}'_p = \{(u_{\xi_1}, v_{\xi_1}), (u_{\xi_2}, v_{\xi_2}), \ldots\} \quad \text{with } u_{\xi_i}(\mathbf{x}) = e^{-ikr\cos(\xi_i - \theta)} \\ \text{and } v_{\xi_i}(\mathbf{x}) = e^{kr\cos(\xi_i - \theta)}$$

where the sequence of angles $\{\xi_1, \xi_2, \ldots\}$ is dense in the interval $[-\pi, \pi[$, u_{ξ_i} and v_{ξ_i} represent the propagating and the evenascent waves respectively travelling in the direction ξ_i.
As before, the transverse displacement w can be written as:

$$w(\mathbf{x}) = \int_{-\pi}^{\pi} D^1(\xi) e^{-ikr\cos(\xi-\theta)}\, d\xi + \int_{-\pi}^{\pi} D^2(\xi) e^{kr\cos(\xi-\theta)}\, d\xi \tag{4.9}$$

where $D^1(\xi)$ and $D^2(\xi)$ are the amplitudes of the propagating wave and evanescent wave travelling in the ξ-direction respectively.
In Cartesian co-ordinates, (4.9) becomes

$$w(\mathbf{x}) = \int_{-\pi}^{\pi} D^1(\xi) e^{-ik(x_1\cos\xi + x_2\sin\xi)}\, d\xi + \int_{-\pi}^{\pi} D^2(\xi) e^{k(x_1\cos\xi + x_2\sin\xi)}\, d\xi \tag{4.10}$$

4.1.3 Numerical analysis

Cartesian co-ordinates will be used in what follows.
Since the PWBM is closely related to the Trefftz method, the integral equations (4.4) and (4.10) may be approximated in the same way [46], i.e., for the membrane, w may be written as:

$$w(\mathbf{x}) \approx \sum_{j=1}^{n} D_j u_{\xi_j} \quad \text{with } u_{\xi_j} \in \mathcal{B}'_m \tag{4.11}$$

For the plate, a similar expression may be obtained:

$$w(\mathbf{x}) \approx \sum_{j=1}^{n} D_j^1 u_{\xi_j} + \sum_{j=1}^{n} D_j^2 v_{\xi_j} \quad \text{with } u_{\xi_j},\, v_{\xi_j} \in \mathcal{B}'_p \tag{4.12}$$

(4.11) and (4.12) represent a discrete superposition of the plane wave travelling in the n different directions ξ_j. The set of angles $\{\xi_j\}_{j=1,\ldots,n}$ should contain the pair of waves that travel in opposite directions because no energy flow in any direction exists in any eigenvalue problems. Thus, as it was remarked by Urata [78], n must be even.
By enforcing the homogeneous boundary conditions, introduced in Chapter 2, the following expression is obtained for the membrane:

$$B(w)(\mathbf{x}) = \sum_{j=1}^{n} D_j B(u_{\xi_j})(\mathbf{x}) = 0, \quad \forall \mathbf{x} \in \partial\Omega \tag{4.13}$$

with $B(w) = w$ for the case of the clamped membrane.
And, for the plate,

$$\left.\begin{aligned} B_1(w)(\mathbf{x}) &= \sum_{j=1}^{n} D_j^1 B_1(u_{\xi_j})(\mathbf{x}) + \sum_{j=1}^{n} D_j^2 B_1(v_{\xi_j})(\mathbf{x}) = 0, \\ B_2(w)(\mathbf{x}) &= \sum_{j=1}^{n} D_j^1 B_2(u_{\xi_j})(\mathbf{x}) + \sum_{j=1}^{n} D_j^2 B_2(v_{\xi_j})(\mathbf{x}) = 0 \end{aligned}\right\} \forall \mathbf{x} \in \partial\Omega \qquad (4.14)$$

where B_1 and B_2 are the two boundary quantities used to enforce the desired boundary condition (see Chapter 2 for their definition).

The unknown parameters D_j or D_j^1 and D_j^2 are determined by the means of the collocation method presented in Section 2.1.1. However, when using the plane wave functions, there are several ways to chose the collocation points $\{\mathbf{x}^j\}_{j=1,\ldots,n}$, at which the equations (4.13) or (4.14) are enforced.
In this work, two types of collocation scheme have been investigated:
Method (a): ξ_j and $\mathbf{x}^i$ are defined by (see Figure 5 (a)):

$$\left.\begin{aligned} \xi_j &= \frac{2\pi(j-1)}{n}, \\ \widehat{(\mathbf{x}^i, X_1)} &= \xi_i \end{aligned}\right\} (i, j = 1, \ldots, n)$$

It may be remarked that this method is an extension of the homothetic collocation seen in Section 3.1.3.
Method (b): ξ_j and $\mathbf{x}^i$ are defined by (see Figure 5 (b)):

$$\left.\begin{aligned} \xi_j &= \frac{2\pi(j-1)}{n}, \\ \mathbf{x}^i &= \frac{iL}{n} \end{aligned}\right\} (i, j = 1, \ldots, n)$$

where L is the length of $\partial\Omega$.
Note that this method is basically equivalent to the equidistant collocation scheme seen in Section 3.1.3.

Using the matrix expression, the following linear system is obtained:

$$[A(k)]\vec{D} = \vec{0} \qquad (4.15)$$

where, for the membrane,

$$[A(k)] = \left[\ B(u_{\xi_j})(\mathbf{x}^i)\ \right]_{n\times n}$$

and,

$$\vec{D} = \left\{ \begin{array}{c} D_1 \\ \vdots \\ D_n \end{array} \right\}_n$$

Whereas, for the plate,

$$[A(k)] = \begin{bmatrix} B_1(u_{\xi_j})(\mathbf{x}^i) & B_1(v_{\xi_j})(\mathbf{x}^i) \\ B_2(u_{\xi_j})(\mathbf{x}^i) & B_2(v_{\xi_j})(\mathbf{x}^i) \end{bmatrix}_{2n\times 2n}$$

and,

$$\vec{D} = \begin{Bmatrix} D_1^1 \\ \vdots \\ D_n^1 \\ D_1^2 \\ \vdots \\ D_n^2 \end{Bmatrix}_{2n}$$

The eigenfrequencies k of the structure are solution of the following complex equation:

$$\det\left([A(k)]\right) = 0,$$

which is solved by using the method presented in Chapter 2.

4.2 Application to a membrane

4.2.1 Numerical results

In this section, the method is applied to the vibration of various membranes. The determination of the matrix $[A(k)]$ is straightforward and the implementation of this method is simple.

The accuracy of the eigenfrequencies of a membrane is confirmed by a simple example problem such as a clamped circular membrane. Indeed, as it is shown in Table 7, the results are very accurate. However, this is due to the fact that the plane wave functions have approximated exactly the solutions of that simple benchmark, which are known to be the positive roots of $J_n(k) = 0$.

Figure 25 shows the general trend of the absolute values of the inverse of the determinant for a square clamped membrane for different values of n and for $\Delta\lambda = 0.001$. The dotted lines indicate the theoretical values of the eigenfrequencies. From this figure, it is understood that $n = 20$ is sufficient to obtain appropriate eigenfrequencies. It may seem obvious that the greater the number of plane waves, the more higher-order eigenfrequencies can be obtained - however, this is not the case on account of the increasingly singular character of the matrix $[A(k)]$, as it will be seen in Section 4.4.2.

The relative error induced by this method was compared with the one induced by the IBEM. The reference values used to compute it were found in [20] and [45]. Figure 26, Figure 27 and Figure 28 show the results for three different types of

membrane. The PWBM is not only more accurate than the IBEM, but it also needs less collocation points to reach this accuracy.

The CPU execution time of the IBEM, the EIBEM and of this method were compared for these three examples, and the results are displayed in Table 8. The latter was found to be ten times quicker than the IBEM and five times quicker than the EIBEM. Such differences are mainly due to the complex calculation of the fundamental solution used in the IBEM and in the EIBEM.

4.3 Application to a plate

In this section, the PWBM is applied to the vibration of plates with various boundary conditions, and some judicious examples will highlight the versatility of the method. The matrix $[A(k)]$ is relatively simple and the expressions of these different boundary conditions for the propagating and evanescent waves are given in Appendix E. Furthermore, all the following results were obtained with the second collocation method because of the higher accuracy obtained.

Due to the different literature source references used, all the results presented in this section are expressed through the use of nondimensional eigenvalue or eigenfrequency λ. For each case, the results from the reference are converted to the corresponding eigenfrequencies by using the relation

$$\lambda^4 = \frac{a^4 \omega^2 \rho h}{D} \tag{4.16}$$

where a is a reference length of the plate.
Almost always the number of significant figures was kept the same as it was in the original publication. In no case were significant figures added. In some few cases the number of significant figures was reduced because the accuracy of the calculations presented in this work did not justify the numbers given.

Unless stated otherwise, the Poisson's ratio ν will be equal to 0.3.

4.3.1 Case of clamped plates

In order to compare this technique with the IBEM, the sample case of a clamped square plate of edge length a was studied. The first five eigenvalues λ obtained by using both methods are shown in Table 9. The accuracy of these results was established by comparison with the work of Bardell [6] who used the hierarchical finite element method. The corresponding relative error is quoted in parentheses next to the current results; three-figure agreement is obtained for all the modes when using the PWBM, while the relative error committed using the IBEM averages 0.46%. Furthermore, the CPU execution time was found to be equal to 1110 s with the PWBM and to 5103 s with the IBEM.

This method was then applied to a fully clamped symmetrical trapezoidal plate shown on Figure 12. The aspect ratios b/a and c/a are equal to 0.8 and 0.75 respectively. The eigenvalues λ for the this plate are classified into mode shapes, being correspondingly indicated by $\lambda_{\alpha\beta}$, in which α and β give the number of anti-nodes in the horizontal and vertical directions respectively. In addition, the numerical values were compared with the experimental ones obtained by Maruyama *et al.* [53] as shown in Table 10. In their investigation, the authors of this reference used the real time technique of time averaged holographic interferometry to determine the natural frequencies and the corresponding mode shapes for the transverse vibrations of clamped trapezoidal plates. A simple look at Table 10 shows a good agreement between the numerical results and the experimental results of the reference [53]. Indeed, the absolute relative error is at most 1.61% and that the average error is 0.70%.

Using the force response technique presented in Chapter 2 and the contour plot capabilities of the software MATLAB [54], the first eight mode shapes of this trapezoidal plate were obtained. As Figure 29 shows, they agree well with the experimental in [53].

4.3.2 Case of simply supported plates

Two different fully simply supported plates have been examined. The first plate is a skew plate of skew angle $\psi = 30°$ shown on Figure 9. The first five eigenvalues λ of it are shown in Table 11. Once again, excellent agreement is observed with the work of Bardell [6]. Several other skew angle were tested and it was found that the eigenvalues were reliable enough for skew angles up to 75°.

The second type of plates tested was a simply supported elliptical plate of aspect ratio $a/b = 2.0$ shown on Figure 13. The eigenfrequencies λ for this plate are given in Table 12, together with the results obtained by Lam *et al.* [49], who used a new set of orthogonal plate functions as the admissible functions in the Rayleigh-Ritz approach. As the relative error shows, the agreement between the results is quite good.

By determining the eigenvector for each eigenfrequency, it was possible to plot the mode shapes for this elliptical plate; these are presented in Figure 30. They were compared with the ones presented in [49], and although they presented the same pattern, it was found that the location of the nodes and anti-nodes differed. However, a closer inspection of the modes shown in the reference [49] reveals that they violate the boundary conditions, and hence it is thought that the present modes are more accurate.

4.3.3 Case of free and sliding-clamped plates

When applying the PWBM to a free plate in combination with any of the collocation methods presented earlier, poor results were achieved. Indeed, even for the case of a square and circular plate, none of the results showed any reasonable agreement

with other work.

The reasons for this apparent anomaly were not obvious, and initially suspicion fell on the implementation of the free boundary condition. To verify this, a square plate with sliding-clamped edge conditions was investigated. As has been seen in Chapter 2, the sliding clamped condition is obtained by prescribing the slope and the equivalent shear force:

$$\begin{cases} \partial_{\mathbf{n}} w = 0 \\ V_n(w) = 0 \end{cases} \tag{4.17}$$

In the case of a square plate of edge length a, when equations (4.17) are used it is seen that:

$$w_{\alpha\beta} = A_{\alpha\beta} \cos\frac{\alpha\pi x}{a} \cos\frac{\beta\pi y}{a} \tag{4.18}$$

satisfies the boundary conditions, where $A_{\alpha\beta}$ is an amplitude coefficient determined from the initial conditions of the problem and a and b are respectively the width and the length of the plate. Substituting (4.18) into (2.70) gives the frequency

$$\omega_{\alpha\beta} = \sqrt{\frac{D}{\rho h}\left[\left(\frac{\alpha\pi}{a}\right)^2 + \left(\frac{\beta\pi}{a}\right)^2\right]} \tag{4.19}$$

where α and β are integers which can take all values from 0 to ∞.
Using this expression, the accuracy of the numerical results was assessed. The relative error, together with the values of the eigenfrequencies are shown in Table 13, and, from the high degree of exactness of the computed values, it can be inferred that the expression of the equivalent shear force is adapted. The good agreement observed when studying simply supported plates ensures the correctness of the expression of the bending moment M_n. Thus, the free boundary condition may be considered to be accurate.

However, since the expressions for the free boundary are usually given for a smooth boundary [14, 74], the effect of a discontinuous boundary such as a corner point was studied. As it is shown in Appendix G, the boundary conditions for corner points differ from the usual ones. For example, in the case of a square plate, they can be represented in the following form [51]:

$$\begin{cases} M_n(w) = 0, \\ \dfrac{\partial^2 w}{\partial x \partial y} = 0 \end{cases} \tag{4.20}$$

It was found that implementing this new set of equations gave more sensible results shown in Table 14 along with the values from the work of Gorman [27], who obtained the *exact eigenvalues* for a free square plate by using the method of superposition. However, the relative errors in Table 14 show that the accuracy is still poor. This type of corner condition was also implemented for skew plates by using

the formulation given in Appendix G

$$\begin{cases} M_n(w) = 0 \\ M_{ns}^+(w) - M_{ns}^-(w) = 0 \end{cases} \tag{4.21}$$

where M_{ns}^+ and M_{ns}^- represent the right-hand and the left-hand limit of the twisting moment at the corner point. This limit is determined by calculating the twisting moment at two points in the neighbourhood of the corner. However, no sensible results were obtained for this type of plates.

Therefore, to further investigate the influence of the corner points, the case of a free circular plate was studied. As said earlier, there was no agreement between the computed frequencies and the ones available in literature. It is believed that this deterioration in agreement is attributable to the fact that the boundary conditions used approximate the circular plate by a polygonal plate. Indeed, they have been derived for straight boundary, i.e., they did not take into account the curvature of the boundary. Hence, a new set of boundary conditions which took account of the curvature of the circle was used. To implement it, polar coordinates are used and the transverse displacement w becomes

$$w(r,\theta) = \sum_{j=1}^{n} D_j^1 e^{-ikr\cos(\theta-\xi_j)} + \sum_{j=1}^{n} D_j^2 e^{kr\cos(\theta-\xi_j)} \tag{4.22}$$

The free boundary condition is now obtained by prescribing the radial bending moment M_r and the radial equivalent shear force V_r [51]

$$\begin{cases} M_r(w) = 0, \\ V_r(w) = 0 \end{cases} \tag{4.23}$$

where M_r and V_r are given by

$$\begin{aligned} M_r(w) &= \frac{\partial^2 w}{\partial r^2} + \nu\left(\frac{1}{a}\frac{\partial w}{\partial r} + \frac{1}{a^2}\frac{\partial^2 w}{\partial \theta^2}\right) \\ V_r(w) &= \frac{\partial}{\partial r}\nabla^2 w + \frac{1}{a}\frac{\partial M_{r\theta}}{\partial r} \end{aligned} \tag{4.24}$$

where $M_{r\theta}$ is the twisting moment defined by

$$M_{r\theta} = (1-\nu)\frac{\partial}{\partial r}\left(\frac{1}{a}\frac{\partial w}{\partial \theta}\right) \tag{4.25}$$

with a the radius of the circle.

The collocation method is used but, instead of enforcing the boundary conditions at the n points $\mathbf{x}^i$ of a n-polygonal plate as it was done before (see Figure 6 (a)), they are now enforced at n points $\mathbf{x}^i$ of the circular plate (see Figure 6 (b)).
Using this type boundary conditions in this manner improved greatly the accuracy of the eigenfrequencies. The results for a circular plate with a Poisson's ratio

$\nu = 0.33$ are given in Table 15. The eigenfrequencies λ, taken from Leissa [51] are also given, and close agreement can be observed.

The response of a free circular plate to a pressure load was then determined. Therefore, it was possible to plot the first seven modes of this plate and the results are shown on Figure 31. The validity of these results is established by comparison with the experimental work of Waller [83]. For every mode shape reported here, excellent agreement with Waller's pictures is observed.

Hence, from these two examples, it may be concluded that when applying the PWBM to the case of free plates, care must be taken with the method of discretization used. Indeed, in the case of the square plate, it has been shown that the method of approximation had to include corner points; in the case of the circular plate, it was found that a polygonal approximation was not appropriate for this kind of shape. Such problem might be due to the fact that the given set of heuristic T-functions may not be T-complete for a boundary value problem which includes free corners.

To overcome the problem of discretization, two other numerical methods were investigated. The first one is the weighted residual method and the second one is the Galerkin method. These two techniques are presented in Appendix F together with the different trial functions employed. However, the added complexity they introduce makes their implementation less easy. Furthermore, no major improvement was noticed for any type of boundary conditions. Therefore, the technique of collocation is thought to be the best compromise between simplicity of implementation and accuracy.

4.3.4 Case of plates with mixed boundary conditions

In this section, the PWBM is applied to the vibration of plates which may have any combination of the previous boundary conditions (free, simply supported or clamped).

The first example is a point supported square plate. This type of mixed boundary condition is realised by having all the edges free and all the corners simply supported. The point supports at each corner are easily incorporated in the analysis, and the first four eigenfrequencies λ for a square plate, are presented in Table 16. The relative errors, determined by comparison with the work of Bardell [6], are well within 2%.

Three other types of mixed boundary conditions are also presented. They involve the triangular plates with the different planforms shown in Figure 14. Letter F, C or SS located along an edge indicates free, clamped or simple support. For convenience, the plates will be referred to by means of a three-letter group, following

established convention [29]. The first letter indicates the type of support along the left edge as shown in the figure. The remaining letters indicate the types of support encountered in moving counterclockwise around the plate. The triangular aspect ratio is determined by b/a where a and b are the length of the base and the height of the triangle respectively.

The first case considered is a SS-C-SS right triangular plate of aspect ratio $a/b = 1.0$ (see Figure 14 (a)). Computed eigenvalues are tabulated in Table 17. These results are compared with the ones obtained by Saliba [68] who used the method of superposition for right triangular plates developed by Gorman [28], and excellent agreement is obtained. Using the corresponding eigenvectors, the first four contour plots of the mode shapes for this plate are shown in Figure 32. Good agreement with the mode shapes in Saliba's work is obtained in term of general proportions and of the shape.

The second case considered is a C-SS-C right triangular plate of aspect ratio $b/a = 2.0$ shown on Figure 14 (b). The corresponding eigenvalues λ are presented in Table 18. Once more, excellent agreement is observed with the work of Saliba [68].

In Table 19, the lowest six frequencies are given for the last case studied, a C-F-C isoceles triangular plate of aspect ratio $b/a = 1.0$ (see Figure 14 (c)). Inspection of the tabulated relative errors shows quite good agreement with the results of Kim *et al.* [44], who used the Rayleigh-Ritz method with simple polynomials as trial functions. Note that the introduction of a free edge does not alter greatly the accuracy of the results. Such a accuracy corroborates the previous study on the exactness of the expression of this boundary condition.

4.4 Corner points and conditioning

When using this method, two problems have been encountered. The first one is the effect of discontinuities of the boundary on the solution, and the second one is the severe singular character of the matrix $A[(k)]$. A description of both these problems is given in this section.

4.4.1 Corner points

All the boundary methods presented in this work suffers from a common drawback: problems with corners. Indeed, in the case of the BEM applied to the biharmonic equation, Jawson *et al.* [40] observed that if the boundary $\partial\Omega$ had corners, the numerically determined source densities tended to oscillate. They concluded that this trouble could to a large extent be eliminated by rounding off the corner: replace the corner zone by a quadrant of an inscribed circle (see Figure 7 (b)) . Bannerjee *et al.* have proposed a similar solution to the problem by modelling corners by two independent nodes placed slightly away from the actual corner (see Figure 7 (a));

such model was used in the IBEM presented in Chapter 2.

In the EIBEM, Zieliński remarked that that the smoothness of the exterior surface Θ may be dependent on the discontinuities of the boundary $\partial\Omega$, and that many authors omitted the zone of the corners. Others, such as Wearing *et al.* [85] proposed their optimised position of the source points in the corner zone.

When using the Bessel expansion method, Urata [76] noted that

> *It remains unknown how to treat reasonably the boundary conditions at corner.*

He proposed different calculating procedures concerning this problem [75, 76]. Among them were a discretization [75] similar to the one proposed by Jawson *et al.* [40], and another one which took the corner condition [76] in consideration.

In this work, several problems with corner points were encountered. They can be classified into two types. The first type regroups the problems which affect the values of the eigenfrequencies. The second type is typified by the problems which modify the modes.

In the case of the membrane, problems of the second type were encountered. When plotting the mode shapes of membranes with sharp corners, it was remarked that the displacement around the corners tended to infinity. An example of this situation can be seen on Figure 33, which represents the forced response of a skew membrane of skew angle $\psi = 70°$ to a pressure load. Note that the problem is localised at acute corners. Such phenomenon may be associated to the one arising the IBEM when the source densities tend to infinity at some corner points. If, for the first few modes, the effects of this type of problem are usually localised and easily identified, they may interfere with the modes of higher frequencies.

In the case of the plates, both types of problems were also encountered. The second type of problem was dealt with in a way similar to the one used for membranes. Furthermore, in most of the cases, i.e. clamped, simply supported and sliding clamped boundaries, the corner point was modelled by using a *single node.* Such technique was used by Zabaras and Mukherjee in work on the application of the BEM to the solidification of pure metals [88]. Such modelling consist in representating the corner point by a single node $\mathbf{x}^i$ and by averaging the normal $\mathbf{n}^i$ at this point by $\mathbf{n}^i = (\mathbf{n}^{i+1} + \mathbf{n}^{i-1})/\|\mathbf{n}^{i+1} + \mathbf{n}^{i-1}\|$ (see Figure 8 (a)). However, in the case of free plates, it has been seen that corner points greatly influence the accuracy of the results, and it was found that this model was not adapted for this type of problem. Hence, two other types of discretization were tried. The first one (see Figure 8 (b)) has been described in Section 4.3.3 and consists in including a corner condition in the boundary conditions by using the set of two different normals $\mathbf{n}^{i+}$ and $\mathbf{n}^{i-}$. The second one, which was used by Jawson *et al.* [40] and Urata [75], rounds the corner by replacing the two intervals adjoining the corner by a quadrant

of an inscribed circle of radius R, and to introduce a nodal point into the middle of the arc (see Figure 7 (b)). The corner can then be approximated by a sequence of circular quadrants of decreasing radius. Two new formulations of the free boundary condition, which took in account the radius of curvature at the corner point, i.e. R, were used. They are written as [56]

$$M_n^R(w) = \nabla^2 w - (1-\nu)\left(\frac{1}{R}\frac{\partial}{\partial \mathbf{n}} + \frac{\partial^2}{\partial \mathbf{s}^2}\right) \tag{4.26}$$

$$V_n^R(w) = \frac{\partial}{\partial \mathbf{n}}\nabla^2 w + (1-\nu)\frac{\partial}{\partial \mathbf{s}}\left(\frac{\partial^2 w}{\partial \mathbf{n}\partial \mathbf{s}} - \frac{1}{R}\frac{\partial w}{\partial \mathbf{s}}\right) \tag{4.27}$$

However, when using the PWBM, it was found that this discretization gave very poor results. The effect of rounding off corners on the accuracy has already been noted by Wearing *et al.* [85] when applying the EIBEM. According to the authors of this reference, the disadvantages of this approach are poor solutions at the corners and edges for all problems, irrespective of their field behaviour, and difficulty in modelling the corners when dealing with problems having regular field behaviour. In the case of the PWBM, it is thought that these conclusions remain valid. Hence, it is still unknown how to model accurately corners in the PWBM, and a modified version of this method, presented in Section 4.5, was studied and was seen to give better results in some cases.

4.4.2 Study of the conditioning of the problem

As it has been said earlier, the accuracy of the results improves with the number of plane wave components. However, when increasing n, the plot of the inverse of the determinant presents some "noise" which renders the determination of the eigenfrequencies impossible. This noise is due to the fact that the value of the determinant of $[A(k)]$ has reached the machine precision. Furthermore, it was also remarked that the conditioning of the same matrix could become extremely high. Hence, in this section, a study of the singularity of this matrix along with its conditioning is presented.

For the sake of simplicity, the special case of a clamped circular membrane of unit radius will be considered. It must be noted that this study on the condition number of the resulting matrix $[A(k)]$ will still be valid for the case of other planforms.

Using the formula for the condition number, introduced in Chapter 3, it was found that the matrix $[A(k)]$ becomes ill-conditioned for large values of n. Indeed, in the simple case of the circular membrane, from Figure 34, it can be deduced that the conditioning is linked to the value of the frequency: the higher the frequency, the better conditioned the matrix gets.

To explain this problem, the linear dependency of the columns j and $j+1$ of the matrix $[A(k)]$ is studied. In the case of a circular membrane of unit radius, these

columns, denoted A_j and A_{j+1}, can be expressed as:

$$A_j = \left\{ \begin{array}{c} e^{-ik\cos(\xi_j-\theta_1)} \\ \vdots \\ e^{-ik\cos(\xi_j-\theta_l)} \\ \vdots \\ e^{-ik\cos(\xi_j-\theta_n)} \end{array} \right\}_n , \quad A_{j+1} = \left\{ \begin{array}{c} e^{-ik\cos(\xi_{j+1}-\theta_1)} \\ \vdots \\ e^{-ik\cos(\xi_{j+1}-\theta_l)} \\ \vdots \\ e^{-ik\cos(\xi_{j+1}-\theta_n)} \end{array} \right\}_n \tag{4.28}$$

and

$$\xi_{j+1} = \frac{2\pi j}{n}. \tag{4.29}$$

Therefore, A_{j+1} can be rewritten as

$$A_{j+1} = \left\{ \begin{array}{c} e^{-jk\cos(\xi_j-\frac{2\pi}{n}-\theta_1)} \\ \vdots \\ e^{-jk\cos(\xi_j-\frac{2\pi}{n}-\theta_l)} \\ \vdots \\ e^{-jk\cos(\xi_j-\frac{2\pi}{n}-\theta_n)} \end{array} \right\}_n \tag{4.30}$$

Since

$$\cos(\xi_j - \frac{2\pi}{n} - \theta_l) = \cos(\xi_j - \theta_l)\cos(\frac{2\pi}{n}) + \sin(\xi_j - \theta_l)\sin(\frac{2\pi}{n}), \tag{4.31}$$

the following approximation can be obtained

$$e^{-ik\{\cos(\xi_j-\frac{2\pi}{n}-\theta_l)\}} = e^{-ik\cos(\xi_j-\theta_l)}\left(1 - \frac{i2\pi k}{n}\sin(\xi_j - \theta_l)\right) + \mathcal{O}\left(\left(\frac{\pi k}{n}\right)^2\right) \tag{4.32}$$

Substituting (4.32) in (4.30), A_{j+1} can be written

$$A_{j+1} = A_j + \frac{2i\pi k}{n}\begin{bmatrix} \alpha_1 & 0 & \cdots & 0 \\ 0 & \ddots & \ddots & \vdots \\ \vdots & \ddots & \ddots & 0 \\ 0 & \cdots & 0 & \alpha_n \end{bmatrix} A_j \tag{4.33}$$

with

$$\alpha_i = \sin(\xi_j - \theta_i) + \mathcal{O}\left(\frac{\pi k}{n}\right) \tag{4.34}$$

A more detailed study of the conditioning of this matrix was realised by Langley [50] who found that the condition number is given by:

$$c([A(k)] \approx \sqrt{\pi n/4}\,(n/ek)^{n/2} \tag{4.35}$$

In both cases, it can be deduced that the singularity of the matrix, thus its condition number, increases with n and $1/k$, as was seen in Figure 34.

A physical explanation of this phenomenon was proposed by Langley [50]: two neighbouring waves become very closely aligned with n increasing and start to interact with a very long beat wavelength. Since the plate or membrane appears relatively small on the scale of this beat wavelength, the two waves produce near identical motion, which gives rise to ill-conditioning.

4.5 The approximate Bessel-function method (ABF)

In order to overcome the problem with free boundary plates, a derived method of the PWBM, called the approximate Bessel functions, was studied. In this method, the amplitude of the waves D^1 and D^2 are expanded as finite Fourier series, and it is shown that the transverse displacement w can be written in terms of a series which approximates to the Bessel function.

4.5.1 Principle

In Appendix D, it is shown that the formulation of the displacement w using plane waves and the one using Bessel functions are equivalent. To do so, the following form of w is used

$$\begin{aligned} w(r,\theta) &= \int_{-\pi}^{\pi} \left\{ \sum_{j=-\infty}^{\infty} c_j^{(1)} e^{ij(\xi+\pi/2)} \right\} e^{-ikr\cos(\xi-\theta)}\, d\xi \\ &\quad + \int_{-\pi}^{\pi} \left\{ \sum_{j=-\infty}^{\infty} c_j^{(2)} e^{ij\xi} \right\} e^{kr\cos(\xi-\theta)}\, d\xi \end{aligned} \tag{4.36}$$

The expressions in braces in (4.36) represent the amplitude $D^1(\xi)$ and $D^2(\xi)$ introduced earlier. These functions are unknown periodic functions of ξ with the fundamental period 2π.

If $D^1(\xi)$ and $D^2(\xi)$ are considered as the unknowns of the problem, the PWBM formulation is obtained, with them being the amplitudes of the plane waves. However, if the series expansions of $D^1(\xi)$ and $D^2(\xi)$ are retained, the unknowns of the problem become $c_j^{(1,2)}$, and the classical Bessel expansion formulation is directly deduced by using the integral representation of the Bessel functions.
By writing

$$D^1(\xi) = \sum_{j=-\infty}^{\infty} \zeta_j^{(1)} e^{ij\xi} \tag{4.37}$$

$$D^2(\xi) = \sum_{j=-\infty}^{\infty} \zeta_j^{(2)} e^{ij\xi} \tag{4.38}$$

with $\zeta_j^{(1)} = c_j^{(1)} e^{ij\pi/2}$ and $\zeta_j^{(2)} = c_j^{(2)}$, it becomes obvious that the series expansions of $D^1(\xi)$ and $D^2(\xi)$ represent the Fourier expansions of these two 2π-periodic functions.

In this technique, this formulation is considered but the infinite series are approximated by N-terms series, hence the name *approximated Bessel functions method.* In the following, the Fourier's formulation involving *sin* and *cos* is preferred. Hence, $D^1(\xi)$ and $D^2(\xi)$ become

$$D^1(\xi) = \frac{a_0^{(1)}}{2} + \sum_{j=1}^{N} \left(a_j^{(1)} \cos j\xi + b_j^{(1)} \sin j\xi \right) \tag{4.39}$$

$$D^2(\xi) = \frac{a_0^{(2)}}{2} + \sum_{j=1}^{N} \left(a_j^{(2)} \cos j\xi + b_j^{(2)} \sin j\xi \right) \tag{4.40}$$

where $a_j^{(1,2)}$ and $b_j^{(1,2)}$ are linked to $\zeta_j^{(1,2)}$ by the following expressions:

$$\left.\begin{array}{l} a_j^{(1,2)} = \zeta_j^{(1,2)} + \zeta_{-j}^{(1,2)} \\ b_j^{(1,2)} = i(\zeta_j^{(1,2)} - \zeta_{-j}^{(1,2)}) \end{array}\right\} (j = 0, 1, 2, \ldots, N) \tag{4.41}$$

Therefore, (4.12), which gives the approximated transverse displacement w of a plate, becomes

$$\begin{aligned} w(\mathbf{x}) = &\sum_{l=1}^{n} \left\{ \frac{a_0^{(1)}}{2} + \sum_{j=1}^{N} \left[a_j^{(1)} \cos j\xi_l + b_j^{(1)} \sin j\xi_l \right] e^{-ik(x_1 \cos \xi_l + x_2 \sin \xi_l)} \right\} \\ &+ \sum_{l=1}^{n} \left\{ \frac{a_0^{(2)}}{2} + \sum_{j=1}^{N} \left[a_j^{(2)} \cos j\xi_l + b_j^{(2)} \sin j\xi_l \right] e^{k(x_1 \cos \xi_l + x_2 \sin \xi_l)} \right\} \end{aligned} \tag{4.42}$$

where $a_l^{(1,2)}$ and $(b_l^{1,2})$ constitute the unknowns of the problem. They are determined in a manner similar to that outlined of Section 4.1.3, i.e. by enforcing the corresponding boundary conditions of the problem B_1 and B_2, and by using an n-point collocation scheme. Hence, the following linear system is obtained:

$$[A(k)][S]\vec{F} = \vec{0} \tag{4.43}$$

where $[A(k)]$ is the matrix defined by (4.1.3), $\vec{F}$ is

$$\vec{F} = \begin{pmatrix} \vec{F}^1 \\ \vec{F}^2 \end{pmatrix}_{4N+2} \tag{4.44}$$

with

$$\vec{F}^{1,2} = \begin{pmatrix} a_0^{1,2} \\ \vdots \\ a_N^{1,2} \\ b_1^{1,2} \\ \vdots \\ b_N^{1,2} \end{pmatrix}_{2N+1} \tag{4.45}$$

And $[S]$ is defined by:

$$[S] = \left[\begin{array}{c|c} [s] & [0] \\ \hline [0] & [s] \end{array} \right]_{2n \times (4N+2)} \tag{4.46}$$

with

$$[s] = \begin{bmatrix} 1/2 & \cos(\xi_1) & \dots & \cos(N\xi_1) & \sin(\xi_1) & \dots & \sin(N\xi_1) \\ \vdots & \vdots & & \vdots & \vdots & & \vdots \\ \vdots & \vdots & & \vdots & \vdots & & \vdots \\ 1/2 & \cos(\xi_n) & \dots & \cos(N\xi_n) & \sin(\xi_n) & \dots & \sin(N\xi_n) \end{bmatrix}_{n\times(2N+1)} \tag{4.47}$$

In order to use a determinant search, a $(4N+2)^2$ square matrix is obtained by multiplying the left-side of (4.43) by the transpose of $[S]$, $[S]^t$:

$$[S]^t[A(k)][S]\vec{F} = \vec{0} \tag{4.48}$$

4.5.2 Application

The case of a clamped square plate was first considered in order to assess the accuracy of this method. The eigenfrequencies λ are tabulated in Table 20 along with the ones obtained by Urata [75] who used a Bessel expansion of the transverse displacement. Since the average relative error, indicated in parentheses and determined by comparison with the results in [6], is equal to 0.08%, the ABFM can be considered to be very accurate.

The next case considered was a free square plate. Table 21 shows the eigenvalues λ obtained with the ABF method and with the Bessel expansion method used by Urata [75]. Both methods are compared with the values from the work of Gorman [27], who obtained the *exact eigenvalues* for a free square plate by using the method of superposition. From the relative errors quoted in parentheses, it is seen that in every case the ABFM gives more accurate results than the Bessel expansion method, and, by comparison with the results in Table 14, the PWBM.

This method was then applied to the vibration of a free skew plate of angle $\psi = 15°$. Unlike the PWBM which did not give any sensible results, the results obtained here have a relative error within 3%, as it shown in Table 22 are accurate. However, for free plates with higher skew angles, no sensible results were obtained and it is thought that it is again due to the presence of acute corners.

4.6 Conclusion

In this chapter, the numerical analysis of eigenfrequencies and modes not only of membranes but also of plates with several different planforms has been carried out and the efficiency and the versatility of the PWB method has been demonstrated. The following may be concluded:

1. In most of the cases, eigenfrequencies obtained by the present method are sufficiently accurate for engineering purposes.

2. Modes can be obtained effectively by either considering the forced response of the structure or by determining the eigenfunctions, or eigenvectors, of the problem.

3. Although the collocation method is the simplest discretization method, it is as efficient as the more complex methods such as the weighted residual methods.

4. The loss of accuracy due to corner points and the ill-conditioning are the two major drawbacks of the PWBM. Hence, this method was found less accurate when applied to free plates. Furthermore, no general solution has been found to cope with these problems.

5. A derived method, called the ABFM, was implemented to overcome the difficulties with free plates, and it has been shown to give better results for plates with simple planform.

5. Conclusions

5.1 General remarks

In this work, three boundary methods have been applied to eigenvalue problems of membranes and thin plates. The feasibility and versatility of all three methods have been verified from a numerical point of view.

The first method is the well-known Indirect Boundary Element Method, which is based on the use of boundary integrals. In order to assess its efficiency, this method was applied to the vibration of clamped membranes and clamped plates. It was found that this method suffered from very complex calculations involving the boundary integrals. Although its application to the determination of eigenfrequencies of structures has previously been demonstrated, a new technique to determine the dynamical forced response of a structure was studied. This technique was seen to produce accurate results for both damped and undamped membranes and was found to be easier to implement than other methods, such as the dual reciprocity method and the multiple reciprocity method.

The second method studied was derived from the IBEM formulation and is called the EIBEM. The main characteristic of this method is to relocate the curve of the source distribution on an imaginary boundary, at a certain distance outside the physical domain of the problem, resulting in a system of regular integral equations, unlike in the IBEM. Though such a technique has previously been applied to different types of problem, it has not been used to solve the resulting eigenvalue problem. It was found that criteria, such as the condition number of a matrix, used to optimise the exterior boundary by other researchers, were not efficient in the present study. Indeed, it was proved that the matrix used in the eigenvalue problem could be severely ill-conditioned but still yield correct eigenfrequencies. Some qualitative criteria were then given but none of them was found to lead to a rigorous treatment of the optimisation of the imaginary boundary.

The third method, called the PWBM, was presented as a Trefftz method with a new set of functions which represent plane waves. However, it was also shown that this method could be derived from the EIBEM formulation by moving the imaginary boundary toward infinity. Hence, some results, such as the technique to determine the forced response and the discretization methods used in the EIBEM were found to be applicable in this case. This method was then applied to the vibration of membranes and plates. In both cases, this method was found to be in perfect agreement with the results found in the literature for most of the cases considered. Not only did it yield accurate results for several different planforms encountered in typical aeronautical applications, such as trapezoidal plates and triangular plates, and for different boundary conditions, but it was also easier to implement and quicker to execute (in average, ten times quicker than

the IBEM and five times quicker than the EIBEM). However, it was shown that this method suffered from two major drawbacks: a severely singular matrix for relatively small numbers of plane waves, and major difficulties when dealing with free corners, thus making it inappropriate to the study of polygonal plates with free boundaries. Such problems were investigated, and a derived method of the PWBM, the ABFM, was studied. This derived method was shown to give better results in the case of free rectangular plates but was not efficient for other plan-forms.

5.2 Suggestions for further research

No general criterion for assessing the accuracy and the robustness of boundary methods when applied to eigenvalue problems has been found; for example, the condition number has not been found to be an adequate measure. Hence, a more detailed study of this aspect is needed.

Although some work has been done on the modelling of corners [76] for the dynamic case, no general results have been derived. Thus, a detailed evaluation of the discontinuities introduced by the corner in the PWBM needs to be addressed. Furthermore, the need to add new terms in the PWBM formulation to represent such discontinuities may be required.

As said earlier, no work has yet been reported on the derivation of a T-complete system for the case of a plate. Therefore, further work in this area would be worthwhile. Indeed, as remarked by Zieliński [89], without any precise mathematical background, the use of heuristic T-functions, such as the ones used in the case of the plate, could be unreliable. Furthermore, such a study would also clarify the effect of corners.

Bibliography

[1] Aircraft accident report: Spectrum Air, Incorporated, Sabre Mark 5, N275X, Sacramento Executive Airport, Sacramento, California, 24 September 1972. NASA Technical Reports NTSB-AAR-73-6, NASA, 1972.

[2] Aircraft accident report: Trans World Airlines, Incorporated, Boeing 707-331C, N15712, Flight 604, San Francisco, California 13 September 1972. NASA Technical Reports NTSB-AAR-73-4, NASA, 1973.

[3] Aircraft accident report: New York Airways, Incorporated, Sikorsky S61-L, N618PA Newark, New Jersey, April 18, 1979. NASA Technical Reports NTSB-AAR-79-14, NASA, 1979.

[4] M. Abramowitz and I.A. Stegun, editors. *Handbook of mathematical functions.* Dover Publications, New York, 1968.

[5] J.P.S. Azevedo and C.A. Brebbia. An efficient technique for reducing domain integrals to the boundary. In *Boundary Elements X*, volume 1, Southampton, 1988. Computational Mechanics Publication and Springer-Verlag.

[6] N.S. Bardell. The free vibration of skew plates using the hierarchical finite element method. *Computers and Structures*, 45:841–874, 1992.

[7] S. Bingnan, T. Jinchun, and X. Yuyin. A new off-boundary element method for analysing plante and shallow shell bending. *Computers and Structures*, 60:297–304, 1996.

[8] A. Bogomolny. Fundamental solutions method for elliptic boundary value problems. *SIAM Journal Numerical Analysis*, 22:644–669, 1985.

[9] C. A. Brebbia and S. Walker. *Boundary element techniques in engineering.* Newnes-Butterworths, London Boston, 1980.

[10] C.A. Brebbia, editor. *Recent Advances in Boundary Elements*, London, 1978. Pentech Press.

[11] C.A. Brebbia. *The Boundary Element Method for Engineers.* Pentech Press, London, 1980.

[12] C.A. Brebbia, editor. *Topics in boundary element method research*, volume 1. Springer-Verlag, Berlin, 1984.

[13] F. Cassot and G. P. Extremet. Détermination numérique du champ sonore et des fréquences propres dans une enceinte circulaire par la méthode de discrétisation (the numerical determination of the sound field and of the characteristic frequencies in a circular enclosure by the method of discretisation). *Acta Acustica*, 27:238–245, 1972.

[14] G. Chen and J. Zhou. *Boundary element methods.* Academic Press, London, 1992.

[15] Y. K. Cheung, W. G. Jin, and O. C. Zienkiewicz. Solution of the Helmholtz equation by Trefftz method. *International Journal for Numerical Methods in Engineering*, 32:63–78, 1991.

[16] Y. K. Cheung, W. G. Jin, and O. C. Zienkiewicz. Trefftz method for Kirchhoff plate bending problems. *International Journal for Numerical Methods in Engineering*, 36:765–781, 1993.

[17] H. D. Conway. The bending, buckling and flexural vibrations of simply supported polygonal plates by point-matching. *Transactions of the ASME, Journal of Applied Mechanics*, 28:288–291, 1961.

[18] H. D. Conway and K. A. Farnham. The free flexural vibrations of triangular, rhombic and parallelograms plates and some analogies. *International Journal of Mechanical Sciences*, 7:811–816, 1965.

[19] G. de Mey. Integral equations for potential problems with the source function not located on the boundary. *Computers and Structures*, 8:113–115, 1978.

[20] S. Durvasula. Natural frequencies and modes of skew membranes. *Journal of the Acoustical Society of America*, 68:1636–1646, 1968.

[21] P. Filippi and J. Vivoli. Vibration de plaques minces: résolution à l'aide de potentiel de couches. *Comptes Rendus de l'Académie des Sciences, Série A*, 279:896–899, 1971.

[22] P. Filippi and J. Vivoli. Vibrations de plaques minces: résolution à l'aide de potentiels de couches. In *7th international congress on Acoustics* [39], pages 617–620.

[23] I. Fredholm. Sur une classe d'équations fonctionelles. *Acta Mathematica*, 27:365–390, 1903.

[24] T.M. Fu, J.G. Xiong, and Y.K. Cheung. Boundary element method with exterior collocation in two-dimensional elastodynamic problems. *Earthquake Engineering and Structural Dynamics*, 24:99–108, 1995.

[25] M. Géradin and D. Rixen. *Théorie des vibrations: Application à la dynamique des structures.* Masson, Paris, second edition, 1996.

[26] G. H. Golub and C. F. Van Loan. *Matrix Computations.* North Oxford Academic, 1983.

[27] D. J. Gorman. Free vibration analysis of the completely free rectangular plate by the method of superposition. *Journal of Sound and Vibration*, 57:437–447, 1978.

[28] D. J. Gorman. A highly accurate analytical solution for free vibration analysis of simply supported right triangular plates. *Journal of Sound and Vibration*, 89:107–118, 1983.

[29] D. J. Gorman. Accurate free vibration analysis of right triangular plates with one free edge. *Journal of Sound and Vibration*, 131:115–121, 1989.

[30] T. Goto and M. Suzuki. A boundary integral equation method for nonlinear heat conduction problems with temperature-dependant material properties. *International Journal of Heat and Mass Transfer*, 39:823–830, 1996.

[31] U. Heise. Application of the singular method for the formulation of plane elastostatical boundary value problems as integral equation. *Acta Mechanica*, 31:33–69, 1978.

[32] I. Herrera. *Boundary methods: an Algebraic Theory.* Pitman Adv. Publ. Program, London, 1984.

[33] I. Herrera and F.J. Sabina. Connectivity as an alternative to boundary integral equations. Construction of bases. *Proceedings of the National Academy of Sciences, USA*, 75:2059–2063, 1978.

[34] I. Herrera and D. A. Spence. Framework for biorthogonal fourier series. *Proceeding of the National Academy of Sciences, USA*, 78:7240–7244, 1981.

[35] R. Heuer and H. Irschik. A boundary element method for eigenvalue problems of polygonal membranes and plates. *Acta Mechanica*, 66:9–20, 1987.

[36] T. Honma, Y. Tanaka, and I. Kaji. Regular boundary element steady-state solutions of the traveling magnetic field problems. *I.E.E.E. Transactions on Magnetics*, 21:2235–2238, 1985.

[37] J. R. Hutchinson. Determination of membrane vibrational characteristics by the boundary-integral equation method. In Brebbia [10], pages 301–315.

[38] J. R. Hutchinson and G. K. K. Wong. The boundary element method for plate vibrations. In *Proc. ASCE 7th Conference on Electronic Computation*, pages 297–311, New York, 1979. American Society of Civil Engineers.

[39] International Commission on Acoustics. *7th International Congress on Acoustics*, Budapest, 1971.

[40] M. A. Jawson, M. Maiti, and G.T. Symm. Numerical biharmonic analysis and some application. *International Journal of Solids and Structures*, 3:309–332, 1967.

[41] M.A. Jawson and G.T. Symm. *Integral Equation Methods in Potential Theory and Elastostatics.* Academic Press, 1977.

[42] Y. Kagawa, Y. Sun, and Z. Mahmood. Regular boundary integral formulation for the analysis of open dielectric/optical waveguides. *I.E.E. Transactions on Microwave Theory and Techniques*, 44:1441–1450, 1996.

[43] O. D. Kellog. *Foundations of Potential Theory.* Springer, Berlin, 1929.

[44] C. S. Kim and S. M. Dickinson. The free flexural vibration of isotropic and orthotropic general triangular shaped plates. *Journal of Sound and Vibration*, 152:383–403, 1992.

[45] Y. Y. Kim and J. H. Kang. Free vibration analysis of membranes using wave-type base functions. *Journal of the Acoustical Society of America*, 99:2938–2946, 1996.

[46] E. Kita and N. Kamiya. Trefftz method: an overview. *Advances in Engineering Software*, 24:3–12, 1995.

[47] M. Kitahara. *Boundary Integral Equation Methods in Eigenvalue Problems of Elastodynamics and Thin Plates.* Elsevier, 1985.

[48] V.D. Kupradze. On the approximate solutions of problems in mathematical physics. *Russian Mathematical Surveys*, 22:58–107, 1967.

[49] K. Y. Lam, M. Liew, and S. T. Chow. Use of two-dimensional orthogonal polynomials for vibration analysis of circular and elliptical plates. *Journal of Sound and Vibration*, 154:261–269, 1992.

[50] R. S. Langley. Some perspectives on wave-mode duality in SEA. In *Symposium on Statistical Energy Analysis*, pages 1–12, Southampton, 1997. University of Southampton.

[51] A.W. Leissa. *Vibrations of Plates.* NASA SP-160, 1969.

[52] G. D. Manolis and D. E. Beskos. *Boundary Element Methods in Elastodynamics.* UNWIN Hyman, 1988.

[53] K. Maruyama, O. Ichinomiya, and Y. Narita. Experimental study of the free vibration of clamped trapezoidal plates. *Journal of Sound and Vibration*, 88:523–534, 1983.

[54] The Math Works, Inc., Natick. *MATLAB Reference Guide.*

[55] R. Mathon and R. L. Johnston. The approximate solution of elliptical boundary-value problems by fundamental solutions. *SIAM Journal of Numerical Analysis*, 14:638–650, 1977.

[56] L. Meirovitch. *Elements of Vibration Analysis.* McGraw-Hill Book Company, London, 2 edition, 1986.

[57] G. De Mey. Calculation of eigenvalues of the Helmholtz equation by an integral equation. *International Journal for Numerical Methods in Engineering*, 10:59–66, 1976.

[58] K. Nagaya. On the analysis of the doubly connected problem of vibrating polygonal plates. *Journal of the Acoustical Society of America*, 66:1795–1800, 1979.

[59] K. Nagaya. Method for solving vibration problems of a plate with arbitrary shape. *Journal of the Acoustical Society of America*, 67:2029–2033, 1980.

[60] K. Nagaya. Vibration of a plate with straight line boundaries. *Journal of Sound and Vibration*, 68:35–43, 1980.

[61] K. Nagaya. Vibration of a plate of arbitrary shape with free and simply supported mixed edges. *Journal of the Acoustical Society of America*, 73:844–850, 1983.

[62] Y. Niwa, S. Kobayashi, and M. Kitahara. Eigenfrequency analysis of a plate by the integral equation method. *Theoretical and Applied Mechanics*, 29:287–307, 1981.

[63] A. J. Nowak and A. C. Neves. *The Multiple Reciprocity Boundary Element Method.* Computational Mechanics Publication, Southampton, 1994.

[64] Numerical Algorithm Group, Inc., Oxford. *NAG Fortran Library Manual - Mark 16.*

[65] P. W. Partridge, C. A. Brebbia, and L. C. Wrobel. *The Dual Reciprocity Boundary Element Method.* Computational Mechanics Publication with Elsevier Applied Science, Southampton, 1992.

[66] C. Patterson and M. A. Sheikh. On the use of fundamental solutions in the trefftz method for potential and elasticity problems. In *Boundary Elements Methods in Engineering*, pages 43–57, Berlin and New-York, 1982. Springer-Verlag.

[67] T. Rudolphi, R. Agarwal, and A. Mitra. Coupling boundary integral equation with nonsingular functional equations by exterior collocation. *Engineering Analysis with Boundary Elements*, 8:245–251, 1991.

[68] H. T. Saliba. Transverse free vibrations of right triangular thin plates with combinations of clamped and simply supported boundary conditions: a highly accurate simplified solution. *Journal of Sound and Vibration*, 183:765–778, 1995.

[69] W. Soedel. *Vibrations of shells and plates.* Marcel Dekker, Inc., New-York, 2 edition, 1993.

[70] A. Sommerfeld. *Partial differential equations in physics.* Academic Press, New-York, 1949.

[71] G. W. Stewart. *Introduction to Matrix Computations.* Academic Press, New York, 1973.

[72] R. Szilard. *Theory and analysis of plates - Classical and Numerical Methods.* Prentice-Hall, New Jersey, 1974.

[73] G. R. C. Tai and R. P. Shaw. Helmholtz-equation eigenvalues and eigenmodes for arbitrary domains. *Journal of the Acoustical Society of America*, 56:796–804, 1974.

[74] S. Timoshenko. *Theory of Plates and Shells.* McGraw-Hill Book Company, London, 1940.

[75] Y. Urata. Analysis of lateral vibration of plates using analytic solutions discretized on boundaries (2nd report, application of collocation method to various kinds of boundary conditions). *Transactions of the Japan Society of Mechanical Engineers, Part C (in Japanese)*, 62:1314–1320, 1996.

[76] Y. Urata. Analysis of bending vibration of plates using analytic solutions discretized on boundaries (3rd report, improvement of calculating scheme in collocation method). *Transactions of the Japan Society of Mechanical Engineers, Part C (in Japanese)*, 63:22–28, 1997.

[77] Y. Urata and A. Horide. Analysis of lateral vibration of plates by the use of analytic solutions discretized on boundaries (1st report, arbitrarily convex shaped plates with clamped and free edges). *Transactions of the Japan Society of Mechanical Engineers, Part C (in Japanese)*, 61:4153–4159, 1995.

[78] Y. Urata and T. Nakagawa. Vibration analysis of continuous bodies using analytic solutions discretized on boundaries (a basic study on two-dimensional problems described by Helmholtz's equation. *JSME International Journal, Serie C*, 38:391–397, 1995.

[79] J. Vivoli. Mise en equation et conditions aux limites pour les problèmes de plaque. In *7th international congress on Acoustics* [39], pages 613–616.

[80] J. Vivoli. Vibrations de plaques de forme quelconque et potentiels de couches. *Comptes Rendus de l'Académie des Sciences, Série A*, 274:993–996, 1972.

[81] J. Vivoli. Vibrations de plaques et potentiels de couches. *Acustica*, 26:305–313, 1972.

[82] J. Vivoli and P. Filippi. Eigenfrequencies of thin plates and layer potentials. *Journal of the Acoustical Society of America*, 55:562–567, 1974.

[83] M. D. Waller. *Chladni Figures: a Study in symmetry.* G. Bell and Sons Ltd, London, 1961.

[84] J. L. Wearing and A. G. Rahman. A regular indirect boundary element method for stress analysis. In C. A. Brebbia, editor, *Boundary Elements IX*, volume 2, pages 183–198, 1987.

[85] J. L. Wearing and M. A. Sheikh. A regular indirect BEM for thermal analysis. *International Journal for Numerical Methods in Engineering*, 25:495–515, 1988.

[86] J. H. Wilkinson. *The Algebraic Eigenvalue Problem.* Clarendon Press, Oxford, 1965.

[87] R. Yuuki, T. Matsumoto, and H. Kisu. The usefulness and the limit of direct regular method in boundary element elastostatic analysis. In C. A. Brebbia and M. Tanaka, editors, *Boundary Elements VII*, pages 715–724, 1986.

[88] N. Zabaras and S. Mukherjee. Analysis of solidification problems by the boundary element method. *International Journal for Numerical Methods in Engineering*, 24:1879–1900, 1987.

[89] A. P. Zieliński. On trial functions applied in the generalized Trefftz method. *Advances in Engineering Software*, 24:147–155, 1995.

[90] A. P. Zieliński and I. Herrera. Trefftz method: Fitting boundary conditions. *International Journal for Numerical Methods in Engineering*, 24:871–891, 1987.

A. Special functions

In this Appendix, the different special functions used in this work are presented briefly.

A.1 The Hankel functions

$H_\alpha^{(1)}$ and $H_\alpha^{(2)}$ are the Hankel functions of the first and the second kinds of order α respectively. They are defined through [4]:

$$\left.\begin{array}{l} H_\alpha^{(1)}(z) = J_\alpha(z) + iY_\alpha(z) \\ H_\alpha^{(2)}(z) = J_\alpha(z) - iY_\alpha(z) \end{array}\right\}, z \in \mathbb{C} \tag{A.1}$$

where

$$\begin{aligned} J_\alpha &= \left(\frac{z}{2}\right)^\alpha \sum_{l=0}^{\infty} \frac{(-1)^l}{l!(l+\alpha)!} \left(\frac{z}{2}\right)^{2l}, \quad \alpha \neq -1, -2, -3, \ldots \\ Y_\alpha &= \frac{1}{\sin \pi\alpha} [(\cos \pi\alpha) J_\alpha(z) - J_\alpha(z)] \end{aligned} \tag{A.2}$$

are respectively Bessel and Neumann functions of order α. (When α is an integer, (A.2) is taken in the sense of limit.)

A.2 Struve function

$\mathcal{H}_0$ and $\mathcal{H}_1$ are respectively the Struve functions of order 0 and order 1, satisfying [4]

$$\mathcal{H}_0(z) = \frac{4}{\pi} \sum_{l=0}^{\infty} \frac{1}{2l+1} J_{2l+1}(z), \tag{A.3}$$

$$\mathcal{H}_1(z) = \frac{2}{\pi} [1 - J_0(z)] + \frac{4}{\pi} \sum_{l=0}^{\infty} \frac{1}{4l^2 - 1} J_{2l}(z) \tag{A.4}$$

B. Some results on linear algebra

In this Appendix, some results on linear algebra from [26] and used to introduce the condition number are presented.

B.1 Vector norms

A useful class of vector norms on $\mathbb{C}^n$ is the *Hölder* or p-norms defined by [26]

$$\|\mathbf{x}\|_p = (|x_1|^p + \ldots + |x_n|^p)^{1/p} \quad p \geq 1 \tag{B.1}$$

of which

$$\|\mathbf{x}\|_1 = (|x_1| + \ldots + |x_n|)$$
$$\|\mathbf{x}\|_2 = \left(|x_1|^2 + \ldots + |x_n|^2\right)^{1/2}$$

and

$$\|\mathbf{x}\|_\infty = \max_i |x_i| \tag{B.2}$$

are the most important. All norms on $\mathbb{C}^n$ are *equivalent*, i.e., if $\|\cdot\|_\alpha$ and $\|\cdot\|_\beta$ are norms on $\mathbb{C}^n$, then there exist positive constants c_1 and c_2 such that

$$c_1\|\mathbf{x}\|_\alpha \leq \|\mathbf{x}\|_\beta \leq \|\mathbf{x}\|_\alpha \tag{B.3}$$

for all $\mathbf{x} \in \mathbb{C}^n$

B.2 Matrix norms

Since $\mathbb{C}^{m\times n}$ is isomorphic to $\mathbb{C}^{mn}$, the definition of a matrix norm should be equivalent to the definition of vector norm. The most frequently used matrix norms in numerical analysis are the p-norms

$$\|[A]\|_p = \sup_{\mathbf{x}\neq\mathbf{0}} \frac{\|[A]\mathbf{x}\|_p}{\|\mathbf{x}\|_p} \tag{B.4}$$

A useful relationship, found in [86], is

$$\|[A]\|_2 = \sigma_1 \tag{B.5}$$

where σ_1 is the smallest *singular value* of $[A]$, i.e. the smallest eigenvalue of $[A]^H[A]$, where $[A]^H$ is the *Hermitian transposed matrix* defined by

$$[A]^H = \bar{A}^T \tag{B.6}$$

C. Derivation of the modal expansion for a vibrating damped square membrane

In this Appendix, the harmonic response of a damped square membrane of unit edge length is derived through the use of normal modes, and a relationship between the response and the damping coefficient is shown.
When using the spectral representation or modal expansion, the general solution of (2.41) is expressed as an infinite series:

$$v(\mathbf{x},t) = \sum_{l=1}^{\infty} \eta_l(t) V_l(\mathbf{x}) \tag{C.1}$$

where the $V_l(\mathbf{x})$ are the natural mode components and the modal participation factor $\eta_l(t)$ are the unknown and have to be determined in the following. Substituting (C.1) in (2.41) gives:

$$\sum_{l=1}^{\infty} \left[\sigma h \eta_l \nabla^2 V_l - \tau \dot{\eta}_l V_l - \rho \ddot{\eta}_l V_l\right] = -b \tag{C.2}$$

However, by definition,

$$\sigma h \nabla^2 V_l = -\rho \omega_k^2 V_l \tag{C.3}$$

Hence, (C.2) can be written as:

$$\sum_{l=1}^{\infty} \left(\rho \ddot{\eta}_l + \tau \dot{\eta}_l + \rho \omega_l^2 \eta_l\right) V_l = q \tag{C.4}$$

Multiplying both sides of (C.4) and applying the orthogonality of the natural modes V_l gives the following equation known as the modal participation factor equation [69]:

$$\ddot{\eta}_l + \frac{\tau}{\rho}\dot{\eta}_l + \omega_l^2 \eta_l = F_l \tag{C.5}$$

where

$$F_l = \frac{1}{\rho N_l} \int_{\Omega} b V_l \, dS \tag{C.6}$$

$$N_l = \int_{\Omega} V_l^2 \, dS \tag{C.7}$$

In the case of steady-state harmonic excitation, the load can be written as:

$$b(\mathbf{x}) = q(\mathbf{x}) e^{-i\omega t} \tag{C.8}$$

Thus,

$$F_l = F_l^* e^{-i\omega t} \tag{C.9}$$

with

$$F_l^* = \frac{1}{\rho N_l} \int_{\Omega} q V_l \, dS \tag{C.10}$$

while the modal participation factor will also be harmonic but lagging behind by a phase angle Φ_l:

$$\eta_l = \Lambda_l e^{-i(\omega t - \Phi_l)} \tag{C.11}$$

Hence, the amplitude of the modal participation factor satisfies:

$$\Lambda_l = \frac{F_l^*}{\sqrt{(\omega_l^2 - \omega^2)^2 + (\omega\tau/\rho)^2}} \tag{C.12}$$

Using the notations introduced in Chapter 2, (C.13) can be written as

$$\Lambda_l = \frac{F_l^*}{c^2\sqrt{(k_l^2 - k^2)^2 + (k\gamma)^2}} \tag{C.13}$$

If a spatially uniform pressure load is considered, q is constant and F_l^* is re-written

$$F_l^* = \frac{q}{\rho N_l}\int_\Omega V_l \, dS \tag{C.14}$$

Hence, if the reduced force $p = q/\sigma h$ is used, (C.13) becomes

$$\Lambda_l = \frac{p\int_\Omega V_l \, dS}{N_l\sqrt{(k_l^2 - k^2)^2 + (k\gamma)^2}} \tag{C.15}$$

In the case of a square membrane of unit edge length, the natural modes are expressed by the well-known formula:

$$V_l = V_{\alpha\beta} = \sin(\alpha\pi x)\sin(\beta\pi y) \tag{C.16}$$

Therefore, (C.15) can be written as:

$$\Lambda_l = \frac{4p}{\alpha\beta\pi^2}\frac{(1-\cos\alpha\pi)(1-\cos\beta\pi)}{\sqrt{(k_l^2 - k^2)^2 + (k\gamma)^2}} \tag{C.17}$$

Hence, for the first natural frequency, α and β are both equal to 1 and $k_1 = \pi\sqrt{2}$. Thus, Λ_1 is equal to:

$$\Lambda_1 = \frac{16p}{\pi^3\sqrt{2}\gamma} \tag{C.18}$$

D. Derivation of the plane wave expansion for the plate

In this Appendix, the plane wave expression of the transverse displacement for a plate is derived by using the heuristic T-functions for a plate. It has been seen in Chapter 3 that w can be expressed:

$$\begin{aligned} w(r,\theta) &= \sum_{j=0}^{\infty} \left\{ a_j^{(1)} J_j(kr) + a_j^{(2)} I_j(kr) \right\} \cos n\theta \\ &\quad + \sum_{j=1}^{\infty} \left\{ b_j^{(1)} J_j(kr) + b_j^{(2)} I_j(kr) \right\} \sin n\theta \end{aligned} \tag{D.1}$$

where $\left\{a_j^{(1,2)}\right\}_{j=0,1,\ldots}$ and $\left\{b_j^{(1,2)}\right\}_{j=1,2,\ldots}$ are complex, J_j and I_j are the Bessel and modified Bessel functions of integer order j respectively. The complex equivalent form of (D.2) can be derived

$$w(r,\theta) = \sum_{j=-\infty}^{\infty} \left\{ c_j^{(1)} J_j(kr) + c_j^{(2)} I_j(kr) \right\} e^{ij\theta} \tag{D.2}$$

with $c_j^{(1,2)}$ given by

$$c_j^{(1,2)} = \overline{c_{-j}^{(1,2)}} = \frac{1}{2}\left(a_j^{(1,2)} - i(-1)^j b_j^{(1,2)}\right) \tag{D.3}$$

One of the integral representations of Bessel functions gives [4]:

$$J_j(kr)e^{ij\theta} = \frac{1}{2\pi}\int_{-\pi}^{\pi} e^{i[j(\xi+\theta)-kr\sin\xi]}\, d\xi \tag{D.4}$$

or

$$J_j(kr)e^{ij\theta} = \frac{1}{2\pi}\int_{-\pi}^{\pi} e^{i[j(\xi+\pi/2)-kr\cos(\xi-\theta)]}\, d\xi \tag{D.5}$$

For the modified Bessel functions:

$$\begin{aligned} I_j(kr)e^{ij\theta} &= e^{-\frac{ij\pi}{2}} J_j(ikr) \\ &= \frac{1}{2\pi}\int_{-\pi}^{\pi} e^{[ij\xi+kr\cos(\xi-\theta)]}\, d\xi \end{aligned} \tag{D.6}$$

Substituting (D.5) and (D.7) in (D.2) gives

$$\begin{aligned} w(r,\theta) &= \int_{-\pi}^{\pi} \left\{ \sum_{j=-\infty}^{\infty} c_j^{(1)} e^{ij(\xi+\pi/2)} \right\} e^{-ikr\cos(\xi-\theta)}\, d\xi \\ &\quad + \int_{-\pi}^{\pi} \left\{ \sum_{j=-\infty}^{\infty} c_j^{(2)} e^{ij\xi} \right\} e^{kr\cos(\xi-\theta)}\, d\xi \end{aligned} \tag{D.7}$$

The expressions in the braces in (D.8) are two unknown periodic functions of ξ with the fundamental period 2π. Let these functions be denoted $D^1(\xi)$ and $D^2(\xi)$. Therefore (D.8) is rewritten as:

$$w(r,\theta) = \int_{-\pi}^{\pi} D^1(\xi) e^{-ikr\cos(\xi-\theta)}\, d\xi + \int_{-\pi}^{\pi} D^2(\xi) e^{kr\cos(\xi-\theta)}\, d\xi \tag{D.8}$$

E. Expressions for the boundary conditions for the PWBM

In this Appendix, the expressions for the boundary quantities B_i $(i = 1, 2)$ presented in Chapter 2, will be derived for a function f of the form

$$\mathrm{f}(\mathbf{x}) = e^{\alpha x_1 + \beta x_2} \tag{E.1}$$

Thus, their corresponding expressions for the propagating and evanescent waves used in the PWBM will be deduced easily by substituting the appropriate expressions for α and β in the formulae.
In what follows, $\mathbf{x} = (x_1, x_2)$ denotes the point of the boundary $\partial\Omega$ at which the boundary quantity is enforced, $\mathbf{n} = (n_1, n_2)$ is the unit outward normal on $\partial\Omega$ at $\mathbf{x}$ and $\mathbf{s} = (-n_2, n_1)$ is the counterclockwise tangential derivative along $\partial\Omega$ at $\mathbf{x}$.

E.1 Boundary quantities for straight element

In this section, the boundary quantities for a straight element, i.e. the radius of curvature of the boundary curve is infinite, are derived.

Transverse displacement

$$f(x_1, x_2) = e^{\alpha x_1 + \beta x_2} \tag{E.2}$$

Slope

$$\frac{\partial f}{\partial \mathbf{n}}(x_1, x_2) = (\alpha n_1 + \beta n_2)\, e^{\alpha x_1 + \beta x_2} \tag{E.3}$$

Bending moment

$$\begin{aligned} M_n(f)(\mathbf{x}) &= \left[\Delta f - (1-\nu)\frac{\partial^2 f}{\partial \mathbf{s}^2}\right](x_1, x_2) && \text{(E.4)} \\ &= \left[\nu(\alpha^2+\beta^2) + (1-\nu)(n_1^2\alpha^2 + n_2^2\beta^2 + 2n_1n_2\alpha\beta)\right] e^{\alpha x_1 + \beta x_2} \end{aligned}$$

Equivalent shear force

$$\begin{aligned} V_n(f)(\mathbf{x}) &= \left[\frac{\partial}{\partial \mathbf{n}}\Delta f + (1-\nu)\frac{\partial}{\partial \mathbf{s}}\left(\frac{\partial^2 f}{\partial \mathbf{n}\partial \mathbf{s}}\right)\right](x_1, x_2) && \text{(E.5)} \\ &= \left[n_1(\alpha^3 + \alpha\beta^2) + n_2(\beta\alpha^2 + \beta^3)\right] e^{\alpha x_1 + \beta x_2} && \text{(E.6)} \\ &\quad + \left\{(1-\nu)\left[n_1n_2(\alpha^3 - \alpha\beta^2) - (n_1^2 - n_2^2)\beta\alpha^2\right] n_2\right\} e^{\alpha x_1 + \beta x_2} \\ &\quad - \left\{(1-\nu)\left[n_1n_2(\beta\alpha^2 - \beta^3) - (n_1^2 - n_2^2)\alpha\beta^2\right] n_1\right\} e^{\alpha x_1 + \beta x_2} \end{aligned}$$

E.2 Boundary quantities for curved element

In this section, the boundary quantities for curved element, i.e. the radius of curvature is finite and equal to R, are derived.

Transverse displacement

$$f(x_1, x_2) = e^{\alpha x_1 + \beta x_2} \tag{E.7}$$

Slope

$$\frac{\partial f}{\partial \mathbf{n}}(x_1, x_2) = (\alpha n_1 + \beta n_2)\, e^{\alpha x_1 + \beta x_2} \tag{E.8}$$

Bending moment

$$\begin{aligned} M_n(f)(\mathbf{x}) &= \left[\Delta f - (1-\nu)\left(\frac{1}{R}\frac{\partial f}{\partial \mathbf{n}} + \frac{\partial^2 f}{\partial \mathbf{s}^2}\right)\right](x_1, x_2) \qquad \text{(E.9)} \\ &= \nu(\alpha^2+\beta^2)e^{\alpha x_1+\beta x_2} \\ &\quad + (1-\nu)\left[n_1^2\alpha^2 + n_2^2\beta^2 + 2n_1n_2\alpha\beta - \frac{1}{R}(n_1\alpha + n_2\beta)\right] e^{\alpha x_1+\beta x_2} \end{aligned}$$

Equivalent shear force

$$\begin{aligned} V_n(f)(\mathbf{x}) &= \left[\frac{\partial}{\partial \mathbf{n}}\Delta f + (1-\nu)\frac{\partial}{\partial \mathbf{s}}\left(\frac{\partial^2 f}{\partial \mathbf{n}\partial \mathbf{s}} - \frac{1}{R}\frac{\partial f}{\partial \mathbf{s}}\right)\right](x_1, x_2) \qquad \text{(E.10)} \\ &= \left[n_1(\alpha^3 + \alpha\beta^2) + n_2(\beta\alpha^2 + \beta^3)\right] e^{\alpha x_1+\beta x_2} \qquad \text{(E.11)} \\ &\quad + \left\{(1-\nu)\left[n_1n_2(\alpha^3 - \alpha\beta^2) - (n_1^2 - n_2^2)\beta\alpha^2\right] n_2\right\} e^{\alpha x_1+\beta x_2} \\ &\quad - \left\{(1-\nu)\left[n_1n_2(\beta\alpha^2 - \beta^3) - (n_1^2 - n_2^2)\alpha\beta^2\right] n_1\right\} e^{\alpha x_1+\beta x_2} \\ &\quad + \left[\frac{(1-\nu)}{R}\left(n_2^2\alpha^2 - 2n_1n_2\alpha\beta + n_2^2\beta^2\right)\right] e^{\alpha x_1+\beta x_2} \end{aligned}$$

E.3 Boundary quantities for free corner points

In this section, the expression of the twisting moment M_{ns}, used in the formulation of the boundary condition for corner points of a free polygonal structure (see Appendix G), is derived.

$$\begin{aligned} M_{ns}(f)(\mathbf{x}) &= (1-\nu)\frac{\partial^2}{\partial \mathbf{n}\partial \mathbf{s}} f(x_1, x_2) \qquad \text{(E.12)} \\ &= \left\{-(1-\nu)\left[n_1n_2(\alpha^2 - \beta^2) - (n_1^2 - n_2^2)\alpha\beta)\right]\right\} e^{\alpha x_1+\beta x_2} \end{aligned}$$

F. Application of the Weighted Residual method and the Galerkin method to the PWBM

F.1 General remarks

The PWBM has been numerically implemented by applying the collocation method. However, it was seen that this technique was less efficient in the study of the vibrations of plates with free edges. In this Appendix, two other approximate methods, namely the Weighted Residual method and the Galerkin method, are presented. As seen earlier, the PWBM approximate the solution of the plate vibration problem by the superposition of propagating and evanescent plane wave functions, i.e.

$$w(\mathbf{x}) = \sum_{j=1}^{n} D_j^1 u_{\xi_j} + \sum_{j=1}^{n} D_j^2 v_{\xi_j} \tag{F.1}$$

where u_{ξ_j} and v_{ξ_j} are the propagating and evanescent waves introduced in Chapter 4 respectively. The unknown parameters D_j^1 and D_j^2 are determined so that the approximate solution satisfies the boundary conditions. There are several different technique to determine them but all of them try to minimise the errors ε_1 and ε_2 on the boundary:

$$\begin{cases} \varepsilon_1 = B_1(w) - 0, & \text{on } \partial\Omega \\ \varepsilon_2 = B_2(w) - 0, & \text{on } \partial\Omega \end{cases} \tag{F.2}$$

where B_2 and B_2 represent the boundary quantities, introduced in Chapter 2, that realize the boundary condition enforced along the edges of the plate.

The weighted residual techniques consists in *distributing* the errors with m weighting functions denoted $\{\psi_i\}_{i=1,\ldots,n}$. The distribution of the errors is carried out by writing:

$$\begin{cases} \int_{\partial\Omega} \varepsilon_1 \psi_i \, dS = 0, & \text{for } i = 1, 2, \ldots, n \\ \int_{\partial\Omega} \varepsilon_2 \psi_i \, dS = 0 & \text{for } i = 1, 2, \ldots, n \end{cases} \tag{F.3}$$

For example, when the weighting functions ψ_i are taken as:

$$\psi_i(\mathbf{x}) = \delta(\mathbf{x} - \mathbf{x}^i), \quad \text{with } \mathbf{x}^i \in \partial\Omega \tag{F.4}$$

where δ is the Dirac delta function, (F.3) becomes

$$\begin{cases} B_1(w)(\mathbf{x}^i) = 0, & \text{for } i = 1, 2, \ldots, n \\ B_2(w)(\mathbf{x}^i) = 0, & \text{for } i = 1, 2, \ldots, n \end{cases} \tag{F.5}$$

The above formulation gives the same numerical results as the collocation method with the points $\mathbf{x}^i$ being the nodal points. Hence, the collocation method may be considered as a particular weighted residual method. This latter is however, more general as other types of ψ_i functions can be used.

F.2 The Weighted Residual method

The conventional weighted residual method was applied to a square plate. The weighting functions ψ_i were composed from two sets ψ_i^1 and ψ_i^2 defined as:

$$\begin{cases} \psi_i^1 = \sin \dfrac{2\pi i s}{L}, & i = 1, \ldots, n/2 \\ \psi_i^2 = \cos \dfrac{2\pi i s}{L}, & i = 1, \ldots, n/2 \end{cases} \tag{F.6}$$

where L is the perimeter of the plate and s is the arc length along the boundary, such that:

$$L = \int_{\partial\Omega} ds \tag{F.7}$$

Substituting (F.6) in (F.3) yields:

$$\begin{cases} \displaystyle\int_{\partial\Omega} \varepsilon_1 \psi_i^1 \, dS + \int_{\partial\Omega} \varepsilon_1 \psi_i^2 \, dS = 0, & \text{for } i = 1, 2, \ldots, n/2 \\ \displaystyle\int_{\partial\Omega} \varepsilon_2 \psi_i^1 \, dS + \int_{\partial\Omega} \varepsilon_2 \psi_i^2 \, dS = 0 & \text{for } i = 1, 2, \ldots, n/2 \end{cases} \tag{F.8}$$

The boundary $\partial\Omega$ is then discretized in N segments. On each of these segments, the integrals in (F.8) are approximated by using a mid-ordinate rule at the middle of the segment $\mathbf{x}^j$. Hence, a linear system similar to the one obtained by using the collocation method is derived:

$$[A^w(k)]\vec{D} = 0 \tag{F.9}$$

where $[A^w(k)]$ is the resulting matrix and $\vec{D}$ is the vector constituted by the coefficient D_j^1 and D_j^2 introduced in (F.1). The eigenfrequencies are determined by solving $\det[A^w(k)] = 0$.

F.3 The Galerkin method

The only difference between the previous weighted residual method and this method consists in the choice of the weighting functions. Indeed, in the Galerkin method, the same functions are used to approximate the solution w and to act as weighting functions. Here, only the propagating waves are used as trial functions, thus

$$\psi_i^1 = u_{\xi_i}, \quad u_{\xi_i} \in \mathcal{B}'_p \tag{F.10}$$

The rest of the process of the Galerkin method is similar to the one of the weighted residual method, and a new linear system is obtained

$$[A^G(k)]\vec{D} = 0 \tag{F.11}$$

where $[A^G(k)]$ is the resulting matrix used to compute the eigenfrequencies.

F.4 Application

Both methods were first applied to a clamped square plate in order to evaluate their accuracy. The results are given in Table A. As can be seen, the Galerkin method introduced three spurious roots marked by the sign†. In the other cases, the agreement between the three method is obvious.

Mode no.	Collocation	WRM	Galerkin
1	6.0	6.0	6.0
			7.0†
2	8.6	8.6	8.6
			8.9†
3	10.4	10.4	10.4
			11.4†
4	11.5	11.5	11.5

†False eigenfrequencies

Table A: Comparison of the eigenfrequencies λ for a clamped square plate obtained with the collocation method, the weighted residual method (WRM) and the Galerkin method ($n = 20$, $N = 40$, $\Delta\lambda = 0.05$)

To explain the cause of these spurious roots produced by the Galerkin method, the matrix $[A^G(k)]$ is written as the product of the matrix $[A(k)]$ used in the collocation method and a matrix $[\Psi(k)]$ holding the different values of the weighting functions:

$$[\Psi(k)] = \left[\begin{array}{c|c} [\psi] & [0] \\ \hline [0] & [\psi] \end{array}\right]_{(2n\times 2N)} \tag{F.12}$$

where $[\psi]$ is the following matrix:

$$[\psi] = \begin{bmatrix} u_{\xi_1}(\mathbf{x}^1) & \dots & u_{\xi_1}(\mathbf{x}_N) \\ u_{\xi_n}(\mathbf{x}^1) & \dots & u_{\xi_n}(\mathbf{x}_N) \end{bmatrix}_{(n\times N)} \tag{F.13}$$

It can easily be shown that

$$[A^G(k)] = [\Psi(k)] \times [A(k)] \tag{F.14}$$

Thus,

$$\det[A^G(k)] = \det[\Psi(k)]\det[A(k)] \tag{F.15}$$

A quick look at $[\Psi(k)]$ shows that this matrix represents the matrix $[A(k)]$ used for a clamped square membrane. Hence, *the spurious eigenvalues are in fact the eigenfrequencies of a clamped square membrane.* If the propagating and the evanescent waves had been used, the situation would have remained the same but the spurious eigenvalues would become the eigenfrequencies of a square clamped plate. Hence, this method is unreliable.
Furthermore, the weighted residual method and the Galerkin method when applied to the case of a free square plate did not improve the poor accuracy of the results.

G. Boundary conditions at corner points of a free plate

One way to derive these expressions is to apply the principle of virtual work [25]. Thus, if w represents the equilibrium state of the plate and if there is no boundary stress acting on $\partial\Omega$, the following expression can be derived for a free plate [25]:

$$\frac{1}{D}\int_{\partial\Omega} Q_n\delta w - M_n\frac{\partial\delta w}{\partial \mathbf{n}} - M_{ns}\frac{\partial\delta w}{\partial \mathbf{s}}\,dS = \int_\Omega \left(\Delta^2 w + k^2 w\right)\,dV \tag{G.1}$$

for all virtual displacements δw. Q_n and M_{ns} are the shear force and the twisting couple respectively. They are defined by

$$\begin{aligned} Q_n &= \frac{\partial}{\partial \mathbf{n}}\Delta w \\ M_{ns} &= (1-\nu)\frac{\partial^2 w}{\partial \mathbf{n}\mathbf{s}} \end{aligned} \tag{G.2}$$

As stated before, multiplying these expressions by $-1/D$ produces the usual expressions. Using (G.2), V_n can be written as

$$V_n = Q_n - \frac{\partial M_{ns}}{\partial \mathbf{s}} \tag{G.3}$$

Thus, (G.1) becomes

$$\delta\int_{\partial\Omega} V_n\delta w - M_n\frac{\partial\delta w}{\partial \mathbf{n}}\,dS - [M_{ns}\delta w]_{\partial\Omega} = \int_\Omega \left(\Delta^2 w + k^2 w\right)\,dV \tag{G.4}$$

Therefore, in the case of a smooth boundary, the previously found boundary conditions and governing equation of vibration are obtained. But, if the boundary presents a discontinuity at the point **P**, (G.4) implies that a different boundary condition must be enforced at **P**, which prescribes the bending moment M_n and a concentrated force equal to:

$$[M_{ns}(w)]_{\mathbf{P}+} - [M_{ns}(w)]_{\mathbf{P}-} \tag{G.5}$$

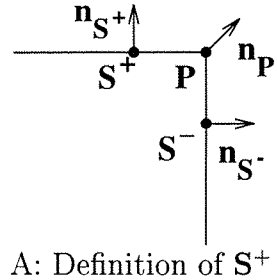

Figure A: Definition of S^+ and S^-

where $\mathbf{P}^+$ and $\mathbf{P}^-$ are respectively defined by

$$\mathbf{P}^+ = \lim_{\|\mathbf{S}^+ - \mathbf{P}\| \to 0} \mathbf{S}^+ \tag{G.6}$$

and,

$$\mathbf{P}^- = \lim_{\|\mathbf{S}^- - \mathbf{P}\| \to 0} \mathbf{S}^- \tag{G.7}$$

with $\mathbf{S}^+$ and $\mathbf{S}^-$ defined as shown in Figure A.
Therefore, two different boundary conditions will be encountered in the case of a free plate. Along a free edge, the boundary condition will be

$$\begin{cases} M_n(w) = 0 \\ V_n(w) = 0 \end{cases} \tag{G.8}$$

and, at a corner point, it will be written as

$$\begin{cases} M_n(w) = 0 \\ M_{ns}^+(w) - M_{ns}^-(w) = 0 \end{cases} \tag{G.9}$$

where M_{ns}^+ and M_{ns}^- represent the right-hand and the left-hand limits defined earlier. In practice, M_{ns}^+ and M_{ns}^- will be determined by evaluating the twisting moment at two points placed slightly away from the corner point.
In the case of a square plate, the corner condition can be rewritten [51]

$$\begin{cases} M_n(w) = 0, \\ \dfrac{\partial^2 w}{\partial x \partial y} = 0 \end{cases} \tag{G.10}$$

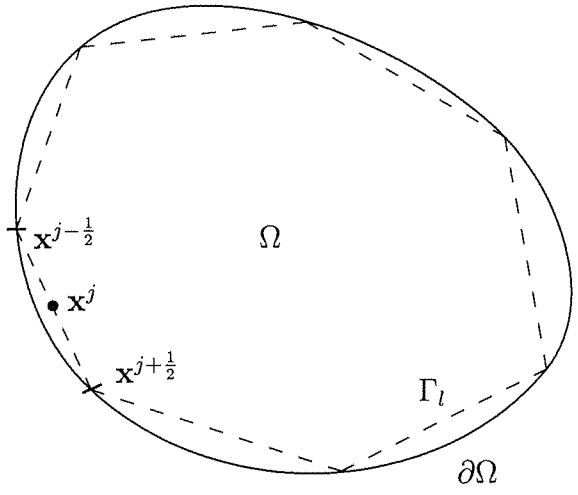

Figure 1: Approximation of the boundary $\partial\Omega$ by straight line segments Γ_l with the interval points $\mathbf{x}^{j\pm\frac{1}{2}}$ and the nodal points $\mathbf{x}^j$ in the IBEM

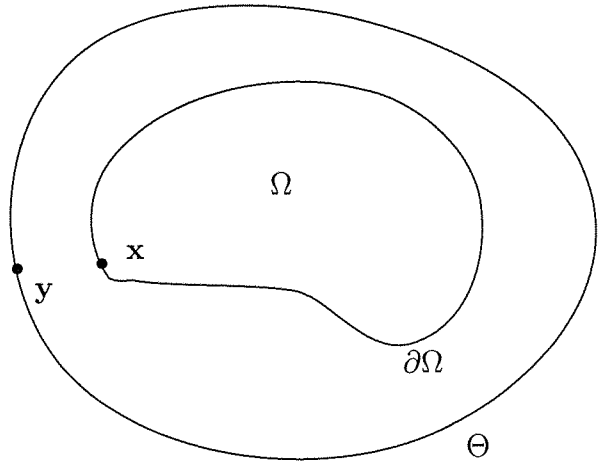

Figure 2: Location of the imaginary source boundary Θ in the EIBEM with $\mathbf{x}$ being the load point and $\mathbf{y}$ being the source point

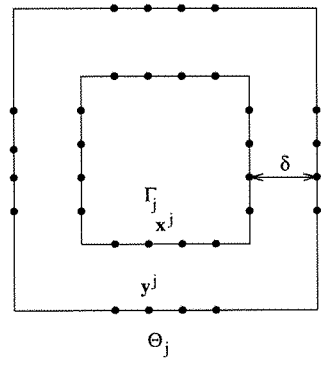

Figure 3: The position of the source points $\mathbf{y}^j$ and the collocation points $\mathbf{x}^j$ when using an homothetic exterior boundary in the EIBEM

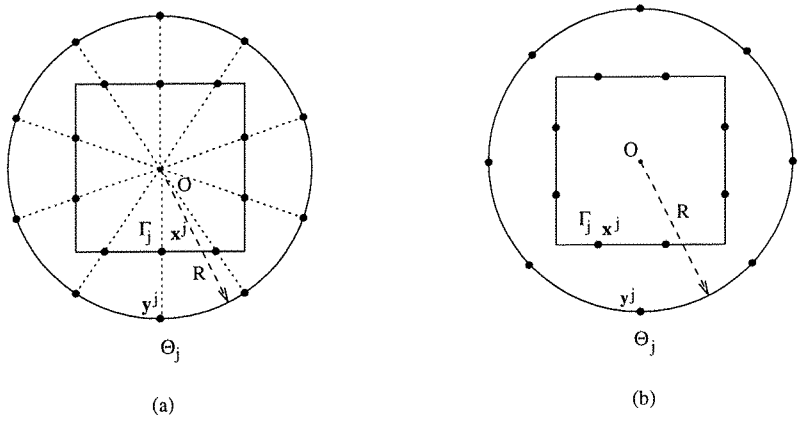

Figure 4: The two methods used to collocate the points $\mathbf{x}^j$ on a square membrane in the EIBEM

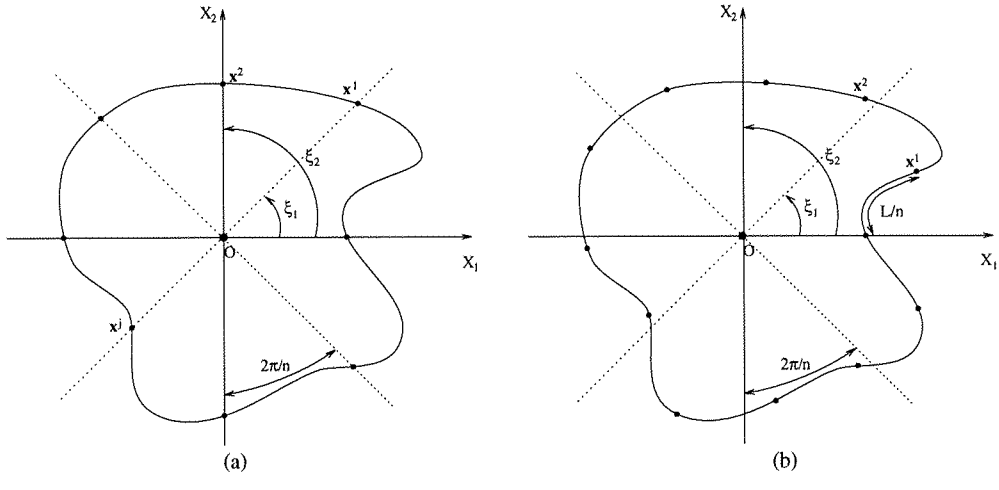

Figure 5: The two types of discretization used in the PWBM

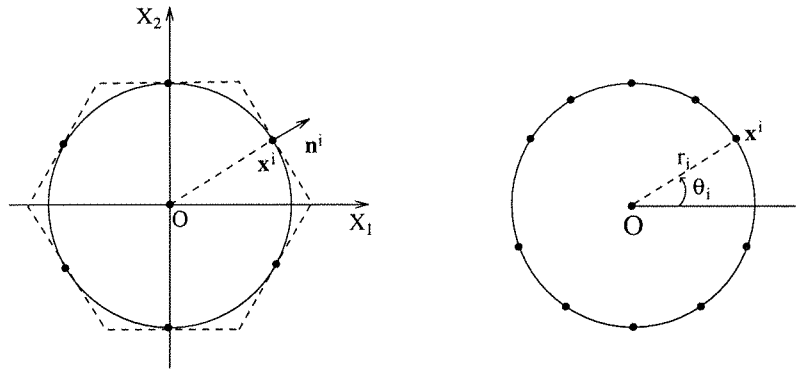

Figure 6: The polygonal and the circle-specific discretizations used in the PWBM for a free circular plate

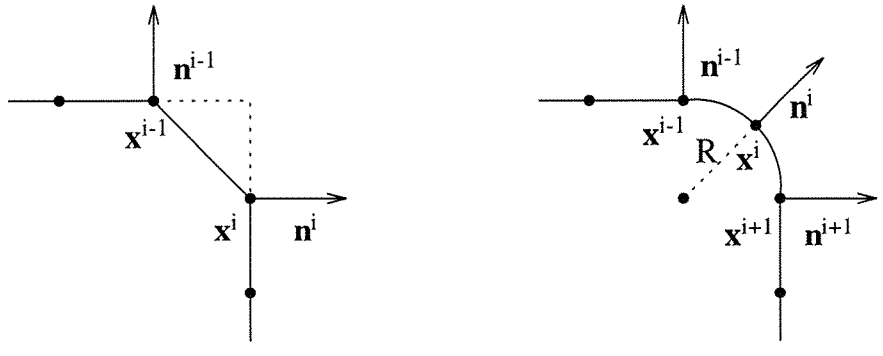

Figure 7: Types of discretizations used for a corner point which round the corner point

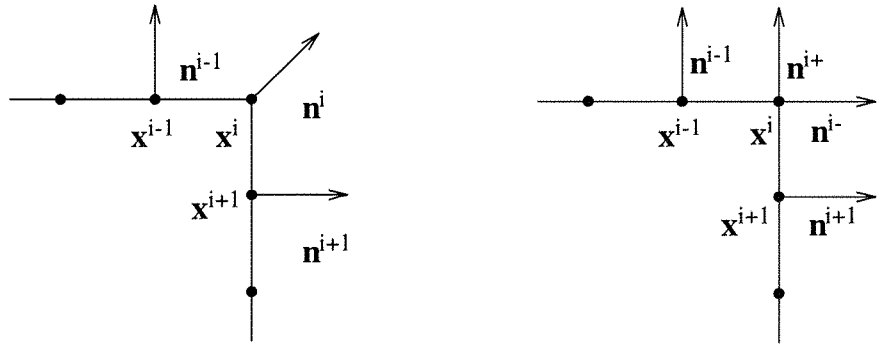

(a) (b)

Figure 8: Types of discretizations used for a corner point which take the corner point into account

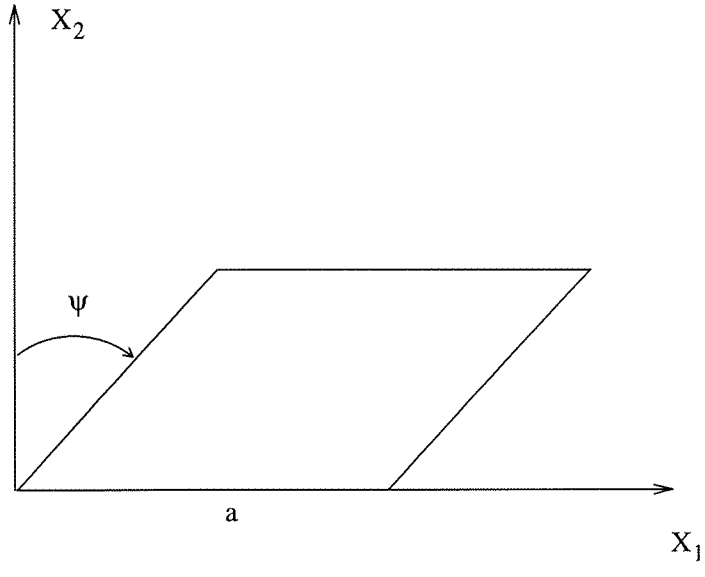

Figure 9: Parameters for the skew planform

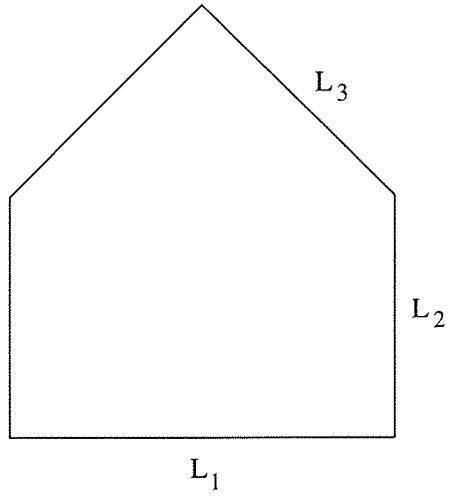

Figure 10: The geometry of the pentagonal membrane
($L_1 = 2.0$, $L_2 = 1.0$, $L_3 = \sqrt{5}$)

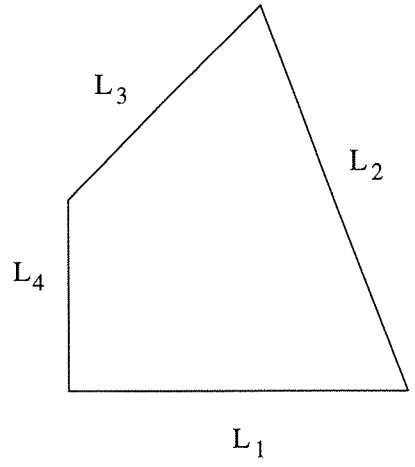

Figure 11: The geometry of a quadrilateral membrane with unequal edges
($L_1 = 2.7$, $L_2 = 3.08$, $L_3 = 2.5$, $L_4 = 1.5$)

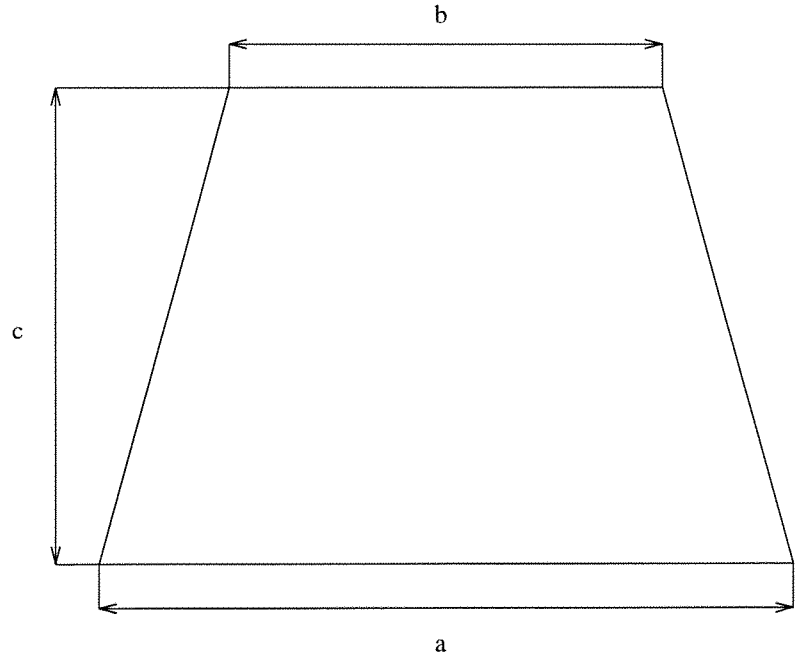

Figure 12: Parameters for a symmetrical trapezoidal plate

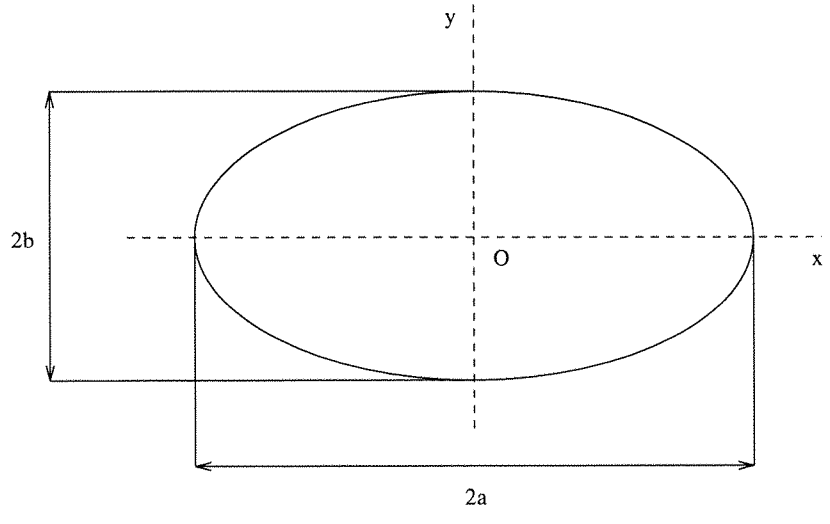

Figure 13: Parameters for an elliptical plate

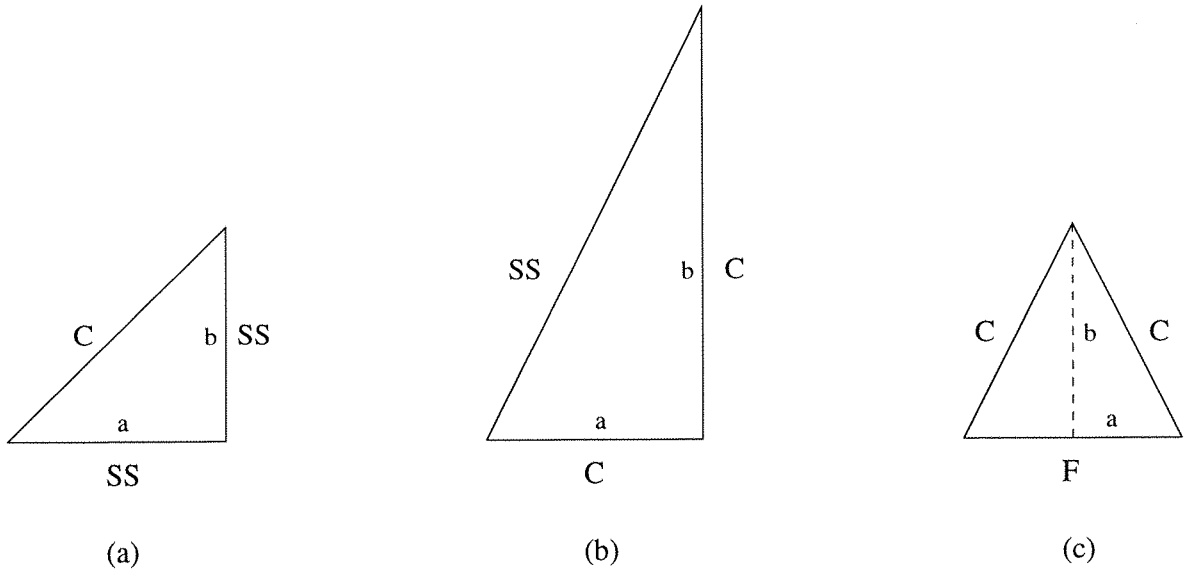

Figure 14: The three types of triangular plates with mixed boundary conditions

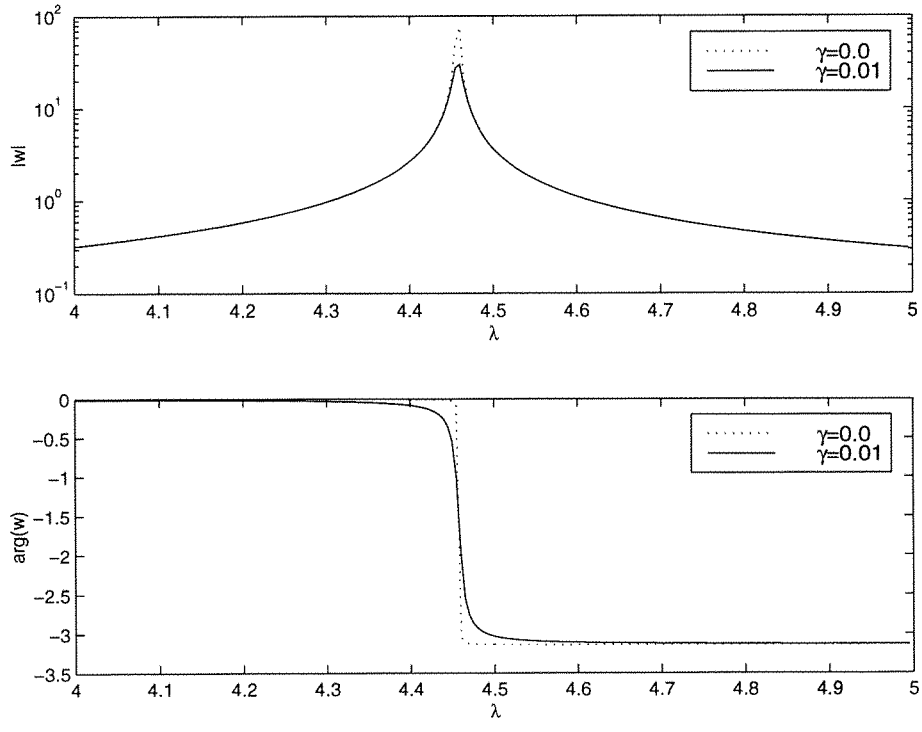

Figure 15: Forced response of a clamped square membrane to a point located force for different damping coefficients γ determined with the IBEM

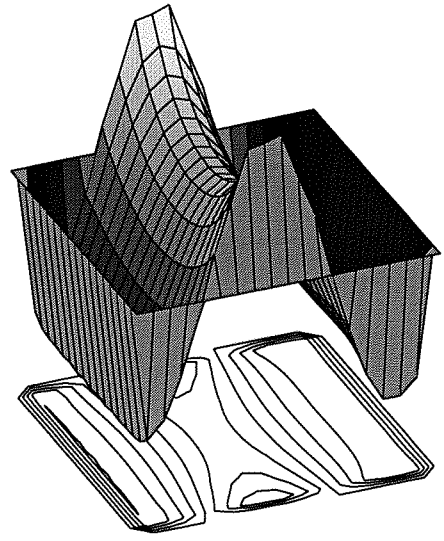

Figure 16: Forced response of a clamped square membrane to a surface wave determined with the IBEM

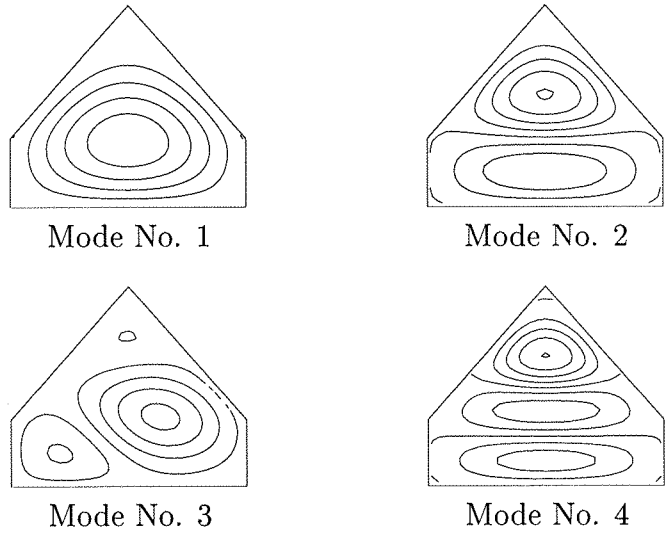

Figure 17: The first 4 modes of the pentagonal membrane shown in Figure 10 determined with the IBEM

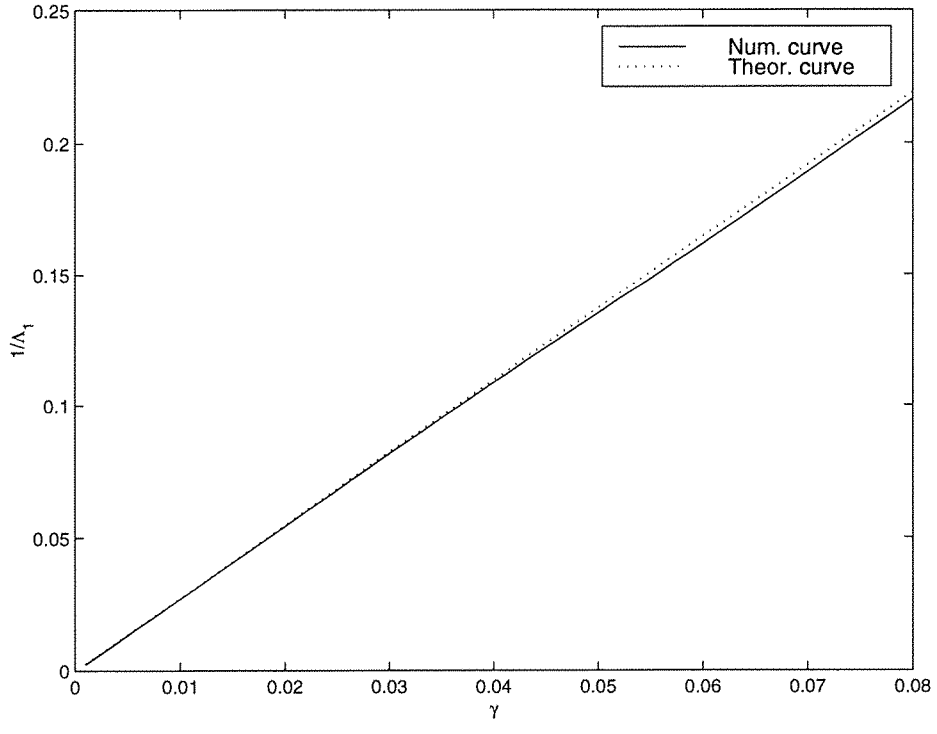

Figure 18: Magnitude of the inverse of the modal factor Λ_1 for different values of the damping coefficients γ determined with the IBEM

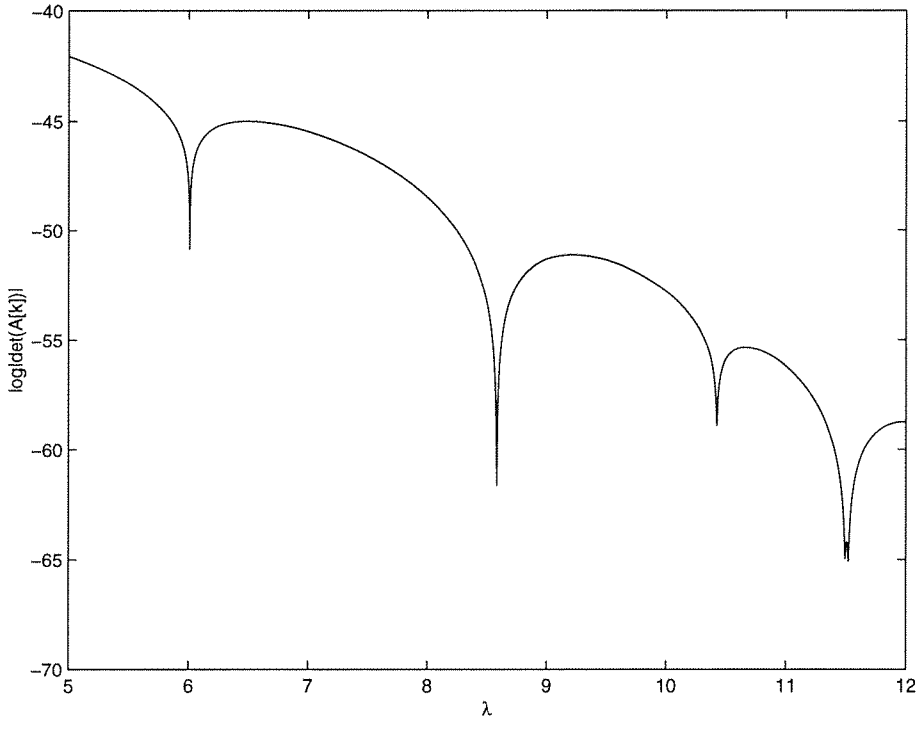

Figure 19: Eigenfrequencies $\lambda = ka$ of a clamped square plate as the minima of $|\det([A(k)])|$ in the IBEM

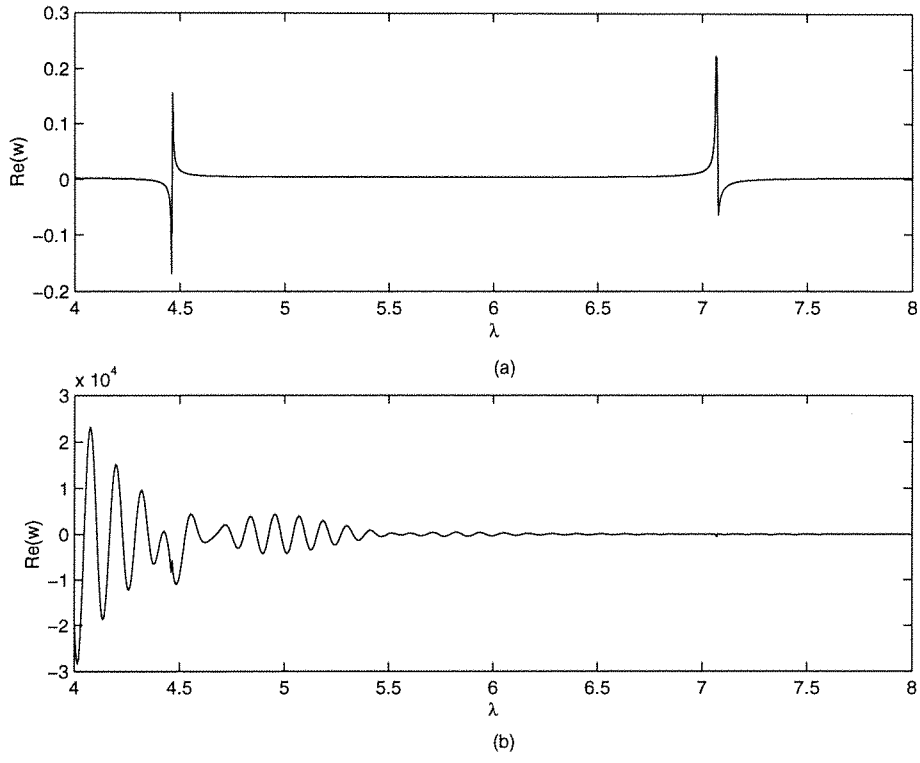

Figure 20: Real part of the forced response of a square membrane to a surface wave travelling in the direction (-10.0,-10.0) for two different condition numbers, determined by using the EIBEM ($n = 24, \Delta\lambda = 0.005$)

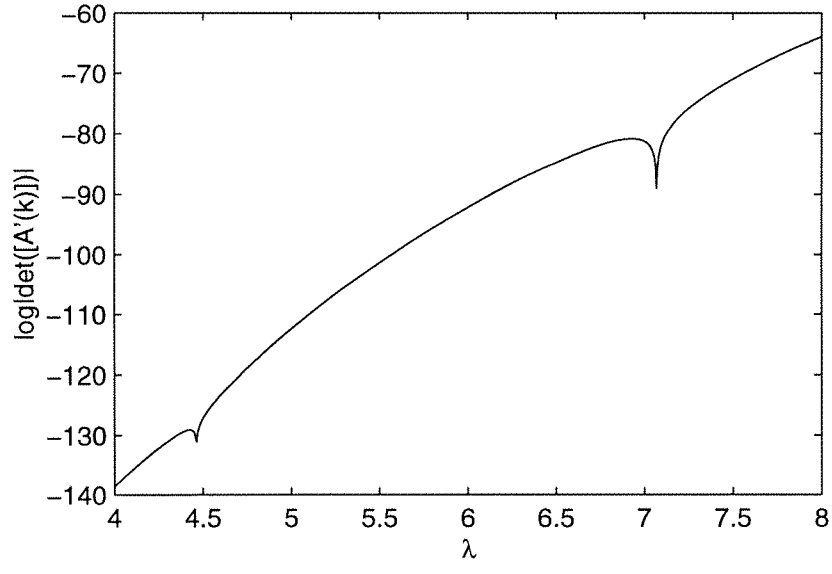

Figure 21: Eigenfrequencies of a clamped square membrane determined with an ill-conditioned matrix and the EIBEM ($n = 24$, $\Delta\lambda = 0.005$)

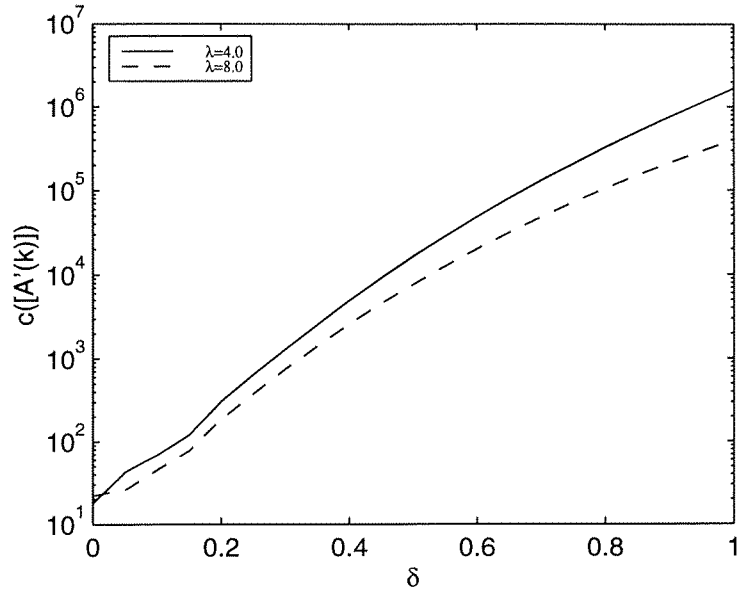

Figure 22: Condition number for a square membrane and an homothetic exterior boundary shown in Figure 3 in the EIBEM

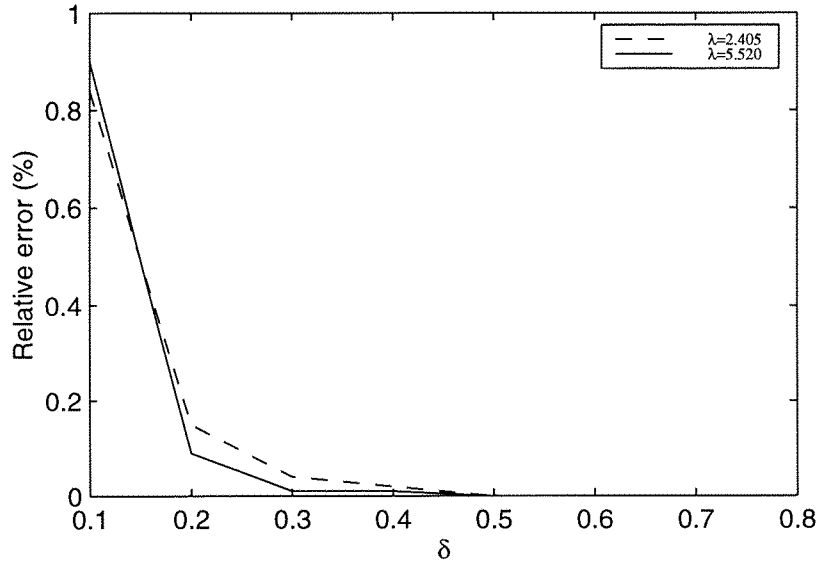

Figure 23: The absolute relative error of the first and sixth eigenfrequencies of a clamped circular membrane when using the EIBEM with an homothetic imaginary boundary ($n = 20$)

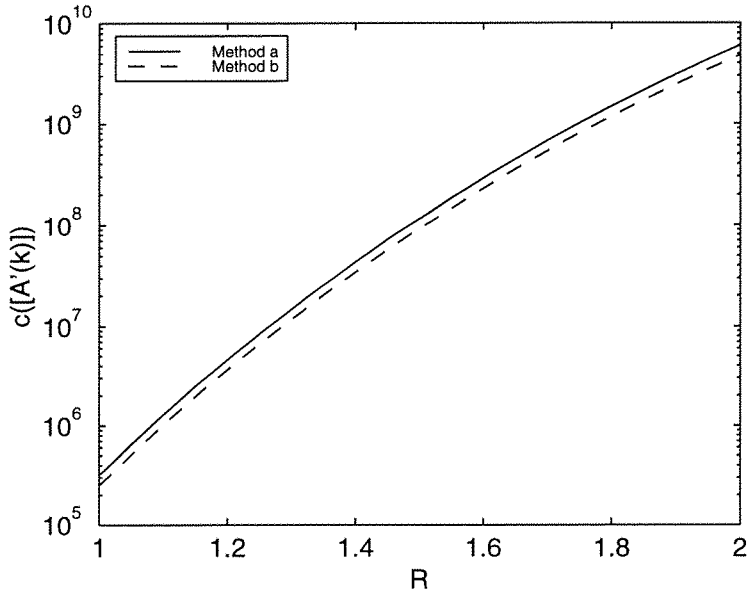

Figure 24: Condition number for a circular exterior boundary of radius R and for the two different types of collocation point shown in Figure 4 in the EIBEM

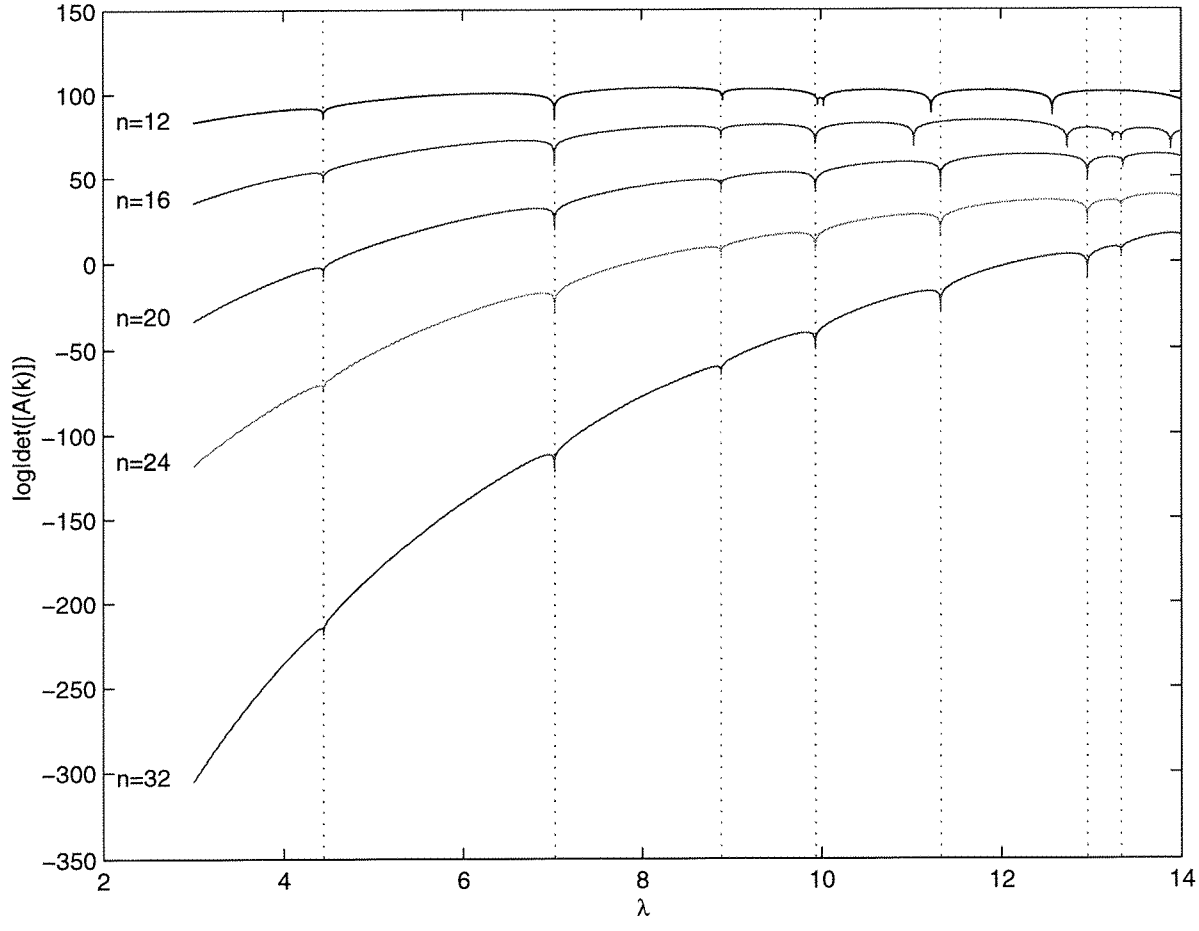

Figure 25: Influence of n upon the eigenfrequencies of a clamped square membrane ($\Delta\lambda = 0.0001$) in the PWBM; dotted lines indicate the theoretical values

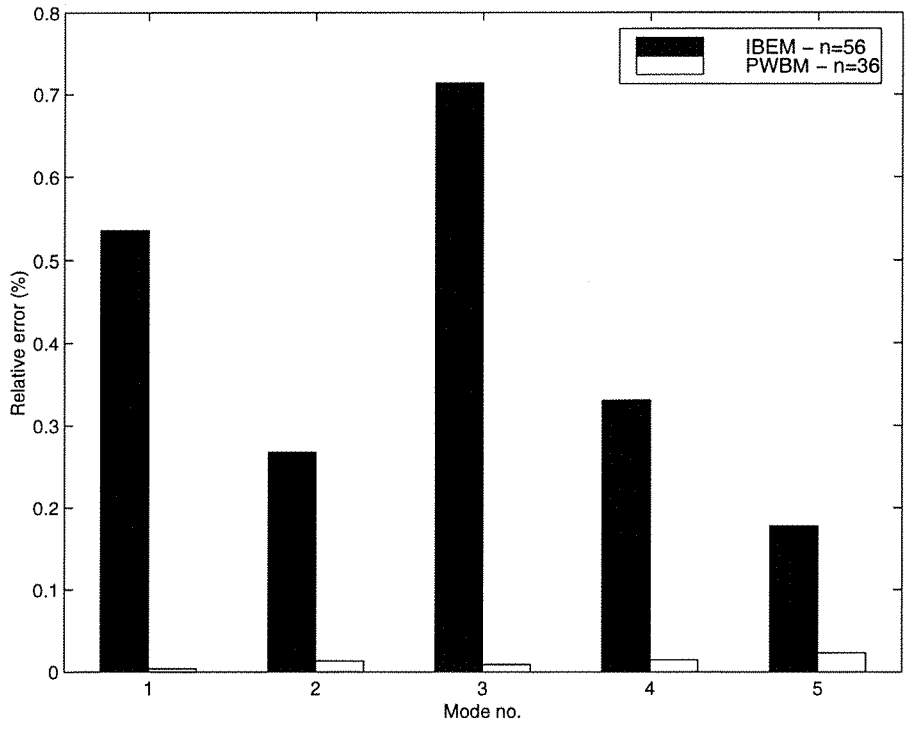

Figure 26: Relative errors on each mode of a clamped skew membrane ($\psi = 35°$) in the PWBM and the IBEM

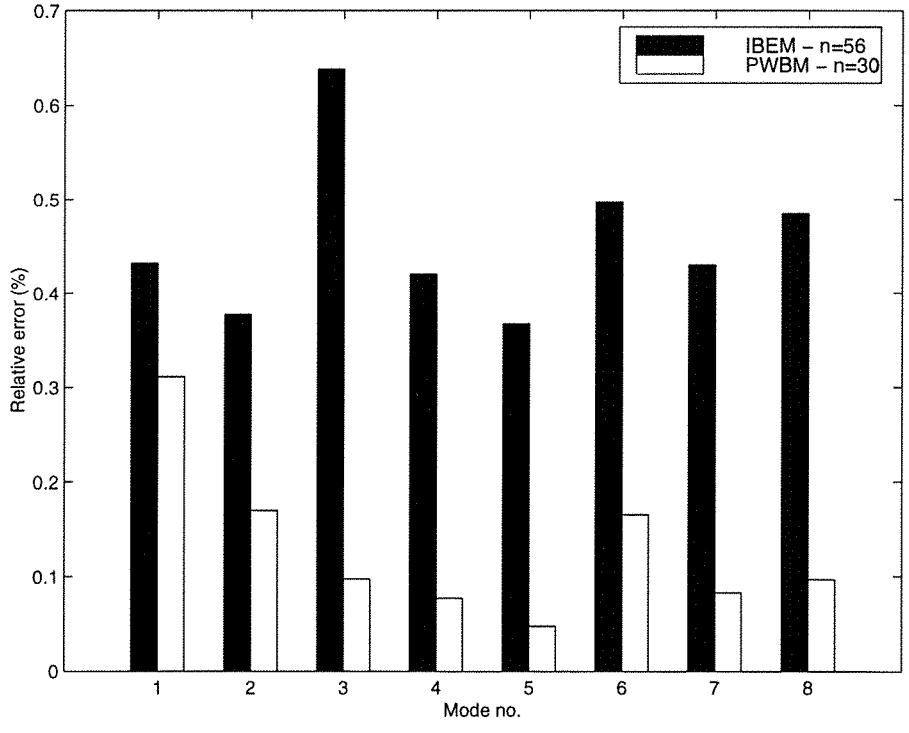

Figure 27: Relative errors on each mode of the clamped pentagonal membrane, shown in Figure 10, in the PWBM and the IBEM

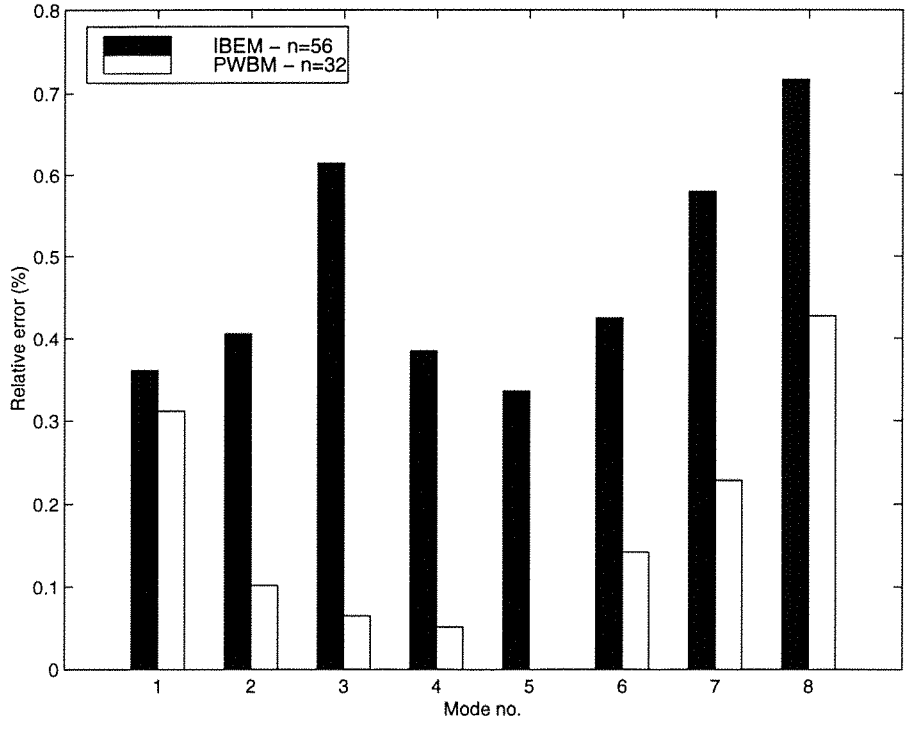

Figure 28: Relative errors on each mode of the clamped quadrilateral membrane with unequal edges, shown in Figure 11, in the PWBM and the IBEM

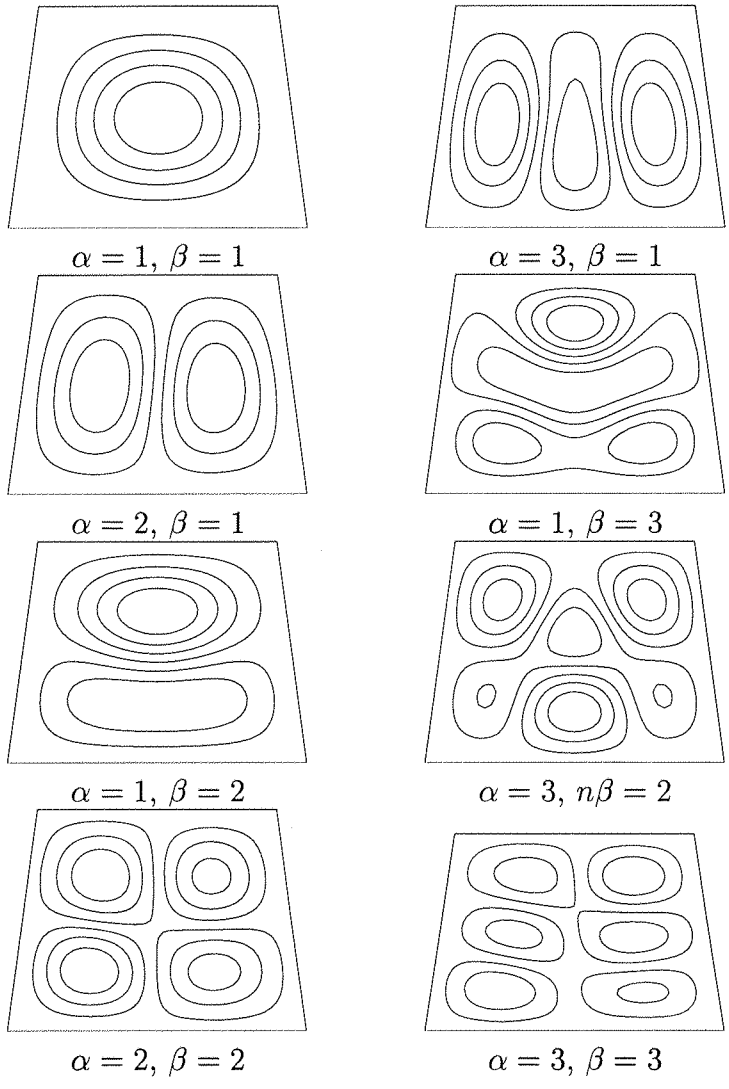

Figure 29: The first 8 mode shapes of a symmetrical trapezoidal clamped plate with $b/a = 0.8$ and $c/a = 0.75$ obtained with the PWBM

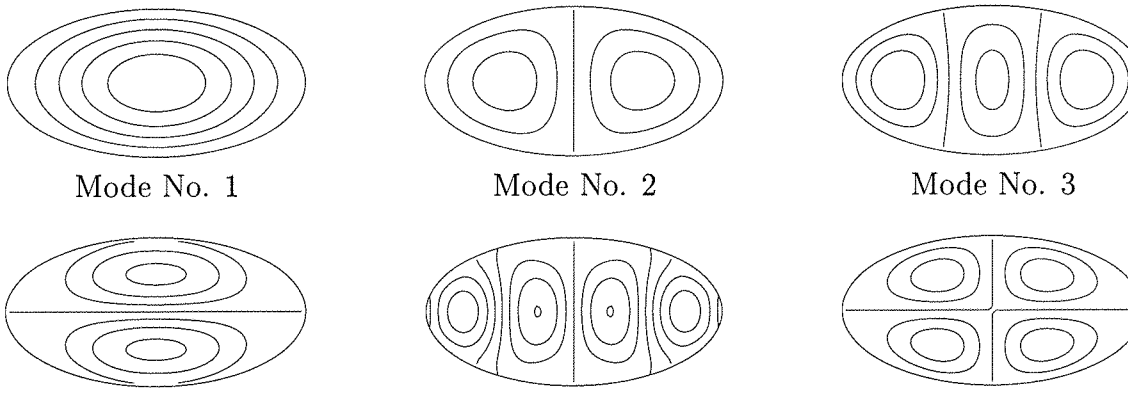

Figure 30: Modes of a simply supported elliptical plate ($a/b = 2.0$) obtained with the PWBM

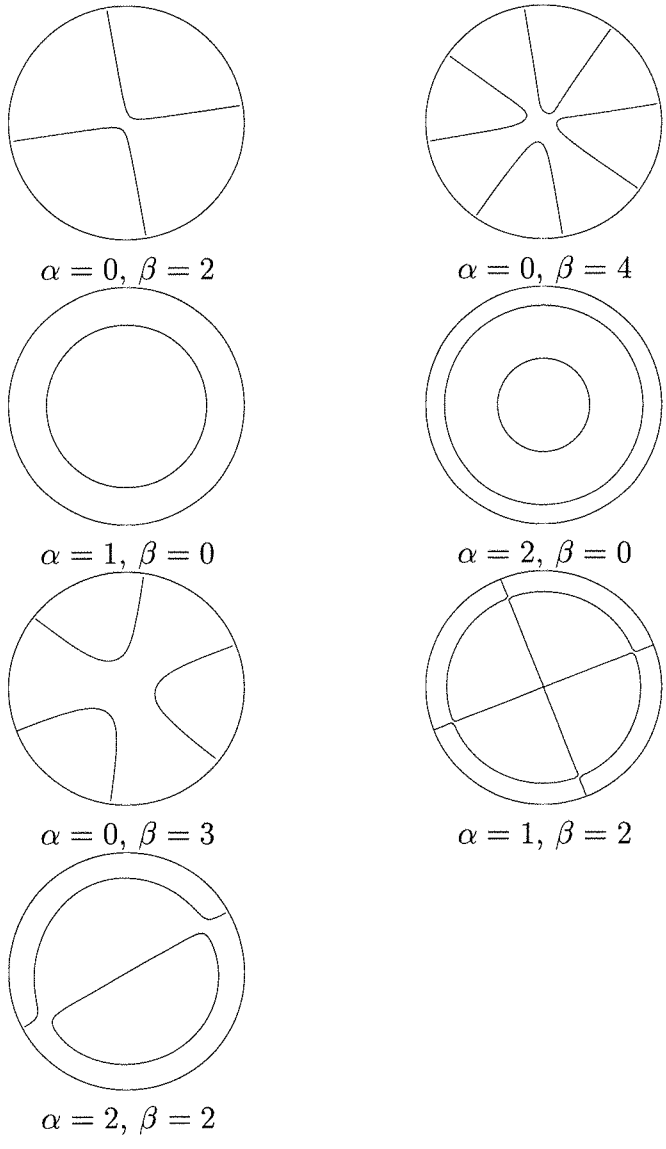

Figure 31: Examples of modes of a free circular plate obtained with the PWBM and the forced response technique ($\nu = 0.33$)

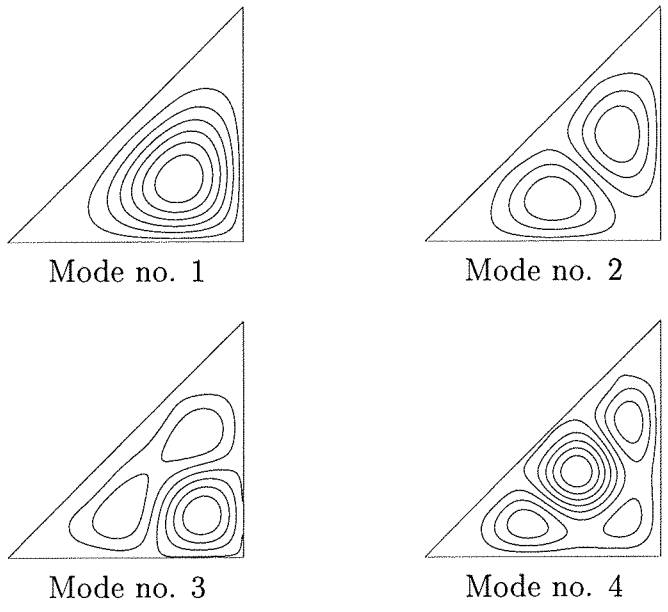

Figure 32: The first 4 modes of a clamped-simply supported-simply supported right triangular shown plate in Figure 14 (a) obtained with the PWBM

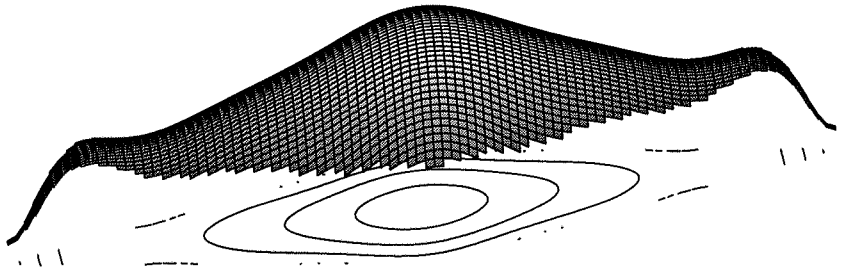

Figure 33: Forced response to a pressure load of a clamped skew membrane of skew angle $\psi = 70°$ obtained with the PWBM

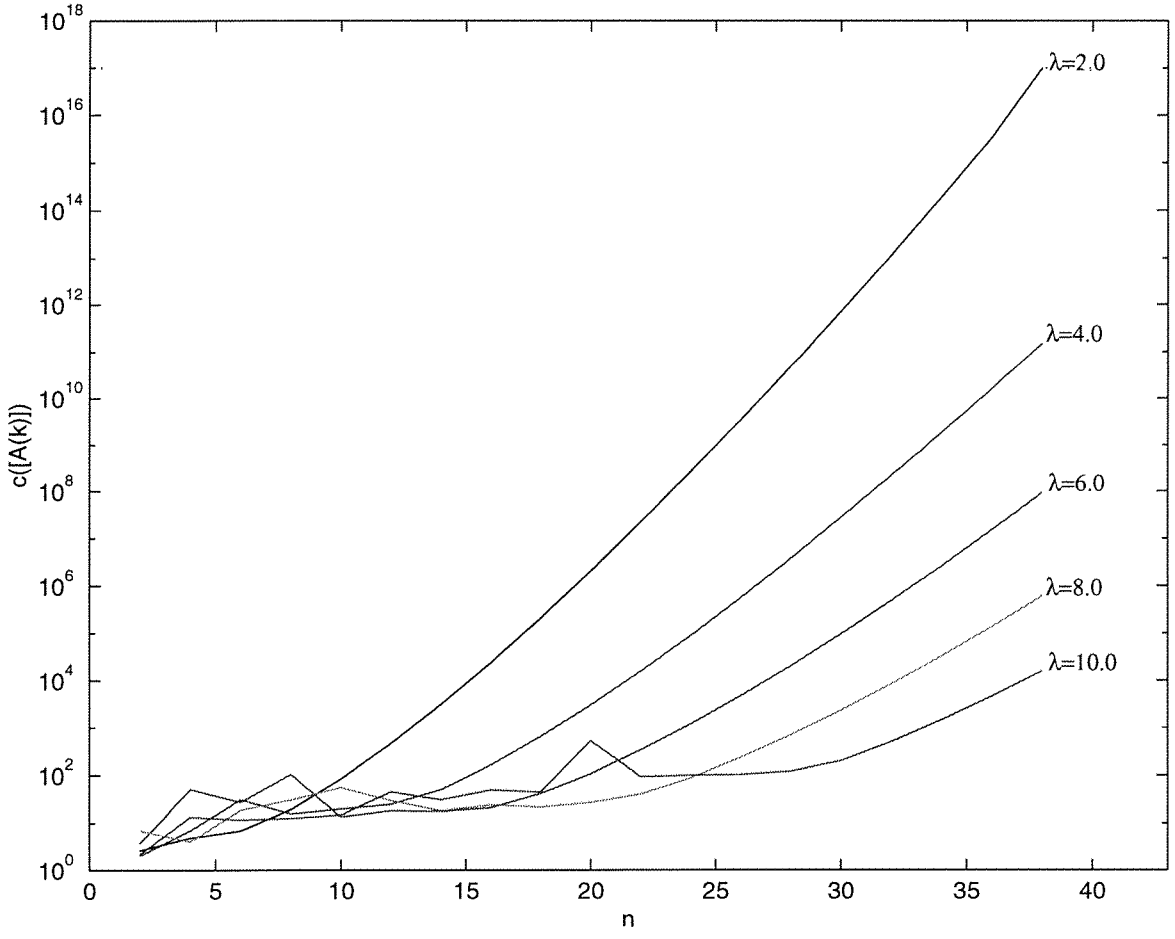

Figure 34: Influence of n upon the condition number for a clamped circular membrane in the PWBM

Skew Angle ψ	Method	Mode No.				
		1	2	3	4	5
15°	IBEM	4.586	6.967	7.526	8.928	10.234
	Rayleigh-Ritz [20]	4.568	6.943	7.493	8.894	10.201
20°	IBEM	4.690	7.024	7.790	8.971	10.451
	Rayleigh-Ritz [20]	4.672	7.025	7.750	8.941	10.418
30°	IBEM	5.016	7.283	8.531	9.198	11.127
	Rayleigh-Ritz [20]	4.992	7.257	8.473	9.161	11.087
35°	IBEM	5.253	7.500	9.040	9.402	11.298
	Rayleigh-Ritz [20]	5.225	7.480	8.976	9.371	11.278
45°	IBEM	5.944	8.179	10.072	10.476	11.924
	Rayleigh-Ritz [20]	5.900	8.146	10.025	10.358	11.875

Table 1: Comparison of eigenvalues λ for skew membranes with various skew angles ($n = 56$, $\Delta\lambda = 0.0005$)

Mode No.	IBEM	FEM [45]
1	2.316	2.300
2	3.442	3.424
3	3.757	3.730
4	4.515	4.493
5	4.896	4.876
6	5.227	5.208
7	5.580	5.560
8	5.983	5.959

Table 2: Comparison of eigenvalues k for the pentagonal membrane shown on Figure 10 ($n = 56$, $\Delta\lambda = 0.0005$)

Mode No.	IBEM	FEM [45]
1	1.939	1.926
2	2.956	2.941
3	3.091	3.074
4	3.903	3.886
5	4.171	4.157
6	4.236	4.224
7	4.828	4.811
8	5.164	5.149

Table 3: Comparison of eigenvalues k for a quadrilateral membrane shown on Figure 11 ($n = 56$, $\Delta\lambda = 0.0005$).

Mode No.	IBEM	HFEM [6]	Relative error (in %)
1	6.009	5.999	0.17
2	8.583	8.567	0.19
3	10.424	10.403	0.20
4	11.495	11.471	0.21
5	11.522	11.498	0.21

Table 4: Comparison of the eigenvalues λ for a clamped square plate ($n = 54$, $\Delta\lambda = 0.001$)

Mode No.	IBEM	HFEM [6]	Relative error (in %)
1	8.144	8.102	0.52
2	10.349	10.320	0.28
3	12.224	12.178	0.38
4	12.644	12.539	0.83

Table 5: Comparison of the eigenvalues λ for a clamped skew plate of skew angle $\psi = 45°$ ($n = 54$, $\Delta\lambda = 0.001$)

Mode No.	Shape of the exterior boundary Θ		
	Homothetic square	Circle Method a	Circle Method b
1	4.450 (0.16)	4.443 (0.00)	4.450 (0.16)
2	7.043 (0.25)	7.025 (0.00)	7.043 (0.25)
3	8.939 (0.60)	8.886 (0.00)	8.939 (0.60)
4	9.934 (0.01)	9.935 (0.00)	9.935 (0.00)
5	11.410 (0.73)	11.330 (0.06)	11.410 (0.73)
6	12.984 (0.24)	12.953 (0.00)	12.983 (0.24)
7	13.474 (1.08)	13.327 (0.01)	13.472 (1.06)

Table 6: Comparison of the eigenfrequencies λ for a clamped square plate, ($n = 24$, $\Delta\lambda = 0.0005$) in the EIBEM; the relative error is shown in parentheses

Mode no.	Exact Solution [14]	Numerical solution
1	2.405	2.405
2,3	3.832	3.832
4,5	5.136	5.136
6	5.520	5.520
7,8	6.380	6.380
9,10	7.016	7.016
11,12	7.588	7.589
13,14	8.417	8.417
15	8.654	8.654
16,17	8.771	8.772
18,19	9.761	9.761
20,21	9.936	9.936

Table 7: Exact and computed eigenfrequencies λ of a clamped circular membrane using the PWBM ($n = 36$, $\Delta\lambda = 0.0005$)

Membrane	CPU execution time (in seconds)		
	For the PWBM	For the IBEM	For the EIBEM
skew $\Psi = 35°$ ($n = 36$)	674	6304	3815
pentagonal ($n = 30$)	200	1962	1230
quadrilateral ($n = 32$)	233	2163	1499

Table 8: Comparison of the CPU execution time for the PWBM, the IBEM and the EIBEM on a SPARC station 2

Mode No.	PWBM	IBEM
1	5.999 (0.00)	6.019 (0.34)
2	8.567 (0.00)	8.603 (0.42)
3	10.402 (0.00)	10.461 (0.56)
4	11.471 (0.00)	11.524 (0.46)
5	11.498 (0.00)	11.568 (0.61)

Table 9: Comparison of eigenvalues λ for a clamped square plate ($n = 32$, $\Delta\lambda = 0.0005$); the relative error is shown in parentheses

Number of anti-nodes α	Number of anti-nodes β	PWBM	Experimental [53]	Relative error (in %)
1	1	2.358	2.320	1.60
2	1	3.173	3.180	0.22
1	2	3.533	3.530	0.09
2	2	4.084	4.100	0.39
3	1	4.153	4.220	1.61
1	3	4.790	4.810	0.42
3	2	4.885	4.889	0.08
2	3	5.176	5.237	1.18

Table 10: Comparison of eigenvalues $\lambda_{\alpha\beta}$ of a fully clamped symmetrical trapezoidal plate; symbols are as shown on Figure 12 with $b/a = 0.8$, $c/a = 0.75$, ($n = 32$, $\Delta\lambda = 0.001$)

Mode No.	PWBM	HFEM [6]	Relative error (in %)
1	4.96	4.992	0.64
2	7.255	7.255	0.00
3	8.428	8.472	0.52
4	9.154	9.156	0.02
5	11.083	11.083	0.00

Table 11: Comparison of the eigenvalues λ for a clamped skew plate of skew angle $\psi = 30°$, ($n = 36$, $\Delta\lambda = 0.0005$)

Mode No.	PWBM	Orthogonal Polynomials [49]	Relative error (%)
1	3.635	3.635	0.00
2	4.862	4.862	0.00
3	6.192	6.191	0.02
4	6.794	6.793	0.01
5	7.582	7.591	0.12
6	7.922	7.7922	0.00

Table 12: Eigenfrequencies λ for a simply supported elliptical plate shown on Figure 13 ($n = 30$, $a/b = 2.0$)

Mode		PWBM	Theory
α	β	k	$k_{\alpha\beta}$
1	0	3.142	3.142
1	1	4.443	4.443
2	0	6.283	6.283
2	1	7.025	7.025
2	2	8.886	8.886
3	0	9.425	9.425
3	1	9.932	9.935

Table 13: Comparison of the eigenvalues λ for a sliding-clamped square plate, ($n = 36$, $\Delta\lambda = 0.001$)

Mode No.	PWBM	Superposition Method [27]	Relative error (in %)
1	3.86	3.67	4.92
2	4.43	4.43	0.00
3	4.98	4.93	1.00
4	6.06	5.90	2.64
5	7.86	7.82	0.51

Table 14: Eigenvalues λ of a free square plate obtained with the PWBM ($n = 32$, $\Delta\lambda = 0.005$)

Mode No. α	Mode No. β	PWBM	Reference [51]	Relative error (in %)
0	2	2.32	2.29	1.29
0	3	3.53	3.50	0.85
0	4	4.67	4.65†	0.43
0	5	5.78	5.75†	0.52
0	6	6.89	6.80†	1.31
1	0	3.00	3.01	0.33
1	1	4.53	4.53	0.00
1	2	5.94	5.94	0.00
1	3	7.28	7.27	0.14
2	0	6.20	6.21	0.16

†Values true within 2 percent [51]

Table 15: Eigenfrequencies $\lambda_{\alpha\beta}$ for a free circular plate ($\nu = 0.33$); α represents the number of nodal circles and β the number of nodal diameters

Mode No.	PWBM	HFEM [6]	Relative error (in %)
1	2.72	2.67	1.87
2	4.04	3.97	1.76
3	4.04	3.97	1.76
4	4.43	4.43	0.00
5	6.340	6.2	2.26

Table 16: Comparison of the eigenvalues λ for a point-supported square plate, ($n = 32$, $\Delta\lambda = 0.005$)

Mode No.	PWBM	Superposition Method [68, 29]	Relative error (%)
1	8.11	8.11	0.0
2	11.00	22.00	0.00
3	12.42	12.43	0.06
4	14.01	14.01	0.00

Table 17: Comparison of the eigenvalues λ for the SS-C-SS right triangular plate shown in Figure 14 (a), ($n = 36$, $\Delta\lambda = 0.005$)

Mode no.	PWBM	Superposition Method [68]	Relative error (%)
1	6.43	6.43	0.00
2	8.21	8.21	0.00
3	9.79	9.78	0.06
4	10.17	10.17	0.00

Table 18: Comparison of the eigenvalues λ for the C-SS-C right triangular plate shown in Figure 14 (b), ($n = 36$, $\Delta\lambda = 0.005$)

Mode no.	PWBM	Rayleigh-Ritz Method [44]	Relative error (%)
1	5.80	5.80	0.00
2	8.87	8.88	0.11
3	9.43	9.44	0.11
4	11.93	11.91	0.15
5	12.90	12.92	0.15
6	13.18	13.19	0.11

Table 19: Comparison of the eigenvalues λ for the C-C-F isosceles triangular plate shown in Figure 14 (c), ($n = 36$, $\Delta\lambda = 0.005$)

Mode No.	ABFM	Bessel expansions [75]
1	6.00 (0.00)	6.00 (0.00)
2	8.57 (0.00)	8.57 (0.00)
3	10.43 (0.25)	10.40 (0.00)
4	11.47 (0.00)	11.47 (0.00)
5	11.51 (0.09)	11.50 (0.00)

Table 20: Comparison of the eigenvalues λ for a free square plate ($n = 32$, $N = 40$, $\Delta\lambda = 0.005$); the relative error is shown in parentheses

Mode No.	ABFM $n = 32$, $N = 40$	Bessel expansions [75]	Superposition Method [27]
1	3.71 (1.08)	3.73 (1.61)	3.67
2	4.43 (0.00)	4.43 (0.00)	4.43
3	4.93 (0.00)	4.94 (0.20)	4.93
4	5.91 (0.17)	5.95 (0.84)	5.90
5	7.85 (0.38)	7.82 (0.00)	7.82

Table 21: Comparison of the eigenvalues λ for a free square plate ($\Delta\lambda = 0.005$); the relative errors is shown in parentheses

Mode No.	ABFM	Superposition Method [6]	Relative error (in %)
1	3.47	3.57	2.88
2	4.51	4.50	0.22
3	5.29	5.21	1.51
4	5.50	5.50	0.00

Table 22: Eigenvalues λ of a free skew plate of skew angle $\psi = 15°$ ($n = 32$, $N = 40$, $\Delta\lambda = 0.005$); the relative error is shown in parentheses